# THERMAL DIFFUSION
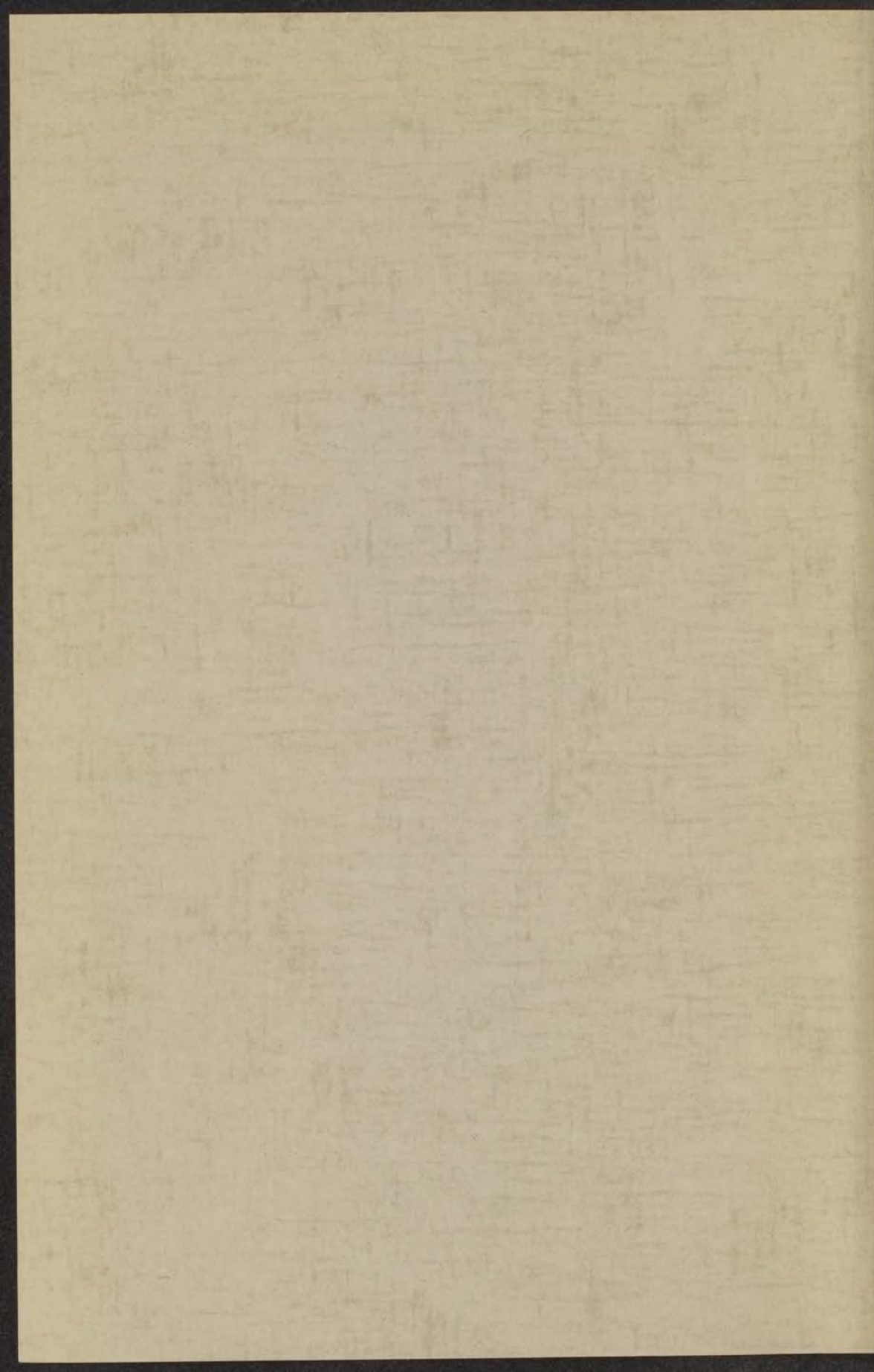# FOR QUASI-LORENTZIAN MIXTURES
# BETWEEN 10 AND 800 °K

AHMED IBRAHIM GHOZLAN

# THERMAL DIFFUSION
# FOR QUASI-LORENTZIAN MIXTURES
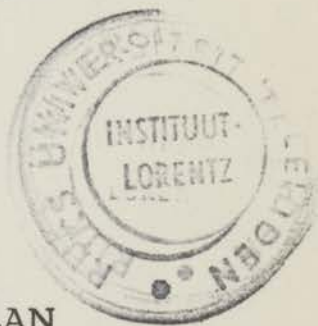# BETWEEN 10 AND 800 °K

## PROEFSCHRIFT

TER VERKRIJGING VAN DE GRAAD VAN DOCTOR IN DE WIS- EN
NATUURKUNDE AAN DE RIJKSUNIVERSITEIT TE LEIDEN OP
GEZAG VAN DE RECTOR MAGNIFICUS Dr. S. DRESDEN, HOOG-
LERAAR IN DE FACULTEIT DER LETTEREN EN WIJSBEGEERTE,
TEGEN DE BEDENKINGEN VAN DE FACULTEIT DER WIS- EN
NATUURKUNDE TE VERDEDIGEN OP WOENSDAG 29 MEI 1963
TE 16 UUR

DOOR

## AHMED IBRAHIM GHOZLAN
geboren te Alexandria (Egypte) in 1926

Promotor : Prof. Dr. J. Kistemaker

to my mother
to my wife and
children

by: A. I. Ghozlan

ERRATA

1. Fig. II-15 replaces fig. II-5 and fig. II-5 is discarded.

2. The figure underneath has to replace fig. II-15.
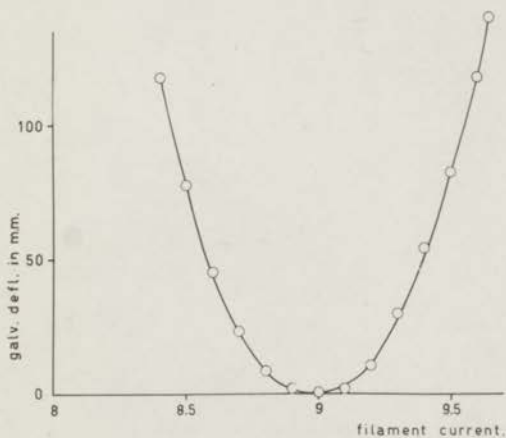


Fig. II-15

N. B. The captions of both figures are correct.
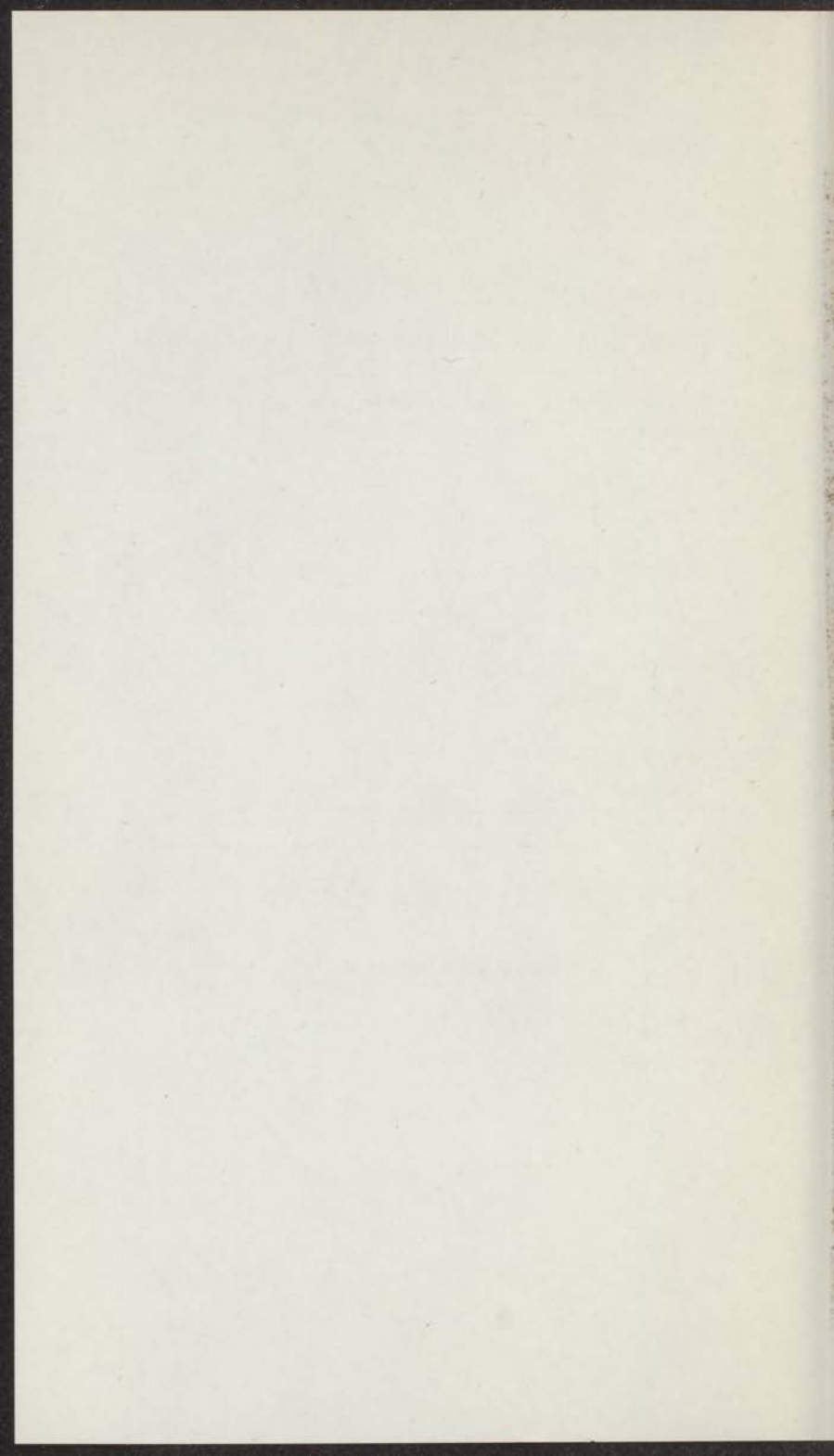
According to the wish of the Faculty for Wis- en Natuur-
kunde of the Leyden University I give here a short des-
cription of my education.

After having finished my studies at the Abbasia Secondary
School in 1946, I studied at the University of Alexandria
from 1946 to 1950 and finished with my B. Sc. in pure
Mathematics. I got my masters degree in Physics in
1955 at the same University.

In the meantime I was employed by the Ministery of
Education and did some exploration research for the
Atomic Energy Commission in the Red-Sea Coast and
Sinai.

In 1955 I was seconded to the University of Khartoum as a
Lecturer in Physics, and in 1958 Prof. Dr. J. Kistemaker
invited me to join his research group in the F. O. M. -
Laboratory for Mass Separation in Amsterdam.

According to the wishes of the Faculty for Mathematics and Natural Sciences of the Leyden University I give here a short description of my education.

After having finished my studies at the Abbasia secondary school in 1944, I studied at the University of Alexandria from 1946 to 1950 and finished with my B.Sc. in pure mathematics. I got my masters degree in Physics in 1954 at the same University.

In the meantime I was employed by the Ministery of Education and did some exploration research for the Atomic Energy Commission in the Red-Sea Coast and Sinai.

In 1955 I was seconded to the University of Khartoum as a Lecturer in Physics, and in 1958 Prof. Dr. J. Kistemaker invited me to join his research group in the F.O.M.-Laboratory for Mass Separation in Amsterdam.

# CONTENTS

# INTRODUCTION

Since several years experience has been obtained with the separation by thermal diffusion of radioactive gases from a carrier gas, by experts like:

Harrison, [1]    using $^{222}Rn$

Mason, [2]    using $^{85}Kr$ and $^{14}C$

Grew, [3]    using $^{222}Rn$, $^{133}Xe$ and $^{85}Kr$    and

Heymann, [4]    using $^{133}Xe$

with various gases like $H_2$, He, Ne, Ar, etc.

They determined the elementary separation factor with an elementary cell, contrary to people like Libby and Arnold[5], De Vries[6] and Dickel[7] who studied the enrichment of $^{14}C$ in various compounds like e.g. CO, $CO_2$ and $CH_4$, using thermal diffusion columns.

The best method to determine the thermal diffusion factor is the method with the elementary cell, and has therefore been chosen as the experimental approach in this thesis.

The reasons for using radioactive gases are:

a. They are easily detectable, and therefore avoid complicate volumetric or mass spectrometric analyses.
b. They make it possible to work with a quasi-Lorentzian gas mixture, being a mixture with only tracer quantities of a heavy, radioactive molecule in it, and on which simplified calculations can be done.
c. As tracer quantities can be used, this opens the possibility to proceed the research in low temperature regions, if only the partial pressure of the tracer remains below its vapour pressure.

Heymann's [8] measurements of the elementary separation factor, done in our laboratory, gave between 300 and 700 °K, qualitative agreement with classically calculated thermal diffusion factors. He used a Lennard-Jones (12, 6) potential model. For the lighter carrier gases ($H_2$, $D_2$, He) his deviations of maximum 10% gave rise to the question how the thermal diffusion factor would behave in lower temperature regions. Of course, there were suspicions to possible quantum effects and this lead us to build a two bulb apparatus, using a Geiger counter at room temperature as a detecting device for the radiation of $^{85}Kr$. Moreover, we realised the possibility to work between 10 and 800 °Kr using cryogenic techniques This was the state of affairs in 1959. In the meantime Grew and Mundy[3] did their beautiful work in England on analogous mixtures, which was not known to us. Their publication came in 1961.

Because of the interesting results which we obtained with $^{85}Kr$ against $^{22}Ne$, $^{4}He$, $^{3}He$ and $H_2$, we decided in 1960 to do some determinations on the thermal separation factor, in about the same apparatus, with tritium ($T_2$) as a radioactive tracer gas. The radiation of $T_2$ having about 10 keV energy, the counting techniques used with $^{85}Kr$ had to be left and to be replaced by an ionisation chamber, at room temperature again, on top of the cryostat. This gave us, moreover, a gain in accuracy of the determination of the separation factor, with a factor ten. We used $T_2$, DT and HT with $^{4}He$, $H_2$ and $D_2$ as carrier gases and worked with liquid hydrogen as a cooling agent.

9

The interesting experiments and calculations on comparable mixtures done at about the same time by Waldmann c.s. [9] gave us a great help.

The $^{85}$Kr measurements should show a more or less classical character till the lowest possible temperature of $50^{\circ}$K, as the reduced wave length $\Lambda^*$ for Kr against ($^4$He, $^3$He or $H_2$) is about 0.8 and the potential minimum (Lennard-Jones) between Kr and these various carrier gases is $\epsilon/K \simeq 44$ $^{\circ}$K and 78 $^{\circ}$K respectively, according to Hirschfelder c.s. [10])

For the tritium mixtures the situation is very different however, where in case of $^4$He as a carrier gas $\Lambda^* \simeq 1.75$ and $\epsilon/k \simeq 19.45$ $^{\circ}$K. Quantum effects in the thermal diffusion factor can be expected below 50 $^{\circ}$K in the latter case.

The object of these two $^{85}$Kr and $T_2$ experimental sequences was to obtain data on the temperature dependence of the experimental thermal diffusion factor $\alpha$. This factor $\alpha$ is, together with the normal diffusion coefficient D, the most sensitive fundamental characteristic for the interaction potential between u n l i k e molecules, whereas these $\alpha$ and D coefficients are only indirectly and insensitively dependent on the interaction of l i k e molecules. The measurement of $\alpha$ and D is therefore of high importance to learn more about the interaction between u n l i k e molecules, and becomes extremely interesting for mixtures with large quantum parameters. The temperature dependent behaviour of $\alpha_{expt.}$ for very asymmetric molecules like HT against spheres like $^4$He in the temperature region where heavy quantum effects can be expected, was the last research object.

10

# CHAPTER I

## THE THERMAL DIFFUSION FACTOR

### PAR. 1.  INTRODUCTION

Before we introduce the way in which the classical theory as well as the quantum theory have performed their calculations for the transport phenomena, we will discuss the basic integro-differential equation given by Maxwell-Boltzmann. [10-12])

The expressions given by the above two theorems are solutions of this equation. The Maxwell-Boltzmann equation is given by:

$$\frac{\partial f}{\partial t} + \bar{c} \frac{\partial f}{\partial \bar{r}} + \bar{F} \frac{\partial f}{\partial \bar{c}} = \sum_j \iint [f_i f_j - f_i' f_j'] \, k_{ij} d\bar{k} d\bar{c}_j \qquad (I-1)$$

where $f = f(\bar{c}, \bar{r}, t)$ is the distribution function, or more simply is analogous to the number of particles per unit volume in the limiting case of equilibrium. The different terms of equation (1) can be explained physically as follows:

a. The term $\frac{\partial f}{\partial t}$ represents the partial time derivative. The physical meaning of this term can be understood if we suppose that we have an observer molecule fixed in position at the centre - for instance - of the unit volume; then the rate of change of the number of molecules in the unit volume with respect to time is given by $\frac{\partial f}{\partial t}$.

b. The second term $\bar{c} \frac{\partial f}{\partial \bar{r}}$ is due to the motion of the molecules themselves If we suppose that our observing molecule has a velocity $\bar{c}$ which is exactly the same as the mean random velocity of the molecules, then when this observer molecule will register the variation of the distribution function f, the effect of its motion will be reflected. The first two terms can be regarded as the substantial time derivative which can be written as $\frac{Df}{Dt}$.

c. The third term $\bar{F} \frac{\partial f}{\partial \bar{c}}$ represents the effects of the external forces on the system. As $\bar{F}$ is the rate of change of momentum and equals $\frac{d\bar{c}}{dt}$ per unit mass, then we see that there is an extra change in the distribution function due to velocity changes by applying external forces.

The left hand side of equation (I-1) can be written as $\not{b}$ , which represents the total change in the unit volume.

The right hand side of equation (I-1) represents the net gain or loss in the volume element due to collisions. This term is usually written as $J(f_i f_j)$.

11

The Boltzmann integro-differential equation can be written now as:

$$\left[\begin{array}{l}\text{rate of change}\\\text{of the distribution}\\\text{function w.r.t. time}\end{array}\right] + \left[\begin{array}{l}\text{rate of change}\\\text{due to particles}\\\text{motion}\end{array}\right] + \left[\begin{array}{l}\text{rate of change}\\\text{due to external}\\\text{forces}\end{array}\right] =$$

$$\left[\begin{array}{l}\text{net gain or loss}\\\text{per unit volume due}\\\text{to collisions}\end{array}\right]$$

PAR. 2.

SOLUTION OF THE BOLTZMANN EQUATION IN CLASSICAL MECHANICS

The Maxwell-Boltzmann integro-differential equation can be written in the short hand form as:

$$\mathcal{D}f = J(f_i f_j) \tag{I-2}$$

In order to solve this equation classically, [11-13] the following steps were followed:

1. Classical mechanics has tried to find an expression for the angle of deflection between two colliding particles. [11] This expression was derived via the two conservation principles of energy and momentum [10, 14] and is given by: [10]

$$x(g, b) = \pi - 2b \int_{r_m}^{\infty} \frac{dr/r^2}{\sqrt{1 - \dfrac{b^2}{r^2} - \dfrac{\Phi(r)}{\frac{1}{2}\mu g^2}}} \tag{I-3}$$

where "g" is the relative velocity of the two colliding particles and "b" is the collision parameter. If the potential field $\Phi(r)$ between two colliding particles is known, then the angle of deflection $x(g, b)$ is completely determined.

2. From the angle of deflection $x(g, b)$, the cross section of two colliding molecules can be determined and is given by the expression: [10]

$$Q^{l}(g) = 2\pi \int_{0}^{\infty} (1 - \cos^{l} x)b\,db \tag{I-4}$$

where the index $l$ denotes the kind of cross section.

3. If the cross section is known, the so called collision integral can be determined and is given by the expression: [10]

$$\Omega^{l,s}(T) = \sqrt{\frac{kT}{2\pi\mu}} \int_{0}^{\infty} e^{-\gamma^2} \gamma^{2s+3} Q^{l}(g)\,d\gamma \tag{I-5}$$

where $\gamma^2 = \frac{1}{2}\mu g^2/kT$

The solution of the Boltzmann differential equation (I-2) without the external forces term has given the following expression for thermal diffusion factor in a binary mixture, in the case one of the components is present in small amounts: [15]

$$\alpha = \frac{-M_2 + \dfrac{3s}{A_{12}} \left[M_1^2(M_1 - M_2)\right] + 4sM_1^2 M_2}{6 M_1^2 + 5 M_2^2 - 4 M_2^2 B_{12} + 8 M_1 M_2 A_{12}} 5(C_{12} - 1) \tag{I-6}$$

12

In this expression for the thermal diffusion factor the temperature effect appears in the factor $(C_{12} - 1)$. The different symbols in this expression[15] are:

$$s = \left(\frac{\sigma_{12}}{\sigma_2}\right)^2 \frac{1}{\sqrt{2 M_1}} \frac{\Omega^{*2,2}(T_{12}^*)}{\Omega^{*2,2}(T_2^*)}$$

$$\left. \begin{array}{lll} A_{12}^* = \dfrac{\Omega_{12}^{*2,2}}{\Omega_{12}^{*1,1}} & B_{12}^* = \dfrac{5\ \Omega_{12}^{*1,2} - 4\ \Omega_{12}^{*1,3}}{\Omega_{12}^{*1,1}} & C_{12}^* = \dfrac{\Omega_{12}^{*1,2}}{\Omega_{12}^{*1,1}} \\[3mm] A_{12} = 0.4\ A_{12}^* & B_{12} = 0.6\ B_{12}^* & C_{12} = 1.2\ C_{12}^* \end{array} \right\}$$

(I-7)

## PAR. 3. SOLUTION OF THE BOLTZMANN EQUATION IN QUANTUM MECHANICS.

The solution of the Boltzmann integro-differential equation in quantum mechanics follows nearly the same way as the classical solution. The main differences between the two theorems are the following:

a. In classical mechanics an expression was given for the angle of deflection by equation (I-3). In quantum mechanics this is not possible due to the uncertainty principle. All what can be said is that, instead of giving the angle of deflection, we give the probability[10] that this angle will lie within a solid angle $d\bar{\omega}$ .
In this case the angle $\varkappa$ is replaced by $\alpha(g_{ij}, \varkappa)$.

b. The second difference is that at very low temperatures - say below 1 or 2 °K- the statistics of the molecules play an important part. This effect is called the symmetry effect;[10,16] and factors of the form $f_i'(1 + \vartheta_i f_i)$ must be introduced in place of $f_i'$, where "i" represents the ith molecule. The factor " $\vartheta_i$" depends on the statistics used. In the case of Fermi-Dirac statistics:

$\vartheta_i = -\left(\dfrac{h}{m}\right)^3/G$, and in Bose-Einstein statistics : $\vartheta_i = +\left(\dfrac{h}{m}\right)^3/G$,

while in Boltzmann statistics $\vartheta_i = 0$. "G" is the statistical weight of the particle. In this case the Boltzmann differential equation becomes : [10]

$$\mathcal{D}f = 2\ \pi \sum_{j=1}^{\nu} \int\int \left[ f_i' f_j' (1 + \vartheta_i f_i)(1 + \vartheta_j f_j) - f_i f_j (1 + \vartheta_i f_i')(1 + \vartheta_j f_j') \right] \alpha(g_{ij}, \varkappa) \sin \varkappa \ d\varkappa \ d\bar{c}_j$$

(I-8)

where the summation extends over all molecules j.

## PAR. 4. NUMERICAL ESTIMATION OF THE CONDITIONS OF THE EXPERIMENT.

a. The influence of the concentration of the tracer gas.

13

The termal diffusion is given in first approximation by an equation of the form : [10]

$$\alpha \, (T, Y) = 5 \left[ C(T) - 1 \right] \beta \; (T, Y) \tag{I-9}$$

In the case of very small amounts of $^{85}$ Kr, which has been used as a tracer gas in our experiments, $\beta$ (T, Y) reduces to $- \dfrac{S_2}{Q_2}$ and equation (I-6) takes the form : [15]

$$\alpha \, (T, Y) = - 5 \left[ C(T) - 1 \right] \frac{\overset{*}{S}_2}{Q_2} \tag{I-10}$$

where $S_2$ and $Q_2$ are expressions given by (I-32a) and (I-32b).

From fig. I-1 we see that the variation of $\dfrac{S_2}{Q_2}$ with temperature is
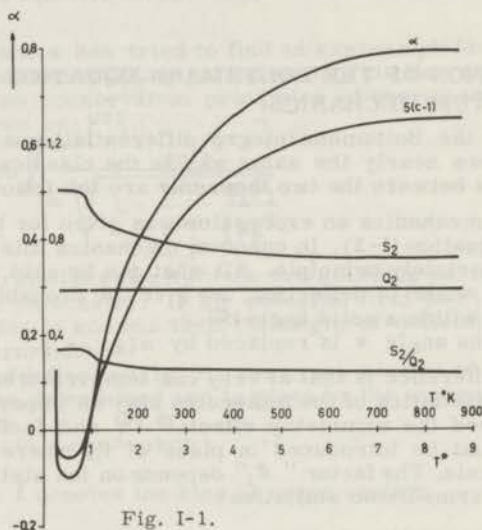


Fig. I-1.

The variation of the quantities $\alpha$, $5(C-1)$, $S_2$, $Q_2$ and $\dfrac{S_2}{Q_2}$ as a function of the reduced temperature $T^*$. The outer scale - on the ordinate axis - is for only, while the inner one is for the quantities $5 (C-1)$, $S_2$, $Q_2$ and $\dfrac{S_2}{Q_2}$. From this graph we see that the variation of $\dfrac{S_2}{Q_2}$ as a function of temperature is small, while most of the variations appear in $5 (C-1)$.

negligible so that $\left[ \dfrac{S_2}{Q_2} \right]_{L.J.}$ can be taken to be approximately equal to

$\begin{bmatrix} S_2 \\ Q_2 \end{bmatrix}_{R.E.S.}$ .Here L. J. stands for Lennard-Jones and R.E.S. for Rigid Elastic Spheres.

The constant $C(T)$ is defined in general by the equation:

$$C(T) = \frac{2 \; \Omega^{1,2}_{12}(T^*_{12})}{5 \; \Omega^{1,1}_{12}(T^*_{12})} \qquad (I-11)$$

where in the case of the R.E.S., these $\Omega$ 's are given by the relation:

$$\Omega^{\ell,s} = \tfrac{1}{2}(s+1)! \left[ 1 - \tfrac{1}{2} \frac{1 + (-1)^{\ell}}{1 + \ell} \right] \pi \sigma^2 \sqrt{\frac{kT}{2\pi\mu}} \qquad (I-12)$$

Substituting we find $C_{R.E.S.} = 1.2$.

For the rigid elastic spheres we have:

$$\alpha_{R.E.S.} = 5 \left[ 1.2 - 1 \right] \begin{bmatrix} S_2 \\ Q_2 \end{bmatrix}_{R.E.S.} = \begin{bmatrix} S_2 \\ Q_2 \end{bmatrix}_{R.E.S.} \qquad (I-13)$$

Therefore equation (I-10) can be written in the form:

$$\alpha_{L.J.}(T) \simeq -5 \left[ C_{L.J.}(T) - 1 \right] \begin{bmatrix} S_2 \\ Q_2 \end{bmatrix}_{R.E.S.}$$

$$\simeq -5 \left[ C_{L.J.}(T) - 1 \right] \alpha_{R.E.S.} \qquad (I-14)$$

or:

$$\alpha^* = \frac{\alpha_{L.J.}}{\alpha_{R.E.S.}} \simeq 5 \left[ C_{L.J.} - 1 \right] \qquad (I-15)$$

b. The temperature region where quantum deviations can be expected. According to the quantum theory, deviations from classical behaviour exist due to the wave nature of the colliding particles. The wave length associated with a particle of reduced mass $\mu$ is given by the De Broglie wave equation;

$$\lambda = \frac{h}{mv} = \frac{h}{\sqrt{2\mu kT}} \qquad (I-16)$$

When this wave length is comparable with the molecular dimensions we have diffraction effects. [10, 16, 17] By dividing equation (I-16) by $\sigma$, we have:

$$\frac{\lambda}{\sigma} = \frac{h}{\sigma \sqrt{\mu kT}} \qquad (I-17)$$

15

where $\mu = \dfrac{m_1 m_2}{m_1 + m_2}$ and $\sigma$ is the molecular diameter.

To compare quantum effects of different gases we measure the temperature in $\dfrac{\epsilon}{k}$ as a unit. The reduced temperature corresponding to $T$ °K is given by:

$$T^* = T / \left(\frac{\epsilon}{k}\right) \tag{I-18}$$

where $\epsilon$ is the depth of the Lennard-Jones potential

Substituting in equation (I-17), we have:

$$\frac{\lambda}{\sigma} = \frac{h}{\sigma\sqrt{2\mu\epsilon}} \frac{1}{\sqrt{T^*}} = \frac{\Lambda^*}{\sqrt{T^*}} \tag{I-19}$$

where $\Lambda^* = \dfrac{h}{\sigma\sqrt{2\mu\epsilon}}$ and is used to compare the quantum deviations of different gases at a reduced temperature $T^*$ equal to 1. [17]

If $\lambda = \sigma$ - the wave length associated with a molecule is equal to its diameter -, then equation (I-19) becomes:

$$1 = \frac{\Lambda^*}{\sqrt{T^*}} \quad \text{or} \quad T^* = \Lambda^{*2} \tag{I-20}$$

Using equation (I-18), we get:

$$T = \Lambda^{*2} \cdot \frac{\epsilon}{k} \tag{I-21}$$

Now the lowest temperature at which measurements can be done, using $^{85}$Kr as a tracer gas, is determined by the vapour pressure. In our counter we cannot have a reasonable number of counts when the pressure of the tracer gas is less than $10^{-6}$ mm-Hg. Substituting this pressure in the vapour pressure formula:

$$\ln \frac{P}{P_c} = K' \left(1 - \frac{T_c}{T}\right) \tag{I-22}$$

where $P_c$ and $T_c$ are the critical pressure and temperature respectively, $P(T)$ is the vapour pressure as a function of $T$ and $K'$ is a constant.

We find that our minimum temperature $T_{min}$ is equal to 50 °K to give the minimum allowed vapour pressure of the krypton gas. Therefore the mixtures which are favourable for measuring the quantum effects, are those mixtures, which have not a too low $\Lambda^*$ together with an $\dfrac{\epsilon}{k}$ exceeding as much as possible the minimum value 50 °K. This means that our temperature region should lie between:

$$T_{min} \leqslant T \leqslant \frac{\epsilon}{k} \tag{I-23}$$

16

To satisfy this equation $^{85}$Kr and another light gas $H_2$ whose $\Lambda^*_{12} = 0.8$ and $\frac{\epsilon_{12}}{k} \simeq 80\,^\circ$K were chosen. The mean value of our temperature range is about $65\,^\circ$K.

In this region of temperature the deviation of the interpolated quantum curve from the classical one might be two to three times the classical value as shown in Fig. I-2.
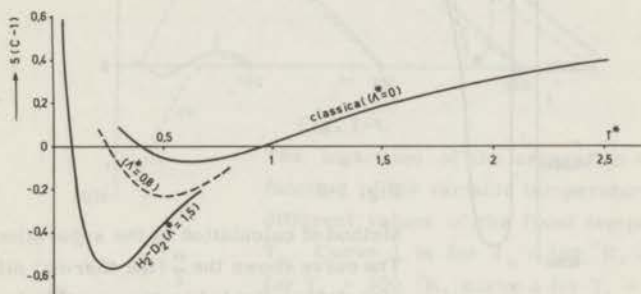


Fig. I-2.

The relation between 5 (C-1) as a function of the reduced temperature $T^*$. The curve for $\Lambda^*=0$ was obtained from Hirschfelder, [1] while for $\Lambda^* = 1.5$ it has been obtained from the theoretical quantum calculations with the Lennard-Jones (12,6) model by De Kerf (see chapter V).
The dotted curve has been interpolated for $\Lambda^* \simeq 0.8$ for the $^{85}$Kr mixtures.

PAR. 5.

APPROXIMATE THEORETICAL CALCULATION OF THE SEPARATION

The thermal diffusion factor $\alpha$ as a function of the separation $Q_s$ is given by: [12]

$$\alpha = \frac{d \ln Q_s}{d \ln \frac{T_c}{T_h}} \qquad (I-24)$$

Integrating this relation, after performing the required differentiation, we get:

$$\ln Q_s = \int_{T_h}^{T_c} \frac{\alpha}{T} \, dT \qquad (I-25)$$

In order to perform this integration a graph of T against $\frac{\alpha}{T}$ was plotted; by varying T from 25 $^\circ$K to 800 $^\circ$K as in fig. I-3. The area under this

17
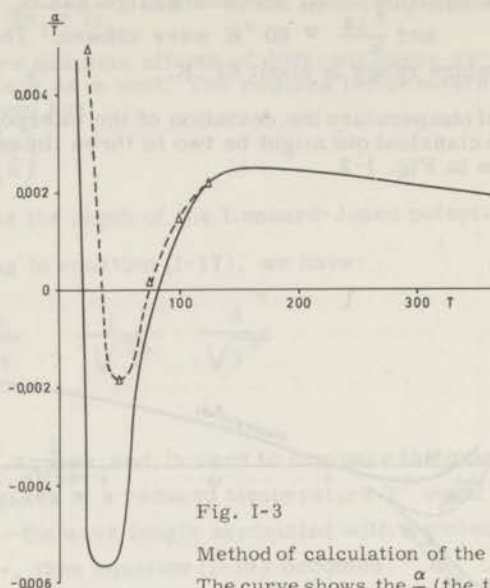
Fig. I-3

Method of calculation of the separation $Q_s$. The curve shows the $\frac{\alpha}{T}$ (the thermal diffusion factor divided by the variable temperature) as a function of the variable temperature T. The area under the curve represents the logarithm of the separation $Q_s$. The dotted curve is classically calculated for the Lennard-Jones (12,6) potential, while the continuous one is obtained from the interpolated curve of fig. I-2.

curve corresponds to the logarithm of the separation $Q_s$. By fixing $T_h$ at 375 °K, 360 °K, 300 °K, 200 °K and 100 °K and varying T to 25 °K in each case, several graphs of log $Q_s$ against T were obtained as in fig. I-4. These graphs have been obtained from the classical and the approximated quantum curve shown in fig. I-3. From these graphs we see that the ratio:

$$\frac{\left[ \left\{ \ln Q_s \right\}_{max} - \left\{ \ln Q_s \right\}_{min} \right]_{classical}}{\left[ \left\{ \ln Q_s \right\}_{max} - \left\{ \ln Q_s \right\}_{min} \right]_{quantum}}$$

does not increase much by lowering the temperature of the top reservoir. Therefore the temperature of the top reservoir was adjusted at room temperature.

## PAR. 6. CLASSICAL CALCULATION OF THE THERMAL DIFFUSION FACTOR $\alpha$.

The calculation of the thermal diffusion factor $\alpha$ was classically performed by using the Lennard-Jones potential which is given by: [10]

18
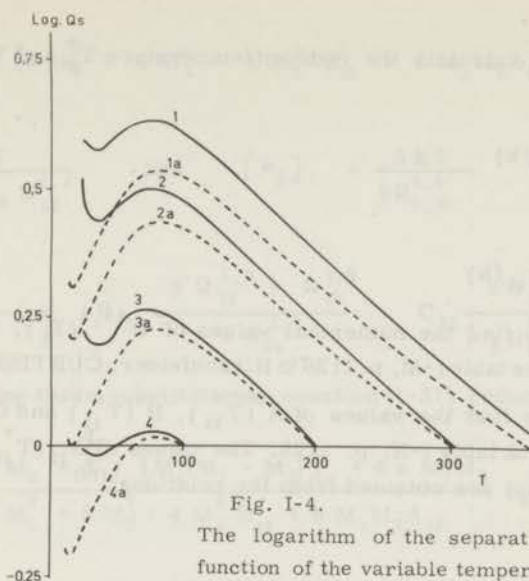
Fig. I-4.

The logarithm of the separation $Q_s$ as a function of the variable temperature $T$ for different values of the fixed temperature $T_h$. Curve 1 is for $T_h = 360\ ^{\circ}K$, curve 2 for $T_h = 300\ ^{\circ}K$, curve 3 for $T_h = 200\ ^{\circ}K$ and curve 4 for $T_h = 100\ ^{\circ}K$. The dotted curves 1a, 2a, 3a and 4a are the same as the curves 1, 2, 3 and 4, only calculated quantum mechanically with the help of the interpolated curve in fig. I-2.

$$\Phi(r) = 4\epsilon \left[ \left(\frac{\sigma}{r}\right)^{12} - \left(\frac{\sigma}{r}\right)^{6} \right] \tag{I-26}$$

This potential shows that at very small distances repulsion prevails and the potential energy decreases with increasing distance; then the attractive forces become more important. As a result of this a minimum in the potential energy curve appears.

The thermal diffusion factor for this model can be obtained from tabulated values of the collison integrals [10] as follows:

1. We have to calculate $\sigma_{12}$ and $\epsilon_{12}$ from the values $\sigma_1$, $\sigma_2$ and $\epsilon_1$, $\epsilon_2$, which are given by the following approximations: [10]

$$\sigma_{12} = \frac{\sigma_1 + \sigma_2}{2} \tag{I-27a}$$

and

$$\frac{\epsilon_{12}}{k} = \frac{\sqrt{\epsilon_1 \epsilon_2}}{k} \tag{I-27b}$$

19

2. We have to calculate the reduced temperature $T_2^*$ and $T_{12}^*$ using the relations :

$$T_2^* = T/(\epsilon_2/k) \qquad\qquad (I-28a)$$

and

$$T_{12}^* = T/(\epsilon_{12}/k) \qquad\qquad (I-28b)$$

3. We have to find the numerical values of $\Omega^{*2,2}(T_2^*)$, $\Omega^{*2,2}(T_{12}^*)$, etc. using the table I-M, p. 1126 in Hirschfelder, CURTISS and Bird.[10]

4. We have to find the values of $A^*(T_{12}^*)$, $B^*(T_{12}^*)$ and $C^*(T_{12}^*)$ from the same book table I-N, p. 1128. The values of $A_{12}(T_{12}^*)$, $B_{12}(T_{12}^*)$ and $C_{12}(T_{12}^*)$ are obtained from the relations :[10]

$$A_{12}^* = \frac{A_{12}}{[A_{12}]_{R.E.S.}} = \frac{A_{12}}{\frac{2}{5}} \qquad\qquad (I-29a)$$

$$B_{12}^* = \frac{B_{12}}{[B_{12}]_{R.E.S.}} = \frac{B_{12}}{\frac{3}{5}} \qquad\qquad (I-29b)$$

$$C_{12}^* = \frac{C_{12}}{[C_{12}]_{R.E.S.}} = \frac{C_{12}}{1.2} \qquad\qquad (I-29c)$$

These quantities are inserted in the expression for $\alpha$ which will be now given.

The first approximation for the thermal diffusion factor[12, 15] is given by the relation :

$$\alpha = 5(C - 1)\frac{S_1 Y - S_2(1 - Y)}{Q_1 Y^2 + Q_2(1 - Y)^2 + Q_{12} Y(1 - Y)} \qquad\qquad (I-30)$$

where Y is the molar fraction of component one and $S_1$, $S_2$, $Q_1$, $Q_2$ and $Q_{12}$ are quantities independant of concentration. (See equations I-32 a and I-32b).

By using a tracer gas we put $Y = O$, and equation (I-32) reduces to :

$$\alpha = 5(C - 1)\left[-\frac{S_2}{Q_2}\right] \qquad\qquad (I-31)$$

where

$$S_2 = \frac{M_2^2 E}{[\mu_2]_1} - M_1\left[3(M_1 - M_2) + 4 M_2 A_{12}\right] \qquad\qquad (I-32a)$$

20

$$Q_2 = \frac{M_2 \, E}{[\mu_2]_1} \left[ 6 \, M_1^2 + 5 \, M_2^2 - 4 \, M_2^2 \, B_{12} + 8 \, M_1 M_2 A_{12} \right] \tag{I-32b}$$

$$E = \frac{kT}{8 \, M_1 M_2 \, \Omega_{12}^{1,1}} \quad \text{and} \quad [\underline{\mu_2}]_1 = \frac{5 \, kT}{8 \Omega_2^{2,2}} \tag{I-32c}$$

$$A_{12} = \frac{\Omega_{12}^{2,2}}{5 \, \Omega_{12}^{1,1}} \qquad B_{12} = \frac{5 \, \Omega_{12}^{1,2} - \Omega_{12}^{1,3}}{5 \, \Omega_{12}^{1,1}} \qquad C_{12} = \frac{2 \, \Omega_{12}^{1,2}}{5 \, \Omega_{12}^{1,1}} \tag{I-32d}$$

By performing these substitutions, equation (I-31) reduces to:

$$\alpha_{\text{at } y=0} = \frac{- M_2 + \dfrac{3s}{A_{12}} \left[ M_1^2 (M_1 - M_2) \right] + 4 \, s \, M_1^2 M_2}{6 \, M_1^2 + 5 \, M_2^2 - 4 \, M_2^2 \, B_{12} + 8 \, M_1 M_2 A_{12}} \; 5(C_{12} - 1) \tag{I-33a}$$

where

$$s = \left( \frac{\sigma_{12}}{\sigma_2} \right)^2 \frac{1}{\sqrt{2 \, M_1}} \; \frac{\Omega^{*2,2}(T_{12}^*)}{\Omega^{*2,2}(T_2^*)} \tag{I-33b}$$

PAR. 7.

THE MEASUREMENT OF THE THERMAL DIFFUSION FACTOR $\alpha$

The thermal diffusion factor $\alpha$ is given by the well known relation: [12]

$$\alpha = \frac{d\ln Q_s}{d\ln \dfrac{T_c}{T_h}} \tag{I-34}$$

where $Q_s$ is the separation factor and is given by:

$$Q_s = \frac{\left[ \dfrac{n_{Kr}}{n_{Kr} + n_{H_2}} \right]_{T_h}}{\left[ \dfrac{n_{H_2}}{n_{Kr} + n_{H_2}} \right]_{T_h}} \Bigg/ \frac{\left[ \dfrac{n_{Kr}}{n_{Kr} + n_{H_2}} \right]_{T_c}}{\left[ \dfrac{n_{H_2}}{n_{Kr} + n_{H_2}} \right]_{T_c}} = \frac{\left[ \dfrac{n_{Kr}}{n_{H_2}} \right]_{T_h}}{\left[ \dfrac{n_{Kr}}{n_{H_2}} \right]_{T_h}}$$

where n denotes the number density.

Our activities are always measured at the top reservoir, at the same pressure and the same temperature. We can say that $\left[ n_{H_2} \right]_{T_c}$ is the as $\left[ n_{H_2} \right]_{T_h}$ since the $^{85}Kr$ concentration is approximately zero.

The above formula reduces to:

$$Q_s = \frac{\left[ n_{Kr} \right]_{T_h}}{\left[ n_{Kr} \right]_{T_c}} \qquad (I-36)$$

But since the specific activity is proportional to the number density, the above relation becomes:

$$Q_s = \frac{(A)_{T_h}}{(A)_{T_c}} = \frac{\text{activity of the hot or top reservoir}}{\text{activity of the cold or bottom reservoir}} =$$

$$= \frac{\text{number of counts/minute in the top reservoir}}{\text{number of counts/minute in the bottom reservoir}} = \frac{n_h}{n_c} \qquad (I-37)$$

This number of counts has to be corrected for the dead time [18] of the counter $\tau$ , using the formula:

$$R_r = \frac{R_o}{1 - R_o \tau}$$

where $R_r$ and $R_o$ are respectively the real and observed number of counts and $\tau$ is the dead time. Then the above formula for $Q_s$ becomes:

$$Q_s = \frac{\left[ \dfrac{R_o}{1 - R_o \tau} \right]_{T_h}}{\left[ \dfrac{R'_o}{1 - R'_o \tau} \right]_{T_c}} \qquad (I-38)$$

where $R_o$ and $R'_o$ stand for $n_c$ and $n_h$.

Once $Q_s$ has been determined, $\alpha$ can be obtained as the slope of the tangent at the required temperature from the graph of $\ln\frac{T_c}{T_h}$ against $\ln Q_s$ . A refined method for drawing the tangent will be discussed later.

22

LIST OF REFERENCES IN CHAPTER I.

1. Harrison, G.E.,
   Proc. Roy. Soc., A 161, 80 (1937) and
   Proc. Roy. Soc., A 181, 93 (1942)

2. Lonsdale, H.K. and Mason, E.A.,
   J. Chem. Phys., 61, 1544 (1957)
   Mason, E.A.,
   J. Chem. Phys., 27, 782 (1957)

3. Grew, K.E. and Mundy, J.N.,
   The Physics of Fluids, 4, 1325 (1961)

4. Heymann, D. and Kistemaker, J.,
   Physica, 25, 556 (1959).

5. Arnold, J.R. and Libby, W.F.,
   Scienne, 110, 678 (1949).

6. Vries, A.E. de, Haring, A. and Slots, W.,
   Physica, 22, 247 (1956).

7. Dickel, G.,
   Proc. of the Symposium on Isotope Separation, Amsterdam (1957).
   Clusius, K. and Dickel, G.,
   Naturwissenschaften, 26, 546 (1938) and
   Naturwissenschaften, 28, 148 (1940).

8. Heymann, D.,
   Thesis, Amsterdam (1958).

9. Schirdewahn, J., Klemn, A. and Waldmann, L.,
   Z. Naturforsch., 16a, 133 (1961).

10. Hirschfelder, J.O., Curtiss, C.F. and Bird, R.B.,
    Molecular theory of gases and liquids,
    John Wiley & Sons, Inc., New York (1954).

11. Chapman, S. and Cowling, T.G.,
    Mathematical theory of non-uniform gases,
    Cambridge University Press (1952).

12. Grew, K.E. and Ibbs, T.L.
    Thermal diffusion in gases,
    Cambridge University Press (1952).

13. Cohen, E.G.D.,
    Institute for Theoretical Physics, Amsterdam,
    Commission I and II, Louvain (1956).

14. Boer, J. de and Kranendonk, J. van
    Physica, 14, 442 (1948).

15. Heymann, D.,
    Reprint from Second United Nations Geneva Conference.

16. Cohen, E.G.D., Offerhaus, M.J. Leeuwen, J.M.L. van,
    Roos, B.W. and Boer, J. de,
    Physica, 22, 791 (1956).

17. Boer, J. de,
    Thesis, Amsterdam (1940)

18. Friedlander, G. and Kennedy, J.W.,
    Introduction to radiochemistry,
    John Wiley & Sons, New York (1949).

## LIST OF SYMBOLS USED IN CHAPTER I

$A$, $B$, $C$, $E$, $S_1$, $Q_1$, $Q_2$ and $Q_{12}$ are numbers involved in the equation of the thermal diffusion factor

| | |
|---|---|
| $A^*$, $B^*$, $C^*$ | reduced values of the above constants |
| $A_{T_c}$ | activity in the cold reservoir |
| $A_{T_h}$ | activity in the hot reservoir |
| $b$ | collison parameter |
| $\overline{c}$ | molecular velocity |
| $f(\overline{c}, \overline{r}, t)$ | distribution function |
| $\overline{F}$ | external forces per unit mass |
| $G$ | statistical weight of a particle |
| $i, j$ | molecular species |
| $k$ | Boltzmann constant $1.38 \times 10^{-16}$ erg/degree |
| $\overline{k}$ | unit vector |
| $m_1$, $m_2$ | masses of the particles |
| $m_o$ | $m_1 + m_2$ |
| $M_1$ | $\dfrac{m_1}{m_1 + m_2}$ $\qquad M_2 = \dfrac{m_2}{m_1 + m_2}$ |
| $n$ | number of particles per c.c. |
| $n_c$ $n_h$ | number of particles in the cold and hot reservoirs per c.c. respectively |
| $Q_s$ | separation factor of the stationary state |
| $R_o$, $R_r$ | observed and real activities respectively |
| $r_m$ | distance of the minimum of the Lennard-Jones potential field |
| $\overline{r}$ | distance between two colliding particles |
| $s$ | a function involved in the thermal diffusion factor |
| $T$ | temperature in $^\circ K$ |

| | |
|---|---|
| $T_c$, $T_h$ | temperature of the cold or lower reservoir and that of the hot or top reservoir |
| $T^*$ | reduced temperature in $^\circ K$ |
| $Y$, $1 - Y$ | mole fractions of components |
| $\alpha$ | thermal diffusion factor |
| $\alpha(g_{ij}, \varkappa)$ | probability of finding a particle within a solid angle $d\omega$ |
| $\epsilon$ | potential energy of the minimum in the Lennard-Jones model |
| $\eta$ | viscosity |
| $\upsilon$ | factor depending on the statistics used |
| $\varkappa$ | angle of deflection of two colliding particles |
| $\mu$ | reduced mass, equals $\dfrac{m_1 m_2}{m_1 + m_2}$ |
| $\sigma$ | particle diameter |
| $\Phi(r)$ | potential field between two particles |
| $\Omega$ | collision integral |

# CHAPTER II

## DESCRIPTION OF THE EXPERIMENT

### PAR. 1. INTRODUCTION

The purpose of this work is to study the thermal diffusion factor for mixtures of gases in temperature regions where the classical theory can be applied, as well as in the low temperature regions where quantum deviations become important. In order to do such research we have to answer the following questions experimentally:

a. What is the order of magnitude of the deviations? Are they actually of the same order as it is predicted by the quantum theory for transport phenomena?

b. Are the discrepancies from the classical calculations in qualitative agreement with the quantum calculations for transport phenomena? Moreover, are the experimental results in quantitative agreement with the quantum calculations?

c. If these discrepancies really exist, can the quantum theory account for them by choosing a specified interaction potential - from the large number of potential models available - and what is the best potential model that will either account for or minimize these discrepancies? As a special case we have to investigate the Lennard-Jones model - which is valid at high temperatures - also on its validity at low temperatures and what are the force constants for this model?

Two apparatuses have been built for measuring the elementary thermal diffusion effect, using the two bulb techniques. In the first one $^{85}$Kr was used as a tracer gas in the carrier gases $H_2$, He and Ne and a GM-counter was used as a detector for measurement. In the second one tritium has been used as a tracer gas and an ionization chamber for the measurement.

It was found from our experimental results that quantum effects are appreciable and that they are nearly of the order as predicted by theory.

Unfortunately, few actual precise calculations have been done quantum mechanically in low temperature regions for transport phenomena. This is due the fact that these calculations are long and tedious. So we have only a rough comparison with our experimental results.

Comparing experimental and theoretical results we notice that the detection of discrepancies is not possible on our early experiment, because the exact quantum curve for the thermal diffusion phenomena is not available, while the comparison with an interpolated quantum curve is not reliable. In our later experiments using tritium as a tracer - for much lower temperatures - this might be possible, however.

Even if exact quantum calculations - for the thermal diffusion phenomena - are available, such a comparison is not possible in the earlier experiment, as this experiment is not accurate enough due to several factors affecting the result, which will be discussed later. Nevertheless in our later experiment - using more refined techniques for measurement - this may be possible.

But the new technique, used in the earlier measurements, has given us an insight in the way of attacking the problem, which has lead to the refined method in our later experiment.

26

At any rate our earlier experiment has shown clearly that the classical calculations for the transport phenomena are not reliable at low tempe - ratures. It may also be that this region - the low temperature region - may decide which of the molecular models is the best and more realistic for the whole range of temperature, whether high or low.

## A) THE KRYPTON APPARATUS :
## PAR. 2. THE TWO BULB DEVICE :

The two bulb apparatus consists of top and bottom reservoirs connected by a tube.

The top reservoir in the first apparatus is made of Pyrex glass. It has a circular opening covered with an aluminium foil 0.06 mm thick, which has an absorbing thickness for $\beta$ - particles of about 16 mg/cm$^2$. This opening is used as a counting window for the counter. This aluminium foil was adhered to the glass by means of warm setting Araldite resin, by heating the whole apparatus in an oven at 130 °C for 24 hours, which is the required period for adhering. A cylindrical glass tube fixed to the circular opening and having the same diameter as the counter - as shown in figure II-1 - is used for adjusting the position of the counter. The top reservoir is surrounded by another glass cylinder to form a cooling jacket. Through this jacket water is allowed to pass from a thermostat, thus keeping the top reservoir at a fixed temperature of about 30 °C. The fluctuations in this temperature will never exceed 0.06 °C. The total volume of this reservoir, with the connecting tubes till the valves, has been determined with water, which was introduced from a calibrated burette at 18 °C. This volume was found to be 14.4 ± 0.1 c.c.

We must notice that during the evacuation of the apparatus, the aluminium foil was bent inside the apparatus. This gives a slight deviation from the measured volume for the top reservoir, which was, however, of the or- der of magnitude of the inaccurancy in the total volume.

The top reservoir has three valves : "a", "b" and "c". "a" is used for pumping the complete apparatus, when "b" is also open; or, for pumping the top reservoir alone, when "b" and "c" are both closed. "b" is used for connecting the top and bottom reservoirs and allowing for thermal diffusion between them, when "c" is closed. "c" is used for filling the upper reservoir from the bottom one. It is also used for taking samples from the bottom reservoir.

The connecting tube between the top and bottom reservoirs is made from stainless steel. It is connected to the top glass reservoir by means of a Kovar joint, and with the bottom copper reservoir through cadmium silver solder.

The cylindrical bottom reservoir consists of Cu and is 20 cm long and has an internal diameter of 5.95 cm. The thickness of the copper wall is 0.1 mm. A stainless steel capillary tube - reaching the centre of the bottom reservoir - is joint to the upper reservoir through the tap "c". The inner diameter of this tube is chosen in such a way that no fractiona- tion takes place, when the upper reservoir is filled from the bottom one. The diameter has to be 2 mm for that purpose.

The lower part of this copper cylinder is used as a gas thermometer. Its length is 4.5 cm and its volume is 125.06 c.c. The bottom of this volume is connected to the rest of the gas thermometer, at room tempe-
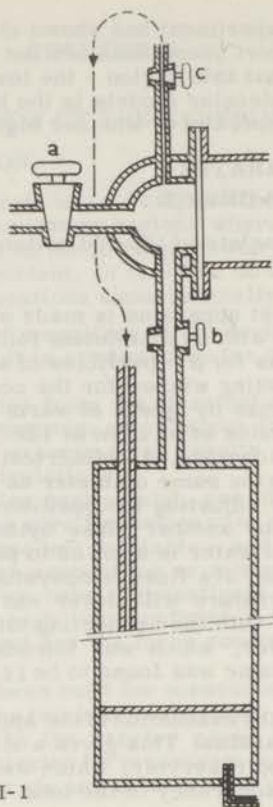
Fig. II-1

Schematic drawing of the two bulb apparatus. The upper part of the apparatus is made of Pyrex glass and the lower part of copper. Valve "a" is used for evacuating the top reservoir alone when "b" and "c" are closed, or the whole apparatus when "b" is open. Valve "c" is used for taking samples from the bottom reservoir to the top.

rature, by a stainless steel capillary of 0.5 mm internal diameter. The dead volume due to this capillary is less than 0.6 c.c.

Both the bottom reservoir and the gas thermometer cylinder are grooved on the outer side with a pitch of about 3 cm. These grooves serve for the winding of a heating element.

## PAR. 3. THE HEATING ELEMENTS AND THE CRYOSTAT

Two heating elements have been used in our first apparatus. The first is used for heating the copper bottom reservoir and the copper cylinder of the gas thermometer. The heating element consist of an insulated constantan wire of 0.15 diameter. The wire is further insulated by pushing it through a glass insulating tape of 0.2 mm inner diameter. This heating

28

element is doubly wound along the grooves of the copper cylinders from
the top to the bottom. The two terminals pass through the cap of the
cryostat. This is done to avoid heat conduction to the reservoir from the
cap of the cryostat.

The other heater is situated at the bottom of the cryostat and is used for
evaporating the liquid. The total resistance of this heater is about 50 $\Omega$
(See fig. II-2).

The cryostat is a large dewar vessel of Pyrex glass about 80 cm long,
10 cm outer diameter and 7.5 cm inner diameter. At the top of the
cryostat is a cap of germanium silver having several holes for the heating
terminals. A long nickel tube of 3 mm inner diameter and of the same
length as the cryostat is also fixed in the cap and is used for filling the
cryostat with the cooling liquids. Through this cap also passes the con-
necting tube of the two bulb thermal diffusion apparatus.

## PAR. 4. THE GAS THERMOMETER

The gas thermometer consists of the copper reservoir and the capillary
mentioned above in par. 3 and the regulating device. From fig. II-2 we
see that this device consists of a glass bulb "e" fitted with two valves
"f" and "g". Joined to this bulb there is also a "U" tube, on the other arm
of which are fixed two photocells. A direct reading open mercury mano-
meter is joined to the bulb through "f". By opening "f" and "h" the gas
thermometer can be pumped high vacuum. "g" is used for filling the gas
thermometer from the helium cylinder.
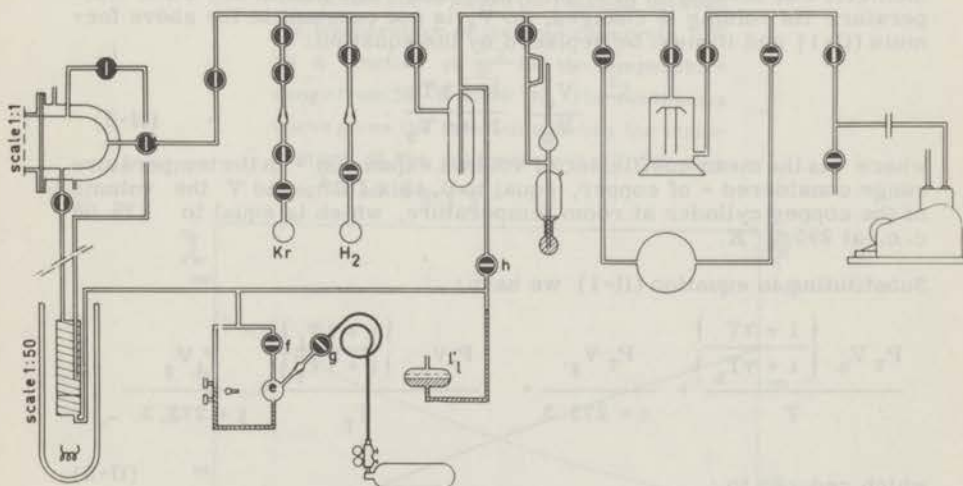


Fig. II-2

Schematic drawing of the whole apparatus.
From the drawing we see the lower part of
the two bulb apparatus fitted in the cryostat
together with the two heating elements for
temperature regulation. At right of the
cryostat we see the regulating device of the
gas thermometer together with the direct
reading manometer.

29

The gas thermometer is the device for measuring and regulating the temperature of the bottom reservoir of the thermal diffusion apparatus.

To get the best results from the gas thermometer, first the cryostat is filled with the cooling liquid - e.g. liquid air or liquid hydrogen - so that the bottom reservoir is cooled by the liquid. Then after a reasonable time, helium gas from the cylinder is introduced via the valves "g" and "f" into the gas thermometer at a continuous slow rate to the required filling pressure $P_f$. The tap "g" is closed. Now, by evaporating the cooling liquid till its level is a few centimeters below the copper cylinder the temperature of the bottom reservoir begins to rise. Accordingly the pressure rises until it reaches the required value, then the stop cock "f" is closed. Let the new pressure be $P_T$. Then, since the number of helium atoms inside the gas thermometer does not change and applying the gas equation:

$$PV = nkT$$

we get:

$$\frac{P_T V_c}{T} + \frac{P_T V_g}{t + 273.3} = \frac{P_f V_c}{T} + \frac{P_f V_g}{t + 273.3} \qquad (II-1)$$

where k is the Boltzmann constant; $P_T$ the pressure at the required low temperature T; t the room temperature in $^\circ$C; $V_c$ and $V_g$ the volumes of the copper cylinder and the glass bulb "e" respectively; $T_f$ and $P_f$ the temperature of the copper cylinder and the pressure at the time of filling.

We must notice that the volume of the copper cylinder of the gas thermometer was measured at room temperature and that at any other temperature its volume is changed. So $V_c$ is not constant in the above formula (II-1) and it must be replaced by the equation:

$$\frac{V_c}{V_h} = \frac{1 + \gamma T}{1 + \gamma T_h} \qquad (II-2)$$

where $\gamma$ is the mean coefficient of volume expansion - in the temperature range considered - of copper, equal to $0.48 \times 10^{-4}$, and V the volume of the copper cylinder at room temperature, which is equal to 125.06 c.c. at 295.3 $^\circ$K.

Substituting in equation (II-1) we have:

$$\frac{P_T V_h \left\{ \dfrac{1 + \gamma T}{1 + \gamma T_h} \right\}}{T} + \frac{P_T V_g}{t + 273.3} = \frac{P_f V_h \left\{ \dfrac{1 + \gamma T_f}{1 + \gamma T_h} \right\}}{T_f} + \frac{P_f V_g}{t + 273.3}$$

$$\qquad (II-3)$$

which reduces to:

$$P_T \left[ \frac{123.311\ (1 + 0.48 \times 10^{-4} T)}{T} + 0.256 \right] = 1.803\ P_f \qquad (II-4)$$

and

$$P_T \left[ \frac{123.311\ (1 + 0.48 \times 10^{-4} T)}{T} + 0.256 \right] = 6.428\ P_f \qquad (II-5)$$

30

for the liquid air filling ($T_f = 80\ ^oK$) and for the liquid hydrogen filling ($T_f = 20.3\ ^oK$) respectively.

By plotting graphs of $\frac{P_T}{P_f}$ against T - using table II-1 - for both equations (II-4) and (II-5) as in fig. II-3, 4 the temperature T is readily known from the measured value of the pressure $P_T$.
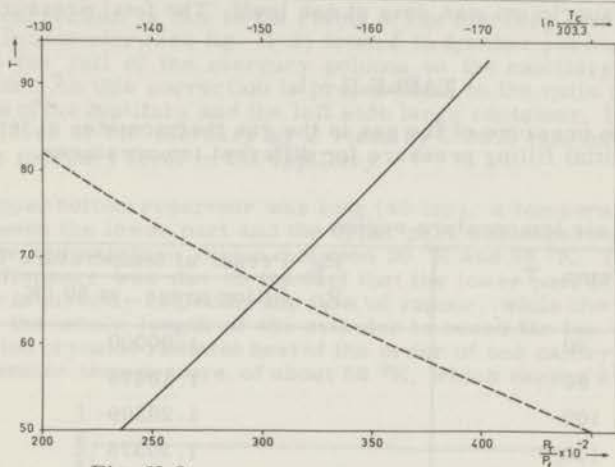


Fig. II-3.

The dotted curve shows the relation between the temperature of the cold reservoir $T\ ^oK$ as a function of $\frac{P_T}{P_f}$ for the temperature range from 50 $^oK$ to 90 $^oK$. The continuous curve gives the relation between the temperature of the cold reservoir $T\ ^oK$ as a function of $\ln \frac{T_c}{303.3}$.
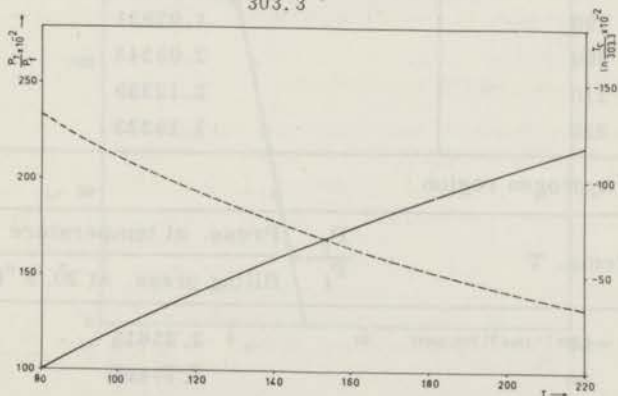


Fig. II-4.

The dotted curve shows the relation between the temperature of the cold reservoit $T\ ^oK$ as a function of $\frac{P_T}{P_f}$ for the temperature range from 80 $^oK$ to 220 $^oK$. The continuous curve gives the relation between the temperature of the cold reservoir $T\ ^oK$ as a function of $\ln \frac{T_c}{303.3}$.

31

The pressures $P_T$ and $P_f$ must be corrected. Everytime an experiment is performed, the atmospheric pressure was asked from the Koninklijk Nederlands Meteorologisch Instituut (K.N.M.I.) by telephone. This pressure is always given at 0 °C and sea level. This pressure must be corrected for the temperature and the height. These corrections are respectively 0.123 mm Hg per decree centrigrade and −0.09 mm - Hg per meter height above sea level. We took no correction for the height since our experiment was done at sea level. The total pressure is given by :

## TABLE II - 1.

Ratio of the pressure of the gas in the gas thermometer at temperature T to the initial filling pressure for different temperatures.

For liquid air temperature region :

| Temp. T. | $\dfrac{P_T}{P_f} = \dfrac{\text{Press. at temperature T}}{\text{filling press. at 80 °K}}$ |
|:---:|:---:|
| 80 | 1.00000 |
| 90 | 1.10475 |
| 100 | 1.20599 |
| 110 | 1.30376 |
| 120 | 1.39820 |
| 130 | 1.48951 |
| 140 | 1.57782 |
| 150 | 1.66329 |
| 160 | 1.74606 |
| 170 | 1.82624 |
| 180 | 1.90394 |
| 190 | 1.97931 |
| 200 | 2.05243 |
| 210 | 2.12339 |
| 220 | 2.19323 |

For liquid hydrogen region :

| Temp. T | $\dfrac{P_T}{P_f} = \dfrac{\text{Press. at temperature T}}{\text{filling press. at 20.3 °K}}$ |
|:---:|:---:|
| 50 | 2.35619 |
| 60 | 2.77415 |
| 70 | 3.17667 |
| 80 | 3.56457 |
| 90 | 3.93862 |

$$P_o + 0.123\,t \quad \text{mm-Hg} \tag{II-6}$$

where $P_o$ is the atmospheric pressure at sea level and $0\ ^\circ C$.

By this way our zero shift can be determined. It was found to be of the order of 1 mm.

Another correction is due to the rising of the mercury level in the left leg of the manometer (see fig. II-2) from $\ell$ to another position $\ell^1$. This is due to the fall of the mercury column on the capillary side of the manometer. As this correction is proportional to the ratio of the inner diameters of the capillary and the left side large container, it was found that the level of the mercury at $\ell$ rises by 0.0025 mm for every mm fall of the mercury level in the capillary.

As our copper bottom reservoir was long (40 cm), a temperature difference between the lower part and the upper part was observed in the intermediate temperature region between 20 $^\circ K$ and 80 $^\circ K$. This temperature difference was due to the fact that the lower part of the bottom reservoir is directly cooled by the flow of vapour, while the vapour has to travel the whole length of the cylinder to reach the top. Moreover, the cap of the cryostat radiates heat of the order of one calory per second at a reservoir temperature of about 80 $^\circ K$, which causes a heat influx
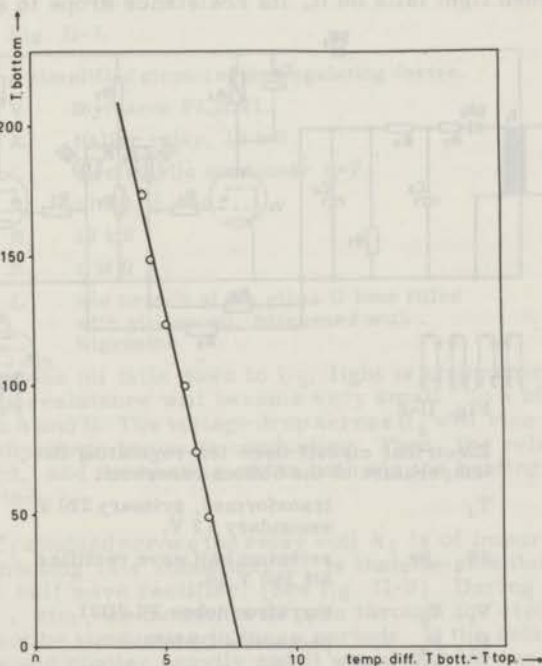


Fig. II-5.

Experimental curve showing the temperature drop along the bottom reservoir at different regulating temperatures. The curve gives the relation between the lower part of the bottom reservoir as a function for the difference in temperature between the lower and upper parts of the bottom reservoir.

on top of the copper reservoir. We were forced to make our bottom reservoir so large due to the fact that we take samples from this reservoir, which would cause pressure changes and disturb our equilibrium.

The temperature difference over the length of the reservoir was measured by means of an iron constantan thermocouple and a Kipp. A 70 galvanometer. This thermocouple was calibrated. The temperature difference between the lower part and the upper part of the cylinder is about 6 $^{\circ}$K. A calibration curve of this temperature difference against the temperature of the lower part of the copper cylinder was drawn, which is approximately a straight line as shown in fig. II-5. The accuracy of these gas thermometer readings is about half a degree Kelvin.

## PAR. 5. TEMPERATURE REGULATION OF THE BATH.

The complete electrical circuit used for regulating the temperature of the gas thermometer is shown in fig. II-6. To understand the working of the circuit, the simplified circuit in fig. II-7 will be discussed.

The photocell ORP60 is a very sensitive cadmium sulphide photocell. The sensitive part lies between the two plates "a" and "b". It has an allowable dissipating power of 100 mW. and a maximum voltage of 100 V. When no light falls on this cell, it has a very high resistance of several M$\Omega$. But when light falls on it, its resistance drops to a few ohms.
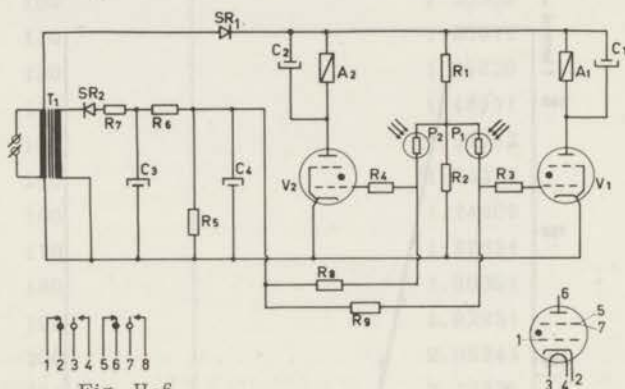


Fig. II-6

Electrical circuit used for regulating the temperature of the bottom reservoir.

| | |
|---|---|
| $T_1$ | transformer, primary 220 V secondary 12 V. |
| $SR_1$, $Sr_2$ | selenium half wave rectifier SR 250 Y 50. |
| $V_1$, $V_2$ | thyratron tubes PL2D21. |
| $P_1$, $P_2$ | photocells ORP60. |
| $R_1$, $R_2$, $R_3$, $R_4$, $R_5$, $R_6$, $R_7$, $R_8$, $R_9$ | resistances of 47 k$\Omega$, 10 k$\Omega$ 1 M$\Omega$, 1 M$\Omega$, 10 k$\Omega$, 1 k$\Omega$ 220 k$\Omega$, 100 k$\Omega$ and 100 k$\Omega$ respectively. |
| $C_1$, $C_2$, $C_3$, $C_4$ | capacitances of 1 $\mu$F, 1 $\mu$F, 100 $\mu$F and 100 $\mu$F respectively |
| $A_1$, $A_2$ | Haller relays, 10 k$\Omega$ |

34

When the level of the oil rises to $L_1$, no light passes through the photo-cell and its resistance is very high. So, the current passes through the potential divider $R_1 R_2 R_3$ and the voltage drop across the points A and B is practically equal to the voltage drop across $R_3$ as $R_2 \ll R_3$, which is far below the cutt off voltage of the thyratron PL2D21.

Hence, no current through the thyratron will pass and the relay contacts of $A_1$ will remain open.
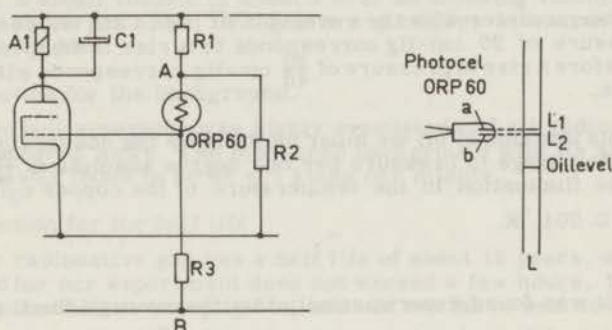


Fig. II-7.

A simplified circuit of the regulating device.

V       thyratron PL2D21.

$A_1$    Haller relay, 10 k $\Omega$

$C_1$    electrolytic condenser 1 $\mu$F

$R_1$    47 k$\Omega$, $\frac{1}{2}$ watt.

$R_2$    10 k $\Omega$

$R_3$    1 M $\Omega$

L       one branch of the glass U tube filled with silicon oil, blackened with Nigrosine

When the level of the oil falls down to $L_2$, light is communicated to the photocell, and its resistance will become very small. So a high current will pass through A and B. The voltage drop across $R_3$ will rise sufficient-ly so that the thyratron becomes conducting. Then, the relay contacts of $A_1$ are closed, and the heating of the bath via the heating coil in the cryostat is started.

The condenser $C_1$ shunted across the relay coil $A_1$ is of importance. The reason for connecting this condenser $C_1$ is that the selenium rectifier SR 250Y50 is a half wave rectifier. (See fig. II-8). During the periods bc, de, ........ etc. , no current will pass through the circuit and the thyratron will not be conducting in these periods. If the relay is closed nominally, it would chatter heavily and it would disturb the regulation. But by inserting the condenser $C_1$ in the circuit, then during the period ab, the thyratron is conducting and the condenser is charged. Hence, during the period be the condenser discharges through $A_1$ and keeps it closed.

By this method of regulation a change of oil level in the tube L of less than 0.3 mm was observable with a filling pressure of 50 cm-Hg helium
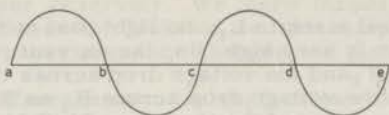
Fig. II-8

Wave form at the input of selenium half wave
rectifier SR 250Y50.

gas in the thermometer with the reservoir at liquid air temperature; a
rise of pressure of 20 cm-Hg corresponds to a rise in temperature of
40 °K. Therefore a rise in pressure of $\frac{20}{40}$ cm-Hg corresponds with a rise
of one degree.

To convert this into cms of oil we must multiply by the conversion factor
15. Thus, the change in pressure per one degree absolute is $\frac{20}{40}$. 15 cm
oil. Thus the fluctuation in the temperature of the copper cylinder is
$\frac{0.03}{\frac{20}{40} \times 15}$ = 0.004 °K.

In this way it was found experimentally that the average fluctuations in
the temperature of the bottom reservoir are 0.006 °K in the temperature
region between 80 and 210 °K and 0.002 °K in the region between liquid
hydrogen and liquid air.

We must notice that, although our regulation of the temperature is of
this accuracy, our measurement of the temperature was not of the same
precision. The reading accuracy of the mercury manometer was only
half a mm-Hg, corresponding to an uncertainty in temperature of about
0.5 °K.

It was found experimentally that, whether the photocell was at a small
distance from the wall of the glass tube L or just touched it, it was always
conducting. This was due to the fact that the glass wall of the tube L work-
ed as a condensor lens; even though the outer wall of the glass tube was
blackened and only a small aperture for the light was used.

To avoid this we made a hole in the glass tube L of the same diameter as
the photocell. The photocell was inserted in this hole and fixed with
kaoline and sodiumsilicate.

The photocell worked then in a magnificient way. No leak was detected
in the gas thermometer.

It is a difficult process to colour oils. Only fews substances can do this .
As our photocell is sensitive to red light, we must colour the silicon oil
dim black. This can be accomplished by Nigrozin, which works in a satis-
factory manner.

PAR. 6.  THE COUNTING METHOD

The evacuation of the apparatus and the introduction of the gas samples
are done in the usual way. When introducing the radioactive substance,
the Geiger-Muller counter is coupled to a counting rate meter. The radio-
active gas is introduced in small doses until the required activity is ob-

36

tained. The other gas is forced into the apparatus through a capillary
until we obtain the required pressure. The apparatus containing the mix-
ture is left over night so that mixing occurs.
The radioactive $^{85}$Kr originates from the fission process of uranium and
is obtained as Kr gas from A. E. R. E. in Harwell (England).

According to the specifications it contains 5% radioactive $^{85}$Kr. It is
supplied in a small glass bulb of about 5 c. c. at N. T. P. This bulb was
connected to a flask of about one litre fitted at the top with two stop cocks
enclosing a small volume of about 3 c. c. as a dozing volume for intro-
ducing the active gas. The $^{85}$Kr gas is a $\beta$ emitter with a particle energy
of about 0. 78 Mev.

a. Correction for the background.

The two bulb apparatus was highly evacuated and all radioactive gases
are removed away. The measured background with its standard de-
viation was found to be $69 \pm 5$ kicks per minute.

b. Correction for the half life

As our radioactive gas has a half life of about 10 years, and the time
needed for our experiment does not exceed a few hours, the correct-
ion for the half life is negligible, and was not taken into consideration.

c. Correction for the dead time of the counter

The dead time $\tau$ of the counter was measured using the two sample
method. [1] The following formula was used for the calculation of $\tau$

$$\tau = \frac{\bar{R}_A + \bar{R}_B - \bar{R}_{A+B} - \bar{R}_b}{\bar{R}_{A+B}^2 - \bar{R}_A^2 - \bar{R}_B^2}$$

where $R_A$ and $R_B$ are the activities of samples A alone and B alone
and $R_{A+B}$ is the activity of the two samples when combined together.
$R_b$ is the background.
The result obtained from our measurement was compared with that
from the graph of the manufacturer. Good agreement was found, The
accepted value of the dead time is taken as 200 micro-seconds.

This dead time introduces in our experiment an uncertainty of about
3%. So we think that this method must be rejected if we want to
measure small discrepancies from an accurately calculated quantum
curve.

d. Mutual interaction of the reservoirs

The activity of the Kr gas at our working pressures is only due to the
first few cms behind the counting window. We wanted to be sure, how-
ever, that no interaction of bottom reservoir activities with the top
reservoir activity took place. An experiment was done by evacuating
the top reservoir, whereas the bottom reservoir was filled with the
radioactive gas mixture. We tried to detect a change in the background.
No effect of this kind was observed, which shows that such interaction
does not exists.

e. Absorption of the activity in the gas.

In order to measure the absorption of the $\beta$ particles by the gas mole-

37

cules, a certain amount of activity was introduced in the top reservoir. The other gas was pushed in the top reservoir through the capillary to different pressures varying from 2 mm to about 50 mm. No change in the activity was observed. So we can conclude safely that, up to 50 mm-Hg pressure, no correction for absorption is needed.

f. Fractionation effect.

By transferring a sample of gas through a capillary (See fig. II-1) from the bottom to the top reservoir, fractionation takes place.
In order to study this fractionation process, the following apparatus was used. (See fig. II-9 ).
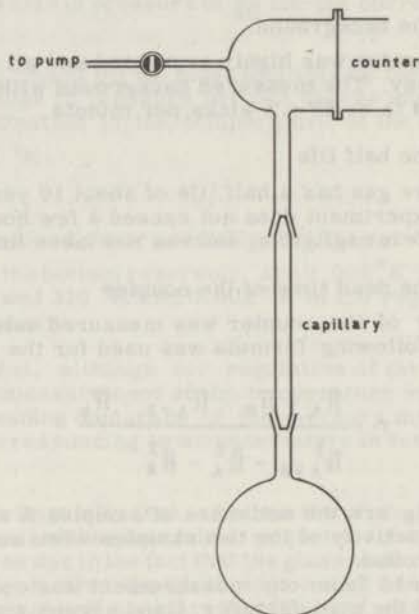


Fig. II-9

Apparatus used to study the effect of fractionation in a two component gas mixture.

The top reservoir is exactly the same as mentioned before, and the bottom reservoir is a glass flask of one litre capacity.

The capillary tubes of different lengths and different diameters are connected in two glass joints by means of black wax as shown in fig. II-9.

The bottom glass bulb was filled with $^{85}$Kr as a tracer gas and hydrogen to a pressure of 1 cm-Hg. The activity of $^{85}$Kr was measured first by connecting the two reservoirs via a short wide bore tube.

The top reservoir is pumped high vacuum and gas is expanded from the bottom reservoir to the top one via the capillary.

The activity of the sample was measured every 5 seconds.

A plot of the time against the ratio $\dfrac{\text{instantaneous activity in top}}{\text{real activity in the bottom}}$

$\frac{\text{reservoir}}{\text{reservoir}}$ for different tube lengths and different tube diameters at different pressures has been made.

From these graphs we saw that:

a. Fractionation increases by increasing the length of the tube at fixed diameter and fixed pressure.
b. It decreases by increasing the inner diameter at a fixed length and fixed pressure.
c. It decreases by increasing the pressure at a fixed length and a fixed diameter.

The length of our capillary is determined by the dimensions of the apparatus. At the same time we cannot increase the pressure much beyond 1 cm-Hg, since our relaxation time would become too long introducing experimental difficulties.The only variable left was the diameter of the tube. This was chosen to compromise with the volume of the top reservoir and at the same time to give us a large safety margin against fractionation. We chose a diameter of 2 mm. The volume of the capillary compared with the top reservoir was 5%.
The relaxation time for this capillary was found to be several hours, which means that diffusion via this capillary is negligible in comparison to diffusion via the wide connection (9 mm diameter) between the two reservoirs.

## B. THE SECOND APPARATUS FOR TRITIUM MEASUREMENTS.

## PAR. 7. THE UPPER RESERVOIR.

The upper reservoir is an ionisation chamber which will be treated later. It has a volume of about 3 c.c. and is maintained always at room temperature. This reservoir is supplied with three glass tubes and three valves as in the previous apparatus. The glass tubes are connected to the brass material of the ionisation chamber with araldite.

Design conditions. [2-9]

The design of an ionisation chamber is extremely simple. We can say that nearly any dimension and shape are good, provided that the electric field between the cathode and collector does not exceed the value required to produce ionisation at any point of the chamber. The simplest design that fulfils this requirement is a cylindrical chamber with a centre rod of fairly large diameter.

The most important thing in the design is the insulation of the collector. The limitation to this insulation is not the bulk resistance, since several insulation materials have good bulk insulating properties. To reduce surface conductivity the humidity is kept as low as possible, but nevertheless the main problem is that of stress currents which are not yet completely understood up to date.

Stress currents appear across an insulator after it has received either electrical or mechanical stress. These currents appear to die away with a half life of the order of 15 minutes, while the magnitude of these currents depends on the magnitude and duration of the stress. It is supposed that these stress currents are due to the fact that charges within the insulator are moved from one place to another, when the stress,changes.

To reduce these stress currents to a minimum, we must take the following points into consideration.

1. We must keep the volume of the insulator to a minimum.
2. The contact area between the insulator and the metal should be minimized as much as possible. Also the insulating material should not be sandwiched between metal if that can be avoided.
3. Polysterene and teflon appear to have the same stress currents.
4. As the stresses are mainly produced by evacuation and filling, it is advisable, that these procedures should be done as quickly as possible. It is also advisable that the pumping and filling lines should be long enough to reduce sudden mechanical shocks.
5. Electrical stress of high-ohmic insulators can be diminished by the use of guard-techniques.
6. It is advisable to ground the collector when it is disconnected from the electrometer, in order to obviate charging up.

Constructional details (See fig. II-10)

The main principles which should be followed in the design especially those of guarding as mentioned above under number 5, were taken into consideration in the construction. The brass part "3" is used as the cathode and is maintained at a negative potential of 135 volt. It is highly polished internally to facilitate evacuation to a high vacuum, and at the same time to reduce surface adsorption of the gases. This brass cylinder is approximately closed, except for the insulating teflon piece "5" fixing the collector. The brass ring "6" has been installed, in order to keep the field inside the cylinder as homogeneous as possible. This brass ring is fitted with a teflon ring "10" at the top to keep the cylinder vacuum tight. The brass cylinder has a diameter of 15 mm and a length of 25 mm and a total volume - including the gaps etc. - of 4 c.c.

The collector is a brass rod "4", shaped in such a way that we can fit a standard plug at its end. This rod has a diameter of 2 mm and working length inside the chamber of 2 cm. This rod passes through a teflon insulator "5" shaped in such a way, that, first it prevents the leakage currents from the cathode to the collector by increasing the leakage path; second it can adapt a teflon ring for making the apparatus vacuum tight. On the plug side the collector rod thickens and is kept short to avoid mechanical vibrations.

The teflon insulator "5" is surrounded by an earthed shield "9" joined with the cap and holding another teflon insulating ring, which centers the collector.

An ebonite plate "7" was used as a secondary insulator between the shield "9" and the cathode cylinder. This avoids sandwiching the teflon between brass pieces according to design conditions. Moreover, any leakage current via the ebonite plate "7" will go to earth via the brass cap "9", and so it will never reach the collector.

The bottom reservoir

The bottom reservoir is a Pyrex glass cylinder of 50 mm internal diameter and 60 mm length. At the bottom of this cylinder there are four Kovar tubes for the four leads of the platinum resistance thermometer. This platinum resistance thermometer is a platinum wire wound over a glass holder of 5 mm diameter and 30 mm length. The thermometer is supported in the middle of this reservoir by means of a thin glass stem. The top part of this reservoir holds two glass tubes of about 40 cm length, and with internal diameters of 3 and 1 mm respectively. The narrower tube extends till the middle of the reservoir. Both tubes are joined to the
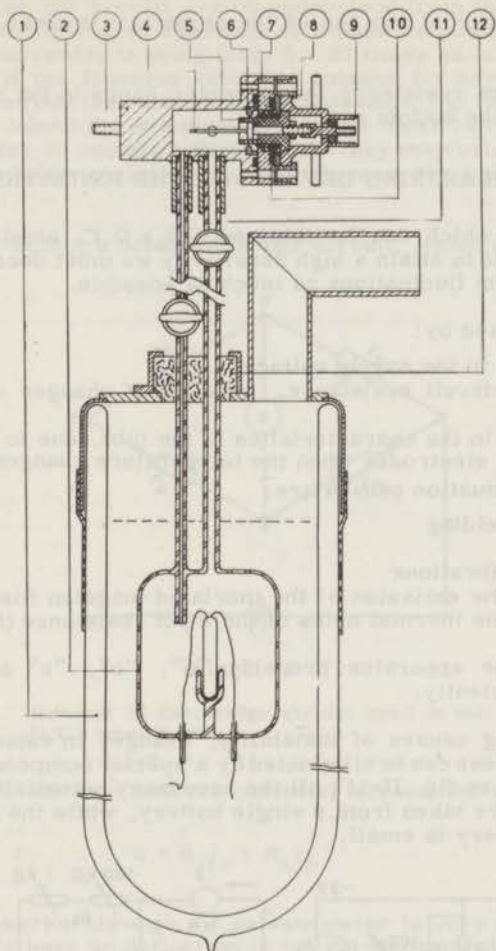
Fig. II-10

The two bulb thermal diffusion second apparatus.

1. cryostat
2. bottom reservoir made of Pyrex glass, inside of which the platinum resistance thermometer is fitted. The leads of the thermometer emerge from Kovar glass joints.
3. the cylindrical part of the ionisation chamber - cathode - made of brass and mirror polished from inside.
4. anode
5. teflon insulator (main insulator)
6. brass ring for maintaining the homogenity of the electrical field inside the ionisation chamber
7. ebonite insulator
8. shield made of brass
9. standard plug with teflon insulation
10. teflon 0-ring for high vacuum
11. glass tube 3 mm internal diameter for thermal diffusion
12. cork

41

ionisation chamber at the top of the cryostat - in small brass tubes - with araldite.

Another platinum resistance thermometer hangs in the cryostat at the same height as the bottom reservoir.

## PAR. 8. THE MEASURING DEVICE FOR THE IONISATION CURRENT.

The sensitivity which can be obtained with a D.C. amplifier, depends on its stability. So to attain a high sensitivity we must decrease the slow drifts and random fluctuations as much as possible.

The drift is caused by:

1. Slow changes in the supply voltages.
2. Changes of circuit resistance, because of changes of the ambient temperature.
3. Slow changes in the characteristics of the tube, due to a geometrical change of the electrodes when the temperature changes.

The random fluctuation causes are:

1. Improper shielding
2. Bad contacts
3. Mechanical vibrations
4. Changes in the emission of the thoriated tungsten filament (Johnson noise), and the thermal noise of the input resistance (Shot effect).

By designing the apparatus properly "a", "b", "c" and "2" can be eliminated sufficiently.

Of the remaining causes of instability, changes in supply voltage are predominant. These can be eliminated by a special compensating circuit. In this circuit (see fig. II-11) all the necessary potentials for the electrometer tube are taken from a single battery, while the current drawn from such a battery is small.
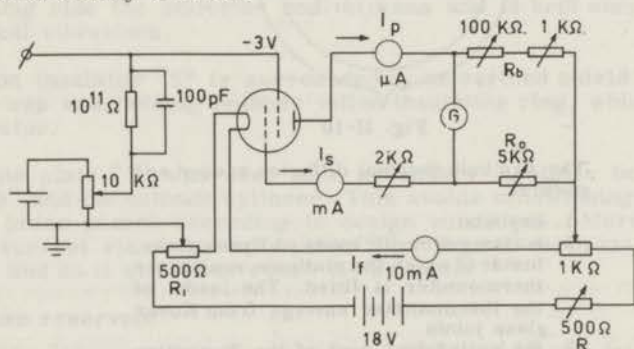


Fig. II-11

The electrical circuit used for measuring the ionisation currents. All resistances except the high ohmic one are wire wound and very stable. The 10 KΩ potentiometer is a high resolution one with a resolution of $\frac{1}{10}$ ohm and a linearity of 0.1%. This potentiometer is shunted across a reference element of 1.5 V. The electrometer tube used is a Philips 4066.
The high ohmic resistance is a Victoreen $10^{11}$ Ω with a tolerance of $\pm$ 10 %.

42

The balancing of the circuit can be understood from the following discussion. As the first grid operates at a positive potential, it collects electrons, the current to it being from 5 - 20 times as large as the plate current. Now if the filament emission changes for any reason, then it would be expected that the currents to the plate and to the first accelerating grid change in about the same ratio. But, as these two currents cross the galvanometer in opposite directions, they may balance each other by choosing suitable resistances. In that case the galvanometer will not be affected.

This circuit is in fact a balanced bridge circuit, which can be drawn as in fig. II-12.
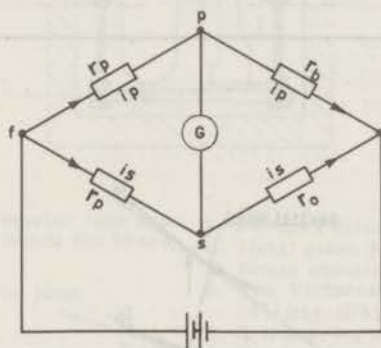


Fig. II-12

Concept of the bridge circuit used in the D.C. amplifier.

From fig. II-11 we see that the potential across the galvanometer is given by:

$$e = R_o I_s - R_{b_1} I_p \qquad (II-7)$$

provided the current through the galvanometer is very small compared to $I_p$ and $I_s$. To have no deflection in the galvanometer e must be zero. Hence,

$$\frac{R_b}{R_o} = \frac{I_p}{I_s} \qquad (II-8)$$

which is the first condition to be satisfied. We must notice that once relation (II-8) is satisfied, then the galvanometer deflection will remain zero, inspite of the fact that there may be small fluctuations in the emission which change $I_p$ and $I_s$ in the same ratio.

Moreover, we have not stabilized the voltage drop "e" across the galvanometer from changes in the battery voltage. As the power supply is common for both the filament current and the electrode voltages, we may consider the supply voltages to be a function of the $I_f$. The condition for stabilisation can be found by differentiating equation (II-7) with respect to the heating current $I_f$. In this case we have:

43

$$\frac{de}{dI_f} = 0 \quad \text{or} \quad \frac{dI_p}{dI_f} = \frac{R_o}{R_b} \cdot \frac{dI_s}{dI_f} \tag{II-9}$$

which is the second condition to be satisfied for neutralisation.

It can be shown that in case that the conditions II-8 and II-9 hold for a fixed value of $R_o/R_b$, the tangent lines of the curves $I_p(I_f)$ and $I_s(I_f)$ intersect in a certain point on the $I_f$ axis. Of course this will not be true in general, but only over a small part of both curves where the required insensitivity (neutralisation) for $I_f$ exists. This condition is illustrated in fig. II-13).
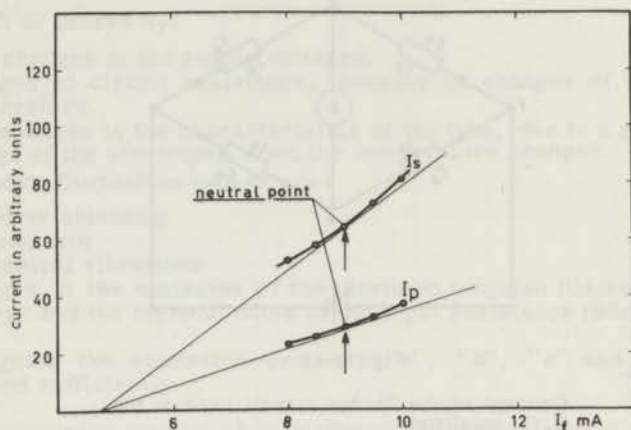
Fig. II-13

Graph showing the relation between the space charge grid current $I_s$ and the plate current $I_p$ as a function of the filament current $I_f$. The slopes of the two tangents at the neutral point meet on the $I_f$ axis. The neutral point was found to be at $\sim 9$ mA.

Constructional details

The D.C. amplifier circuit shown in fig. II-11 has been constructed in the following way.

The input circuit which consists of the high ohmic resistance and the electrometer tube with the bandwidth determining capacitor is all arranged inside a heavy wall brass cylindrical box as shown in fig. II-14. A condenser has been inserted in the circuit in parallel with the high ohmic resistance giving a time constant of about 10 seconds. The measuring part of the D.C. amplifier was built in an aluminium box, which was well earthed. All resistances are wire wound and of good stability.

A separate balancing circuit consisting of a high quality potentiometer, shunted across a reference voltage and opposing the voltage developed by the ionisation current across the input resistor, is inserted in the grid circuit of the electrometer valve.

The galvanometer used is a Kipp. 70, having a sensitivity of $10^{-6}$ V/mm approximately and is introduced between the plate and the accelerating grid.
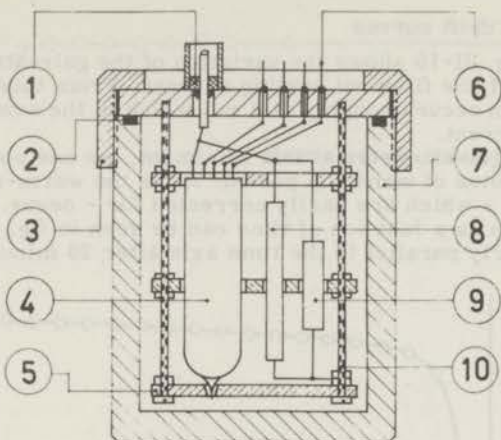
Fig. II-14

Arrangement of the electrometer tube and the high ohmic resistance inside the brass shield.

1. Standard plug with teflon joint
2. Rubber 0-ring
3. Brass cap
4. The Philips electrometer tube no. 4066
5. Perspex discs.
6. Metal glass joints.
7. Brass container
8. The Victoreen high ohmic resistance $10^{11}\Omega$ (± 10%).
9. A trimering condenser of ~ 100 pF.
10. Brass screws.

Adjustment of the circuit

First, all the variable resistances are adjusted to give the necessary voltages and currents for the different electrodes of the electrometer tube. Then the filament current is varied with the aid of the rheostat R (see fig. II-11) to give a parabolic galvanometer deflection as a function of the filament current. If the galvanometer deflects outside the scale, it can be returned back to scale by adjusting $R_b$. Finally with the highest sensitivity of the galvanometer a last adjustment is performed and the galvanometer is returned to zero.
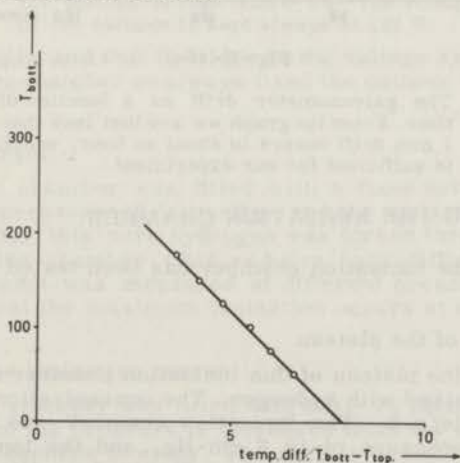


Fig. II-15

The adjustment of the filament current for minimum value of galvanometer deflection. This minimum value is seen to be 9 mA.

45

Adjustment and drift curves

The graph in fig. II-15 shows the variation of the galvanometer current
as a function of the filament heating current. From this graph we see
that the minimum occurs roughly at 9 mA which is the nominal value for
the filament current.
By keeping the galvanometer at this minimum, we see some changes in
the first 20 minutes of warm-up period. After the warm-up period very
minute changes - which are easily corrected for - occur. The galvano-
meter deflection as a function of time can be seen in fig. II-16. We see
that it runs nearly parallel to the time axis after 20 minutes.
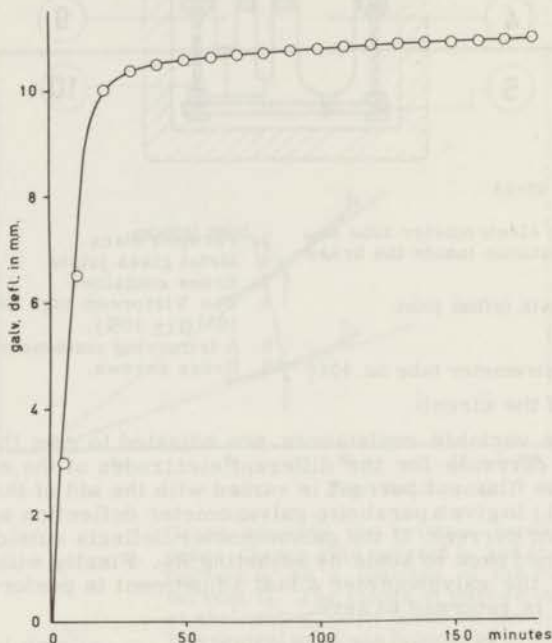


Fig. II-16

The galvanometer drift as a function of
time. From the graph we see that less than
1 mm drift occurs in about an hour, which
is sufficient for our experiment.

PAR. 9.   TESTING THE IONISATION CHAMBER.

The function of the ionisation chamber has been tested in the following
way:

1. Determination of the plateau

    To determine the plateau of this ionisation chamber a known amount
    of tritium is mixed with hydrogen. The concentration of tritium was
    about $10^{-9}$ curie/c.c. The ionisation chamber was filled with this
    mixture to a pressure of 12.6 cm-Hg, and the ionisation current
    measured at varying cathode voltages from a few volts to 1000 volt as
    shown in graph II-17. From the graph we see that the plateau begins

46
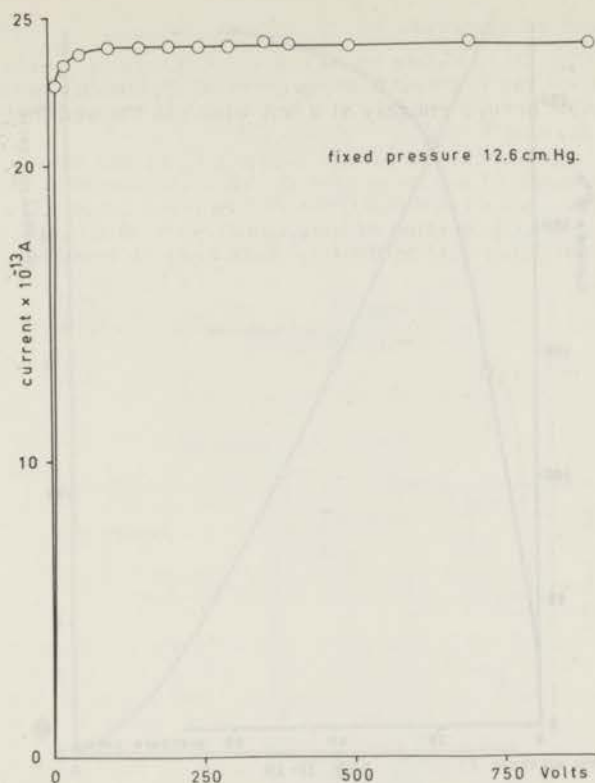
Fig. II-17

Determination of the plateau of the ionisation chamber. From the graph we see that the plateau begins at about 50 V. The slope of the plateau is less than 0.5%. The voltage of the cathode is kept always at 135 V.

at about 50 volts and that its slope to the voltage axis is negligible. In our ionisation chamber we always fixed the cathode voltage at about 130 volts.

2. Saturation current

The ionisation chamber was filled with a fixed activity of a $T_2$-$H_2$ mixture of a pressure of 5 cm-Hg, and the ionisation current was measured. After this pure hydrogen was forced through a capillary to the ionisation chamber (this reduces back diffusion), and the ionisation current was measured at different pressures. From fig. II-18 we see that the maximum ionisation occurs at about 50 cm-Hg.

3. Linearity of the ionisation current.

The ionisation chamber was filled with a $H_2$-$T_2$ mixture to a certain pressure. Then the pressure is increased from the same mixture to about one atmosphere in steps. The results are shown in fig. II-19, from which we see that at pressures below 1 cm the ionisation current is not porportional to the pressure. But above 1 cm-Hg the curve is approximately straight.

47
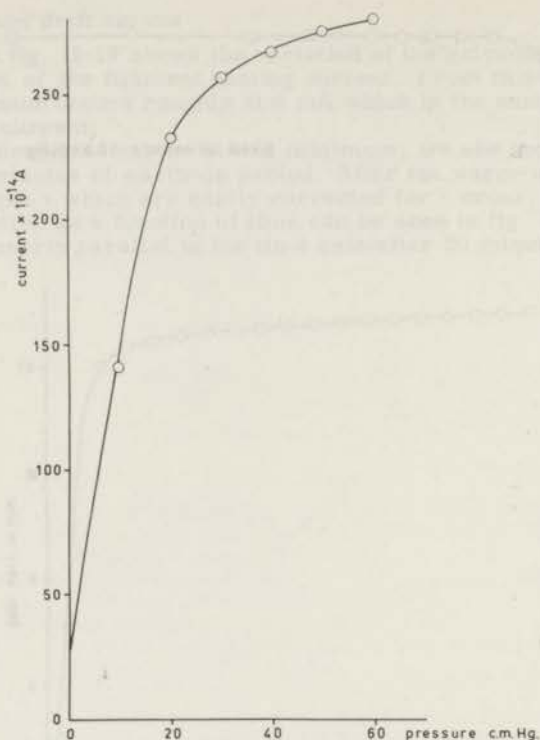
Fig. II-18

Curve showing the ionisation current with
a fixed activity as a function of the pressure
of the pure gas. The gas used was $H_2$. The
increase in the ionisation current for
pressures above 50 cm. Hg is very small.

Other mixtures have been tested, which give approximately the same
results. The reproducibility of the results was extremely good.


PAR. 10.   THE PUMPING SYSTEM. (See fig. II-20).

The cryostat is the same as before. The only change is that the cap of
the cryostat is fitted with a pumping line with two connections. One
connection for the rotary pump via the valves "1" and "2" and the other
to the atmosphere. The needle valve "2" is joined in parallel with "1"
and is used for fine regulation. The regulation is facilitated with the
regulating oil devices "a", "b" and "c". When the manometer "4" reads
the required pressure the tap "b" of the regulating device "3" is closed
and the needle valve "2" is turned clockwise or anticlockwise to maintain
the oil level L in a fixed position.

The manometer "4" is used for the rough measurement of the pressure
and hence the temperature. Moreover, it is used as a safety valve for
the cryostat.

The exact measurement of the temperature is done with the platinum
resistance thermometer.
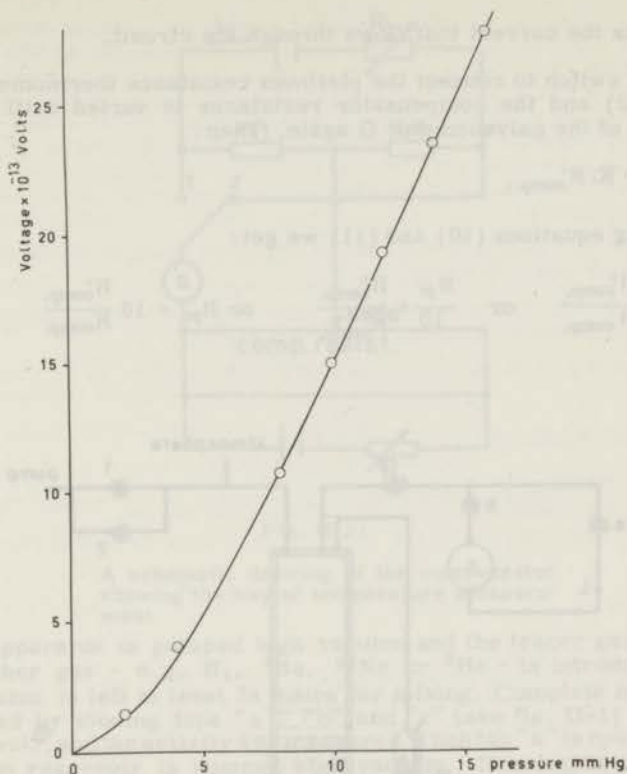
Fig. II-19

Graph showing the linearity of the ionisation current in arbitrary units as a function of pressure. From the graph we see that above about 0.5 cm-Hg the ionisation current is directly proportional to the pressure.

## PAR. 11. TEMPERATURE MEASUREMENT.

The temperature is measured by means of a Diesselhorst compensation bank, which is an instrument of extremely high accuracy. In this instrument changes in the power supply have been prevented by measuring with very small currents. Besides, the instrument has a low internal resistance of only $15\,\Omega$, which makes it suitable to be matched to a high sensitive galvanometer. This galvanometer gives 1 mm deflection on the scale corresponding with approximately $2.4 \times 10^{-7}$ volts. The compensation bank can be read to 5 digits.

In our measurement of the temperature we have not standardised the current, but we have measured relative values. The principle of the measurements is as follows : The compensator resistance is fixed at a certain position. Then the compensation voltage is adjusted with $R_1$ until we get no deflection in the galvanometer. In this case we get : (see fig. II-21).

$$i_x R_{st} = K . R_{comp.}$$  (II-10)

49

where $i_x$ is the current that flows through the circuit.

Next, we switch to connect the platinum resistance thermometer ($R_{pt}$) (position 2) and the compensator resiatance is varied until we get no deflection of the galvanometer G again, Then:

$$i_x R_{pt} = K. R'_{comp.,}.$$  (II-11)

By dividing equations (10) and (11) we get:

$$\frac{R_{pt}}{R_{st,}} = \frac{R'_{comp.}}{R_{comp.}} \quad \text{or} \quad \frac{R_{pt}}{10} = \frac{R'_{comp.}}{R'_{comp.}} \quad \text{or } R_{pt} = 10 \frac{R'_{comp.}}{R_{comp.}} \quad \text{(II-12)}$$
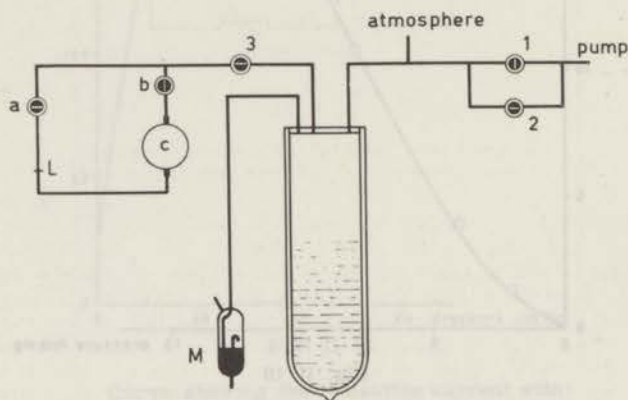


Fig. II-20

Schematic drawing for the pumping system with regulation for adjusting the temperature of the cooling liquid in the cryostat. The valve "2" is a by-pass for regulating the pump speed. The device, "a", "b", "c" and "L", is an oil manometer to facilitate the regulation of the pump speed.

From equation (12) and the calibration table of $R_{pt}$ the temperature of the bath is known.

The temperature was always measured in two ways; inside the bottom reservoir, which means that we measure the temperature of the gas, and outside the bottom reservoir, giving the temperature of the bath. In all cases we have found no differences between these two temperatures.

The temperature of the upper reservoir was measured by an ordinary mercury thermometer accurate to 0.1 °C.

PAR. 12.  METHOD OF PERFORMING THE EXPERIMENT.

The way in which we have done our experiment can be explained as follows :

50
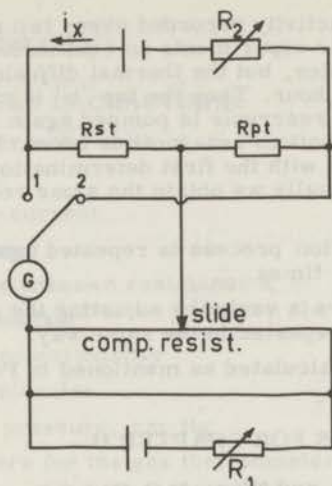
Fig. II-21

A schematic drawing of the compensator
showing the way of temperature measure-
ment.

1. The apparatus is pumped high vacuum and the tracer gas $^{85}$Kr and the other gas - e.g. $H_2$, $^4$He, $^{22}$Ne or $^3$He - is introduced. The apparatus is left at least 24 hours for mixing. Complete mixing is checked by closing taps "a", "b" and "c" (see fig. II-1) in the top reservoir, and the activity was measured. Then tap "a" is opened, and the top reservoir is pumped high vacuum. This can be checked by counting the background. A sample of gas from the bottom reservoir is obtained by closing "a" and opening "c" for about 15 seconds. If we measure the same activity, then we have complete mixing. It was found that 24 hours is enough.

2. The pressure from the K. N. M. I. is asked and corrected as in Par. 4. Then the gas thermometer is filled to the required pressure. The apparatus is left in this condition for some time to attain equilibrium. After that the cooling liquid is evaporated by the lower heater, by short circuiting the photocell till the level of the cooling liquid is a few cms below the copper cylinder. Then the heater is switched off. The copper cylinder is then heated gently by the upper heater till we obtain the required pressure in the gas thermometer. At that moment the heating current is switched off and tap "f" is closed. (See fig. II-2) The lower and upper heaters are adjusted so that the rate of change of the oil level in "L" is slow. It was found experimentally that the best results will be attained by letting the lower heater work continuously at an extent such that the cooling due to the flow of vapour is slightly greater than the heat gained by the copper cylinder due to heat radiation and conduction via the cap. We leave the apparatus in this situation for a sufficient time to obtain equilibrium.

3. The valves "b" and "c" in the top reservoir are closed, while "a" is opened and the top reservoir is pumped high vacuum. A sample of gas is taken from the bottom reservoir by closing "a" and opening "c" for 15 seconds, and the activity is measured. This is repeated till we obtain the same number of counts. The tap "b" is opened for thermal

diffusion, and the activity recorded every two minutes during     one hour. In most of our experiments an equilibrium time  was obtained after about 19 minutes, but the thermal diffusion is allowed to  take place for about one hour. Then the tap "b" is closed and the activity measured. The top reservoir is pumped again in the same way, and a sample from the bottom reservoir is taken. The activity of   this sample was checked with the first determination at the beginning of the experiment. Usually we obtain the same result within the statistical fluctuations.

4. The thermal diffusion process is repeated again at the same temperature for several times.

5. Then the temperature is varied by adjusting the gas thermometer  and the whole process repeated in the same way.

6. The separation is calculated as mentioned in Par. 7. of Chapter I.

## LIST OF REFERENCES FOR CHAPTER II

1. Wright Wilson, D. and Nier, A.O.C.,
   Preparation and measurement of isotopic tracers,
   a symposium prepared for the Isotope Research Group (1948).

2. Gordon, L. Brawnell and Helen, S. Lochart,
   Nucleonics, 10, 26 (1952).

3. Rossi, B.B. and Staub, H.H.,
   Ionization chambers and counters,
   National Nuclear Energy Series V-2
   McGraw-Hill Book Co., Inc., New York (1949).

4. Wilkinson, D.H.,
   Ionization chambers and counters,
   Cambridge University Press, Camvridge, England (1950).

5. Bearden, T.A.,
   Rev. Sci. Instr., 4, 271 (1933).

6. Henriques, F.C. and Marghetti, Ir. C.,
   Ind. Eng. Chem. Anal. Ed., 18, 417 (1946).

7. Janney, C.D. and Moyer, B.J.,
   Rev. Sci. Instr., 19, 667 (1948).

8. Robley, D. Evans,
   Rev. Sci. Instr., 6, 99 (1935).

9. Bearden, J.A.,
   Rev. Sci. Instr., 4, 271 (1933).

10. Penick, D.B.,
    Rev. Sci. Instr., 6, 115 (1935).

11. Harnwell, G.P. and Voorhis, S.N. van,
    Rev. Sci. Instr., 5, 244 (1934).

12. Turner, Louis A.,
    Rev. Sci. Instr., 4, 665 (1933).

13. Bridge,
    Phys. Rev., **37**, 392 (1931).

## LIST OF SYMBOLS USED IN CHAPTER II.

| | |
|---|---|
| e | potential difference, volts |
| $I_p$ | plate current |
| $I_s$ | space charge current |
| $I_f$ | filament current |
| $i_x$ | current in the unknown resistance x |
| k | Boltzmann constant |
| K | constant of proportionality |
| n | number of molecules |
| $P_o$ | atmospheric pressure, cm-Hg |
| $P_f$ | filling pressure for the gas thermometer |
| $P_T$ | pressure of the gas thermometer at the unknown temperature T |
| P | pressure |
| R | resistance |
| $R_b$ | plate resistance |
| $R_o$ | resistance in an arm of a Weatstone bridge |
| $R_{st}$ | standard resistance, $10\,\Omega$ |
| $R_{comp.}$ | resistance of the compensator |
| $R_{pt}$ | platinum resistance |
| $\bar{R}_A$ | activity of sample A |
| $\bar{R}_B$ | activity of sample B |
| $\bar{R}_{A+B}$ | activity of both samples A and B when put beside each other |
| $\bar{R}_b$ | background activity |
| t | temperature, $^{\circ}C$ |
| T | unknown temperature, $^{\circ}K$ |
| $T_f$ | filling temperature for the gas thermometer |
| $T_h$ | temperature of the hot reservoir |
| $T_c$ | temperature of the cold reservoir |
| V | volume, c.c. |
| $V_c$ | volume of copper cylinder of gas thermometer |
| $V_g$ | volume of glass bulb for regulating pressure of gas thermometer |
| $\gamma$ | coefficient of volume expansion for copper |
| $\tau$ | dead time of counter |

# CHAPTER III

## MEASUREMENTS ON GASEOUS MIXTURES OF $^{85}$Kr WITH $^{22}$Ne, $^{4}$He, $^{3}$He AND $H_2$.

### PAR. 1. INTRODUCTION

In the temperature region from room temperature to 1000 °K the theoretical values for the different transport coefficients agree very well with the measured values, provided that we use one of the more sophisticated molecular models like the Lennard-Jones model or the Buckingham exp.-6 model. However, the agreement for diffusion and viscosity is better than for the thermal diffusion.

We choose in our calculations the Lennard-Jones model, this being a very realistic model, while most of the quantum calculations have been done for this model.

This will not nullify the fact that the other models - e. g. the Buckingham 6-exponent or a Lennard-Jones (4,8) potential model - can be used in the quantum calculations in the low temperature region later as refinements for getting better agreement between experiment and theory.

In this work the force constants in the Lennard-Jones model - $\sigma$ and $\frac{\epsilon}{k}$ - which we have used in the calculation of $\alpha \frac{L.J.}{theor.}$, were taken from Hirschfelder. [1]

### PAR. 2. THE $^{4}$He-$^{85}$Kr EXPERIMENT

Some importance will be given to this mixture, since $^{85}$Kr as well as $^{4}$He are both spherical molecules, fulfilling the requirements for the classical calculations.

The experimental results as well as the theoretical ones are shown in table III-1. In this table the $\ln Q_s$ is the logarithm of the separation, while $\ln \frac{T \text{ var.}}{303.3}$ is the logarithm of variable temperature - the oven temperature $T_h$ or the low temperature $T_c$ - divided by the fixed temperature.

By plotting a graph of $\ln Q_s$ against $\ln \frac{T_c}{303.3}$ as in fig. III-1 and measuring the slope of the tangents* at the different temperatures, the values of the

---

*The above results have been obtained by a refined way of drawing the tangent. The method consists of a rectangular parallelopiped piece of hard material the sides of which are optically flat. One side of the parallelopiped is a mirror. To draw the tangents first we have to draw the curve; this is drawn by means of a flexible piece of plastic fixed in position by heavy weights. The piece of plastic was adjusted symmetrically between the points as much as possible; then a curve is drawn. By facing the mirror side of the parallelopiped to the curve, the image of the curve is seen. The curve and its image are adjusted to be parallel as much as possible and then the slope is measured. The best results were obtained when the mirror face of the parallelopiped was not in contact with the curve.
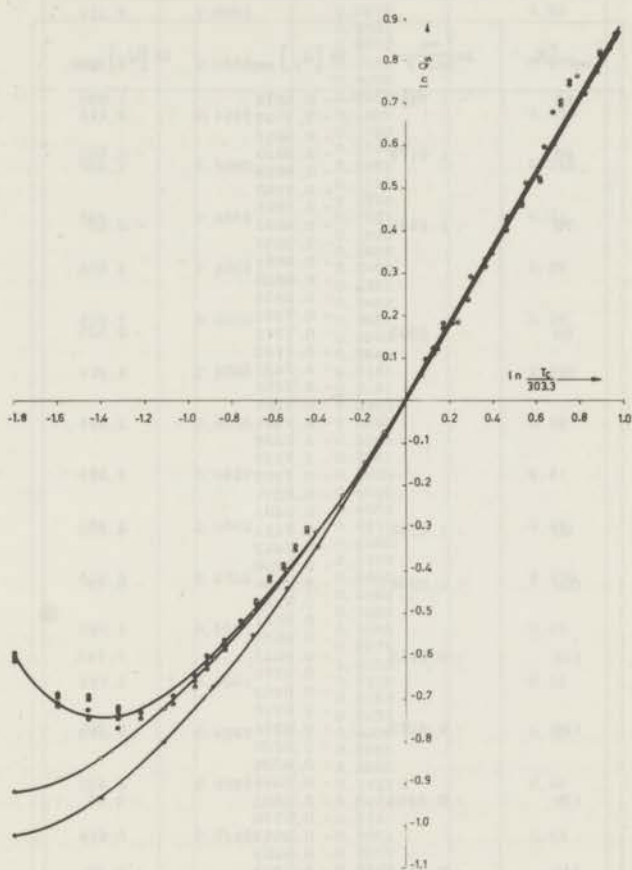
Fig. III-1.

The logarithm of the separation $\ln Q_s$ as a function of $\ln \frac{T_c}{303.3}$ for the $^{85}Kr$-$^4He$ mixture form 50 °K to 800 °K.

⊙ Experimental points

• Theoretical points calculated according to the classical theory with the Lennard - Jones (12,6) potential using the best parameters $\epsilon_{12}$ = 44.1 °K and $\sigma_{12}$ = 3.095.

○ Theoretical points calculated according to the classical theory with the Lennard - Jones (12, 6) potential by decreasing the parameter $\sigma_2$ of the $^4He$ molecule by 10%.

## TABLE III - 1.

Experimental and theoretical values of the separation factor for the mixture ⁸⁵Kr-⁴He at different temperatures.

| $T_{var.}$ °K | $\ln\dfrac{T_{var.}}{303.3}$ | $\ln\left[Q_s\right]$ expt. | $\ln\left[Q_s\right]$ theor. |
|---|---|---|---|
| 50 | - 1.7998 | - 0.5874 | - 1.025 |
|  |  | - 0.6102 |  |
|  |  | - 0.6017 |  |
| 60 | - 1.6176 | - 0.6929 | - 0.995 |
|  |  | - 0.6848 |  |
|  |  | - 0.7163 |  |
|  |  | - 0.7085 |  |
| 70 | - 1.4637 | - 0.6937 | - 0.95 |
|  |  | - 0.6956 |  |
|  |  | - 0.6681 |  |
|  |  | - 0.6827 |  |
|  |  | - 0.6975 |  |
|  |  | - 0.7242 |  |
| 80 | - 1.3303 | - 0.7242 | - 0.905 |
|  |  | - 0.7143 |  |
|  |  | - 0.7437 |  |
|  |  | - 0.7401 |  |
|  |  | - 0.7285 |  |
|  |  | - 0.7691 |  |
|  |  | - 0.7228 |  |
|  |  | - 0.7237 |  |
|  |  | - 0.7302 |  |
|  |  | - 0.7371 |  |
|  |  | - 0.7401 |  |
| 90 | - 1.2126 | - 0.7481 | - 0.855 |
|  |  | - 0.7442 |  |
|  |  | - 0.7290 |  |
| 100 | - 1.0778 | - 0.7159 | - 0.79 |
|  |  | - 0.7223 |  |
|  |  | - 0.6931 |  |
|  |  | - 0.6977 |  |
| 110 | - 0.9915 | - 0.6627 | - 0.745 |
|  |  | - 0.6776 |  |
|  |  | - 0.6882 |  |
|  |  | - 0.6740 |  |
| 120 | - 0.9253 | - 0.6378 | - 0.70 |
|  |  | - 0.6330 |  |
|  |  | - 0.6226 |  |
|  |  | - 0.6394 |  |
| 130 | - 0.8453 | - 0.5862 | - 0.65 |
|  |  | - 0.5770 |  |
|  |  | - 0.5653 |  |
|  |  | - 0.5883 |  |
| 140 | - 0.7714 | - 0.5303 | - 0.60 |
|  |  | - 0.5195 |  |
|  |  | - 0.5248 |  |
|  |  | - 0.5218 |  |
| 150 | - 0.7024 | - 0.4762 | - 0.55 |
|  |  | - 0.4792 |  |
|  |  | - 0.4725 |  |
|  |  | - 0.4651 |  |
| 160 | - 0.6380 | - 0.4244 | - 0.505 |
|  |  | - 0.4161 |  |
|  |  | - 0.4278 |  |
|  |  | - 0.4200 |  |
| 170 | - 0.5773 | - 0.4009 | - 0.46 |
|  |  | - 0.4009 |  |
|  |  | - 0.3928 |  |
|  |  | - 0.3841 |  |
| 180 | - 0.5203 | - 0.3514 | - 0.435 |
|  |  | - 0.3470 |  |
|  |  | - 0.3521 |  |
|  |  | - 0.3378 |  |
| 190 | - 0.4665 | - 0.2970 | - 0.37 |
|  |  | - 0.3030 |  |
|  |  | - 0.2987 |  |
|  |  | - 0.3060 |  |

TABLE III - 1

| $T_{var.}$ °K | $\ln \dfrac{T_{var.}}{303.3}$ | $\ln [Q_s]_{expt.}$ | $\ln [Q_s]_{theor.}$ |
|---|---|---|---|
| 321.6 | 0.0583 | 0.0573 | 0.05 |
| | | 0.0601 | |
| | | 0.0573 | |
| 329.8 | 0.0836 | 0.1062 | 0.075 |
| | | 0.0988 | |
| | | 0.0988 | |
| 343.5 | 0.1248 | 0.1292 | 0.105 |
| | | 0.1283 | |
| | | 0.1133 | |
| 359.1 | 0.1690 | 0.1881 | 0.145 |
| | | 0.1715 | |
| | | 0.1734 | |
| 385 | 0.2383 | 0.1831 | 0.21 |
| | | 0.1840 | |
| | | 0.1856 | |
| 403.4 | 0.2853 | 0.2406 | 0.25 |
| | | 0.2351 | |
| | | 0.2406 | |
| 408.7 | 0.2986 | 0.2957 | 0.26 |
| | | 0.2940 | |
| | | 0.2940 | |
| 439.4 | 0.3709 | 0.3161 | 0.325 |
| | | 0.3161 | |
| | | 0.3392 | |
| 449.2 | 0.3928 | 0.3562 | 0.35 |
| | | 0.3548 | |
| | | 0.3541 | |
| 482.3 | 0.4637 | 0.4023 | 0.41 |
| | | 0.4030 | |
| | | 0.4002 | |
| 484.3 | 0.4683 | 0.4357 | 0.42 |
| | | 0.4285 | |
| | | 0.4278 | |
| 517.3 | 0.5340 | 0.4656 | 0.470 |
| | | 0.4644 | |
| | | 0.4608 | |
| 527.1 | 0.5526 | 0.5068 | 0.49 |
| | | 0.5075 | |
| | | 0.5153 | |
| 563.9 | 0.6201 | 0.5225 | 0.55 |
| | | 0.5183 | |
| | | 0.5236 | |
| 572.9 | 0.6362 | 0.6005 | 0.56 |
| | | 0.5961 | |
| | | 0.5955 | |
| 598.5 | 0.6797 | 0.6823 | 0.60 |
| | | 0.6727 | |
| | | 0.6781 | |
| 619.5 | 0.7143 | 0.7051 | 0.63 |
| | | 0.7076 | |
| | | 0.6965 | |
| 644.5 | 0.7536 | 0.7527 | 0.665 |
| | | 0.7490 | |
| | | 0.7451 | |
| 665.6 | 0.7856 | 0.7681 | 0.70 |
| | | 0.7654 | |
| | | 0.7649 | |
| 690.3 | 0.8225 | 0.7276 | 0.73 |
| | | 0.7272 | |
| | | 0.7253 | |
| 701.9 | 0.8388 | 0.8133 | 0.74 |
| | | 0.8124 | |
| | | 0.8124 | |
| 731.5 | 0.8805 | 0.7767 | 0.78 |
| | | 0.7852 | |
| | | 0.7794 | |
| 740.6 | 0.8929 | 0.8236 | 0.79 |
| | | 0.8220 | |
| | | 0.8176 | |
| 775.5 | 0.9388 | 0.8363 | 0.83 |
| | | 0.8386 | |
| | | 0.8328 | |
| 792.3 | 0.9599 | 0.8658 | 0.85 |
| | | 0.8681 | |
| | | 0.8363 | |

57

thermal diffusion factor $\alpha$ as a function of temperature are obtained. These values are shown in table III-2.

## TABLE III - 2.

Experimental and theoretical values of the thermal diffusion factor for the mixture $^{85}Kr$-$^4He$ at different temperatures.

| T. °K | $\alpha_{classical}$ L.J. | $\alpha_{expt.}$ tang. | $\alpha_{expt.}$ calc. from 14 | $\alpha_{expt.}$ tang. $- \alpha_{expt.}$ calc. from 14 |
|---|---|---|---|---|
| 50 | + 0.10 | - 0.55 | - 0.53 | 0.02 |
| 60 | + 0.23 | - 0.34 | - 0.34 | 0.00 |
| 70 | + 0.32 | - 0.16 | - 0.17 | 0.01 |
| 80 | + 0.40 | 0.00 | - 0.02 | 0.02 |
| 90 | + 0.47 | + 0.10 | + 0.10 | 0.00 |
| 100 | + 0.52 | + 0.24 | + 0.25 | 0.01 |
| 110 | + 0.57 | + 0.33 | + 0.34 | 0.01 |
| 120 | + 0.61 | + 0.41 | + 0.41 | 0.00 |
| 130 | + 0.64 | + 0.48 | + 0.50 | 0.02 |
| 140 | + 0.67 | + 0.54 | | |
| 150 | + 0.69 | + 0.58 | | |
| 160 | + 0.72 | + 0.62 | | |
| 170 | + 0.74 | + 0.66 | | |
| 180 | + 0.76 | + 0.69 | | |
| 190 | + 0.77 | + 0.72 | | |
| 200 | + 0.78 | + 0.74 | | |
| 250 | + 0.83 | + 0.81 | | |
| 300 | + 0.85 | + 0.85 | | |
| 350 | + 0.87 | + 0.87 | + 0.87 | 0.00 |
| 400 | + 0.88 | + 0.88 | + 0.88 | 0.00 |
| 450 | + 0.89 | + 0.89 | + 0.89 | 0.00 |
| 500 | + 0.89 | + 0.89 | + 0.89 | 0.00 |
| 550 | + 0.89 | + 0.89 | + 0.89 | 0.00 |
| 600 | + 0.89 | + 0.90 | + 0.90 | 0.00 |
| 650 | + 0.89 | + 0.90 | + 0.90 | 0.00 |
| 700 | + 0.90 | + 0.91 | + 0.91 | 0.00 |
| 750 | + 0.90 | + 0.91 | + 0.91 | 0.00 |
| 800 | + 0.90 | + 0.91 | + 0.91 | 0.00 |

From this graph we see that there are appreciable deviations from the classical curve, even at room temperature.

These deviations are attributed to diffraction effects due to the wave nature of the particles which become noticeable at low temperatures.

To interpret these deviations as quantum deviations, it is necessary to show in a satisfactory way that the classical theory does not account for the experimental curve by any means below a certain region of temperature and that it holds above this temperature.

To do this we must notice that $\sigma$ and $\frac{\epsilon}{k}$ are not very well known. [2-5)] Surely we have taken the best known values for these parameters, but this does not guarantee their absolute acuuracy. So an allowable deviation in each of them of about 10% could be considered. Therefore we have tried to fit our experimental curve by varying the parameters

$\sigma_{12}$ and $\frac{\epsilon_{12}}{k}$. [6, 7)]
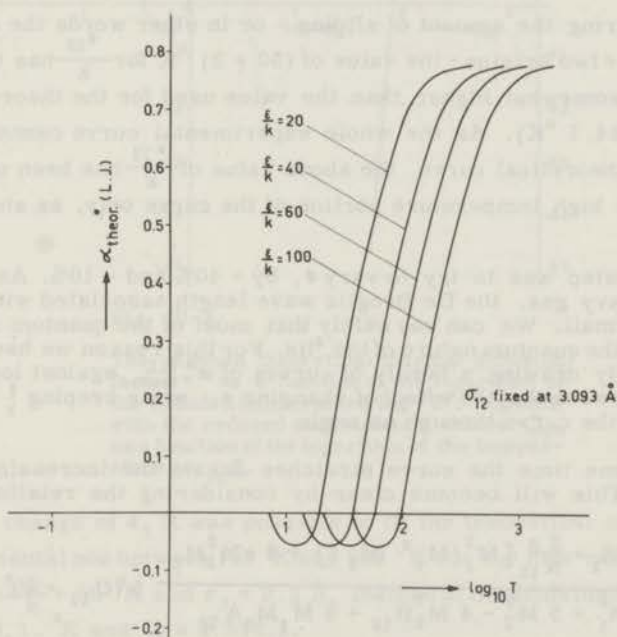


Fig. III-2.

The reduced theoretical thermal diffusion factor $a^*$ as a function of the logarithm of the temperature with $\epsilon$ as a parameter ; $\sigma_{12}$ is fixed at 3.093 Å.

59

First we have examined the effect of the variation of $\frac{\epsilon_{12}}{k}$. Fig. III-2 shows a family of curves for different values of $\frac{\epsilon_{12}}{k}$. From this figure we see that all curves are parallel to each other. This suggests an easy way to find an unknown value - or to check a known value - of $\frac{\epsilon_{12}}{k}$

By considering the relation:

$$T^* = T / \left(\frac{\epsilon}{k}\right)$$

and taking the logarithm of both sides we get

$$\log T^* = \log T - \log \frac{\epsilon}{k} \tag{III-1}$$

Relation (1) is of considerable importance. It shows that the logarithm of $\frac{\epsilon}{k}$ can be obtained from two curves, viz. an experimental and a theoretical one, showing respectively the relation between $\alpha^*_{\text{theor.}}$ against $\log T^*$ and $\alpha^*_{\text{expt.}}$ against $\log T$ by mere sliding one curve over the other along the temperature axis, as has been indicated in fig. III-3.

By measuring the amount of sliding - or in other words the difference between the two origins - the value of $(50 \pm 2)$ $^\circ$K for $\frac{\epsilon_{12}}{k}$ has been found, which is somewhat higher than the value used for the theoretical calculation (44.1 $^\circ$K). As the whole experimental curve cannot be fitted with the theoretical curve, the above value of $\frac{\epsilon_{12}}{k}$ has been obtained by fitting the high temperature portion of the curve only, as shown in fig. III-3.

The next step was to try to vary $\sigma$, by + 10% and - 10%. As $^{85}$Kr is a rather heavy gas, the De Broglie wave length associated with it is extremely small. We can say safely that most of the quantum deviations are due to the quantum nature of the $^4$He. For this reason we have changed only $\sigma_2$. By drawing a family of curves of $\alpha^*_{\text{theor.}}^{\text{L.J.}}$ against $\log T^*$ as in fig. III-4 we see that the effect of changing $\sigma$ - while keeping $\frac{\epsilon}{k}$ constant - is to turn the curve through an angle.

At the same time the curve stretches due to the increasing value of $\alpha^*_{\text{theor.}}^{\text{L.J.}}$ . This will become clear by considering the relation between $\alpha$ and $\sigma$:

$$\alpha = \frac{- M_2 + \frac{3 s}{A_{12}} \left[M_1^2 (M_1 - M_2)\right] + 4 s M_1^2 M_2}{6 M_1^2 + 5 M_2^2 - 4 M_2^2 B_{12} + 8 M_1 M_2 A_{12}} \; 5 \, (C_{12} - .1) \tag{III-2}$$

where:

$$s = \left(\frac{\sigma_{12}}{\sigma_2}\right)^2 \frac{1}{\sqrt{2} \, M_1} \frac{\Omega^{*2,2} (T_{12}^*)}{\Omega^{*2,2} (T_2^*)}$$

Hence, s will increase if $\sigma_2$ decreases.

Correspondingly $\alpha$ will increase if $\sigma_2$ decreases.
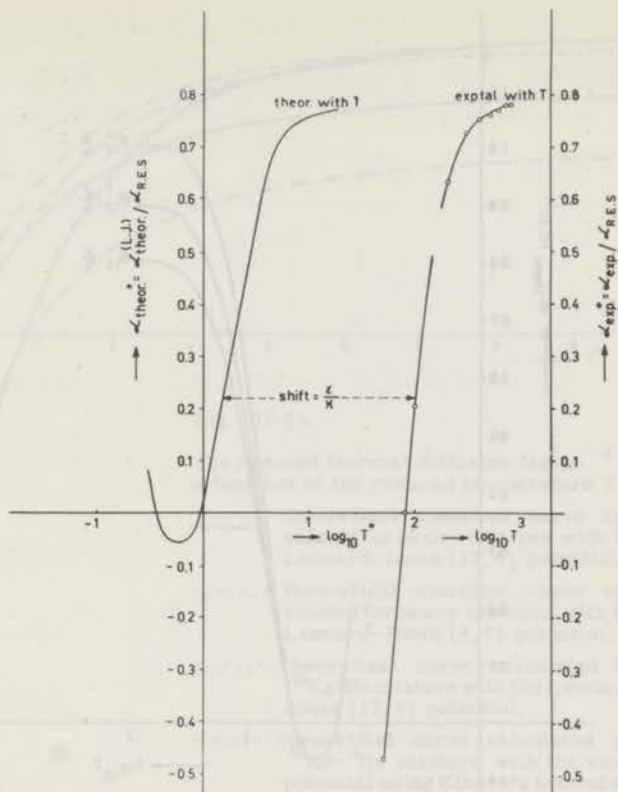
Fig. III-3.

The reduced theoretical thermal diffusion factor $\alpha^*$ as a function of the logarithm of the reduced temperature log $T^*$; together with the reduced experimental values $\alpha^*_{expt.}$ as a function of the logarithm of the temperature $\log_{10} T$.

By such a change of $\sigma_2$ it was possible to fit the theoretical curve with the experimental one between 100 $^{\circ}$K and 800 $^{\circ}$K for the new values of the parameters $\frac{\epsilon_{12}}{k}$ = 50 $^{\circ}$K and $\sigma_2$ = 2.3 Å, instead of Hirschfelder's values of $\frac{\epsilon_{12}}{k}$ = 44,1 $^{\circ}$K and $\sigma_2$ = 2.576 Å.

We must notice that such a fitting was only possible over the temperature range from 800 $^{\circ}$K till about 100 $^{\circ}$K. Below 100 $^{\circ}$K a large discrepancy appears between the theoretical curve and the experimental one as shown in fig. III-1 in the second calculated curve with the decreased $\sigma$ value (see subscript). This discrepancy at low temperatures can never be explained by changing the parameters of the Lennard-Jones model. We can say in principle that the classical theory is not valid below 100 $^{\circ}$K.

For the sake of completeness we have considered still two other potential fields, viz. :

61
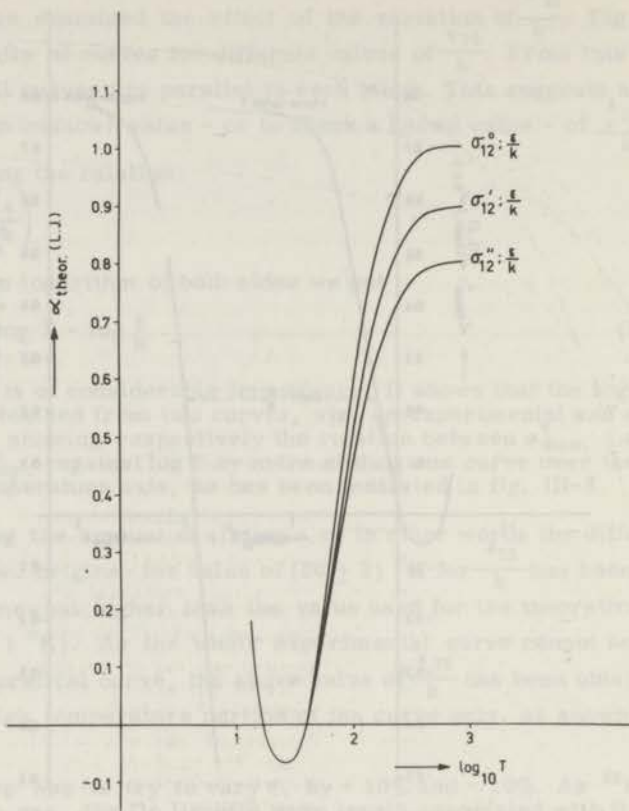
Fig. III-4.

The theoretical thermal diffusion factor $\alpha$
as a function of the logarithm of the temp-
erature $\log_{10} T$; for different values of
($\sigma_{12}^{\circ} = 2.965$ Å, $\sigma_{12}' = 3.093$ Å, $\sigma_{12}'' = 3.225$
Å) and fixed value of $\epsilon$ = 44.1 °K.

1. the Lennard-Jones (4, 8) potential
2. the Buckingham 6-exponent potential
in order to compare them with our experimental points.

The Lennard-Jones (4, 8) potential was published in 1940 and 1941 by
Clark Jones[8] and afterwards represented by Waldmann[9] in the same way
as we have treated in this thesis. We have represented Waldmann's
graphs for the $\alpha^*{}_{theor.}^{L.J.}$ for both the (12, 6) and the (4, 8) model in fig.
(III-5a). We must remark, however, that Waldmann's two curves were
calculated for heavy isotopic mixtures which fact means that deviations
from $\alpha^*{}_{theor.}^{L.J.}$ for Kr-He mixtures can be expected. The character of
the curves is quite the same, however, as indicated by the extra curve
for $\alpha^*{}_{theor.}^{L.J.}$ (12, 6) for our ($^{85}$Kr-$^4$He) mixture as calculated by us and
shown in the same fig. III-5a.
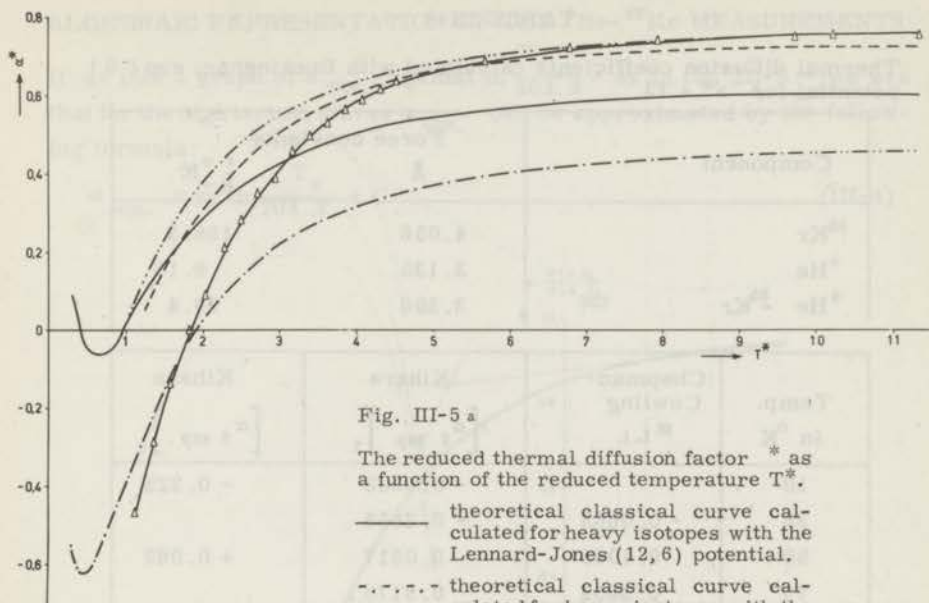
Fig. III-5 a

The reduced thermal diffusion factor $\alpha^*$ as a function of the reduced temperature $T^*$.

——————— theoretical classical curve calculated for heavy isotopes with the Lennard-Jones (12, 6) potential.

-.-.-.- theoretical classical curve calculated for heavy isotopes with the Lennard-Jones (4, 8) potential.

-..-..- theoretical curve calculated for $^{85}$Kr-$^4$He mixture with the Lennard-Jones (12, 6) potential.

- - - - theoretical curve calculated for $^{85}$Kr-$^4$He mixture with the exp-6 potential using Kihara's second approximation.
△ experimental points for the $^{85}$Kr-$^4$He mixture.

The Buckingham 6-exponent[1] which we have used for our calculations has the shape:

$$\Phi(r) = \frac{\epsilon}{1 - \frac{6}{a}} \left[ \frac{6}{a} \exp \left\{ a\left(1 - \frac{r}{r_{min}}\right)\right\} - \left(\frac{r_{min}}{r}\right)^6 \right] \qquad (III-3)$$

where $r_{min}$ was obtained from Mason's tables;[7,10,12] $r_{min}$ holds for the distance of the minimum in the potential curve, whereas $\epsilon$ is the energy depth of the potential well at that point. The factor "a" gives the steepness of the potential well, which we took equal to 12 to get the closest approach to our experimental results (see also Grew and Mundy [11] fig. 1). All force constants for our Kr-He mixture were taken from Mason's tables [7,10,12] and are in table III-3, together with the results of our first and second order Kihara approximation.[13-16]. The second Kihara approximation of $\alpha^*_{theor.}$ is indicated also in fig. III-5a. We see that this $\alpha^*_{theor.}$ behaves in much the same way as the $\alpha^*_{theor.}^{L.J.}$ with (12, 6) potential. It is therefore not able to explain our experimental results below $T^* = 4$.

63

## TABLE III-3

Thermal diffusion coefficients calculated with Buckingham exp ( 6 ) potential for "a" = 12.

| Component | Force constants | |
|---|---|---|
| | Å | $\frac{\epsilon}{k}$ °K |
| $^{85}$Kr | 4.056 | 158.3 |
| $^{4}$He | 3.135 | 9.16 |
| $^{4}$He - $^{85}$Kr | 3.596 | 39.4 |

| Temp. in °K | Chapman-Cowling $\alpha_{L.J.}$ | Kihara $\left[\alpha_{6\ exp}\right]_1$ | Kihara $\left[\alpha_{6\ exp.}\right]_2$ |
|---|---|---|---|
| 10 | | - 0.3302 | - 0.325 |
| 25 | - 0.0665 | - 0.2555 | |
| 50 | 0.1068 | 0.0517 | + 0.062 |
| 75 | 0.3652 | 0.3170 | |
| 100 | 0.5229 | 0.4628 | + 0.463 |
| 125 | 0.6250 | 0.5725 | |
| 150 | 0.6919 | 0.6204 | + 0.628 |
| 175 | 0.7375 | 0.6625 | |
| 200 | 0.7808 | 0.6845 | + 0.700 |
| 250 | | 0.7209 | + 0.730 |
| 300 | 0.8468 | 0.7299 | + 0.748 |
| 400 | 0.8866 | 0.7379 | + 0.760 |
| 500 | 0.8928 | 0.7343 | + 0.762 |

$$\left[\alpha_{R.E.S.}\right]_{\text{with exp.-6 force const.}} = 1.05 \qquad \left[\alpha_{R.E.S.}\right]_{\text{with L.J. force const.}} = 1.16$$

In the same fig. III-5a there is also a fifth curve indicated for our experimentally determined $\alpha^*$ expt. ( $^{85}$Kr- $^{4}$He) using the $\epsilon/k$ value of the Lennard-Jones potential. We see that above $T^* = 4$ our results agree with the Lennard-Jones (12, 6) model, whereas for $T^* < 3$ we observed an approach of the experimental curve to a Lennard-Jones (4, 8) model. This result is interesting so far it indicates that the collisons between Kr and He for the temperature region below 120 °K ($T^* = 3$) get a softer character than for the higher temperature region. This same fact was observed already by Clark Jones[8] who made in 1940 the remark: "It can hardly be doubted that the decrease in $\alpha$ expt. is due to the increased "softness" of the repulsive force at low temperatures."

# ALGEBRAIC REPRESENTATION OF THE $^4$He-$^{85}$Kr MEASUREMENTS

If we plot a graph of $\alpha_{expt.}$ against $\ln \dfrac{T_c}{303.3}$ - as in fig. III-5 -, we see that for the high temperatures $\alpha_{expt.}$ can be approximated by the following formula:

$$\alpha_{expt.} = \overline{m} \ln \frac{T_c}{303.3} + C \tag{III-4}$$
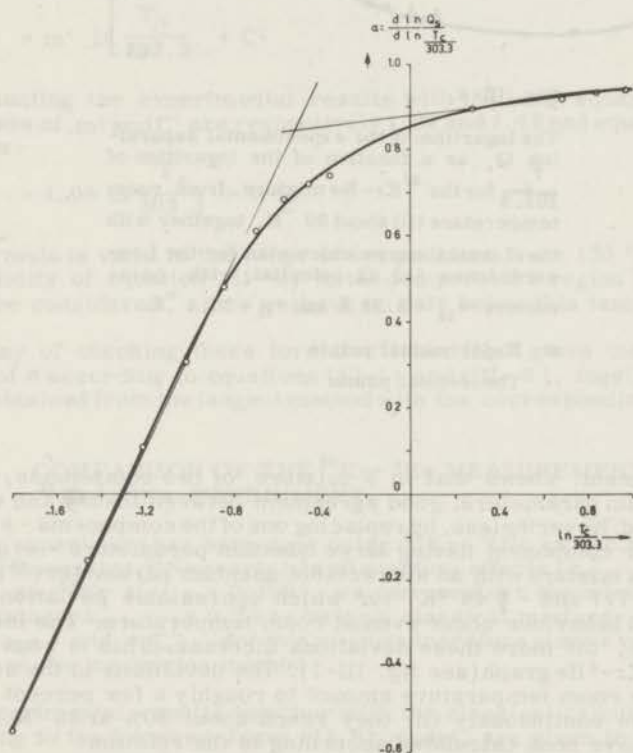


Fig. III-5.

The experimental thermal diffusion factor $\alpha$ as a function of the logarithm of $\dfrac{T_c}{303.3}$, where $T_c$ is the variable temperature, and the temperature of the top reservoir was kept always at 303.3 °K.

By plotting $\ln \dfrac{T_c}{303.3}$ against $\ln Q_s$ as shown in fig. III-6 we see that the experimental points lie nicely on the classical, calculated curve. This fit of the experimental points with the classical curve extends over the temperature region from 80 °K till 800 °K. This is consistent with the fact that this mixture has a $\Lambda^* = 0.28$ and an $\dfrac{\epsilon}{k} = 77$ °K which means that the deviations from the classical behaviour at 77 °K are not appreciable.

65
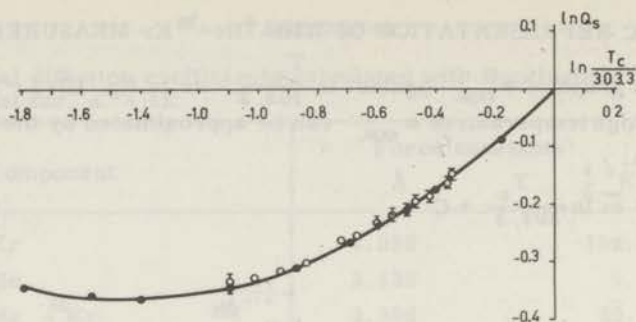
Fig. III-6.

The logarithm of the experimental separation $Q_s$ as a function of the logarithm of $\frac{T_c}{303.3}$ for the $^{85}$Kr- Ne mixture, from room temperature till about 80 $^{\circ}$K, together with the classical curve calculated for the Lennard-Jones (12,6) potential, with parameters $\sigma_{12} = 3.22$ Å and $\epsilon_{12} = 77.1$ $^{\circ}$K.

⊙   Experimental points

·   Theoretical points

This experiment shows that in a mixture of two components, with small quantum parameters, good agreement between theory and experiment is found. Nevertheless, by replacing one of the components - e.g. Ne - by an other component having large quantum parameters - e.g. $^4$He- will give us a mixture with an appreciable quantum parameter ($^{85}$Kr-$^4$He with $\Lambda^* = 0.777$ and $-\frac{\epsilon}{k}$ 44 $^{\circ}$K) for which appreciable deviations from the classical behaviour occur even at room temperature. The lower the temperature, the more these deviations increase. This is what we see from the $^{85}$Kr-$^4$He graph (see fig. III-1). The deviations in the separation near the room temperature amount to roughly a few percent ($1\rightarrow2\%$) and increase continuously till they reach about 30% at 50 $^{\circ}$K. These deviations have been calculated according to the relation:

$$\text{percent deviation} = \frac{\text{classical value - experimental value}}{\text{classical value}} \times 100$$

By fitting the experimental results with the least square method [17], we obtain the values 0.0604 and 0.88 for $\bar{m}$ and $C$ respectively and equation III-4 takes the form:

$$\alpha_{\text{expt.}} = 0.0604 \ln \frac{T_c}{303.3} + 0.88 \tag{III-5}$$

This formula is valid in the temperature range from 425 $^{\circ}$K to 800 $^{\circ}$K. Heymann [18] in his thesis has suggested the formula:

$$\alpha = A - \frac{\beta}{T} \tag{III-6}$$

66

which is the same formula suggested by Heymann, and which he supposed to be valid from 300 °K to 700 °K. At 300 °K the curve of $\ln \frac{T}{303.3}$ against $\alpha$ bends a little and is no more linear. The error at 300 °K between the value calculated according to equation(III-6) and the value obtained by drawing the tangent, is not due to the drawing of the tangent, but to the unvalidity of equation (III-8) at 300 °K.

From the same plot of $\alpha_{expt.}$ against $\ln \frac{T}{303.3}$, we see that - in the low temperature region - the thermal diffusion factor $\alpha$ can be estimated by the following formula:

$$\alpha_{expt.} = m' \ln \frac{T_c}{303.3} + C' \tag{III-7}$$

By evaluating the experimental results with the least squares method, the values of $m'$ and $C'$ are respectively 1.09 and 1.42 and equation (III-7) becomes:

$$\alpha_{expt.} = 1.09 \ln \frac{T_c}{303.3} + 1.42 \tag{III-8}$$

This formula is valid in the range of temperature from 130 °K to 50 °K. The validity of equation (III-8) in the temperature region below 50 °K cannot be considered, since we have no data below this temperature. -

As a way of checking these formulae table III-2 gives the calculated values of $\alpha$ according to equations (III-5) and (III-8), together with the values obtained from the tangent method with the corresponding deviation.

## PAR. 4. COMPARISON OF THE $^{85}$Kr-$^4$He MEASUREMENTS WITH A $^{85}$Kr-$^{22}$Ne EXPERIMENT.

Another experiment has been done using $^{85}$Kr-$^{22}$Ne as our mixture. As it is well known that $^{22}$Ne nearly has no quantum effects ($\Lambda^*_{Ne-Ne} = 0.593$), as well as $^{85}$Kr $\Lambda^*_{Kr-Kr} = 0.192$), we can consider the mixture $^{85}$Kr - $^{22}$Ne having a $\Lambda_{Kr-Ne\ L.J.} = 0.28$ as being a classical mixture. Comparison of the $\alpha_{expt.}$ and $\alpha_{theor.}$ for this mixture therefore gives a very valuable control on the measuring method.

The experimental results together with the classical calculated values, according to the Lennard-Jones (12,6) model, are given in table III-4.

## PAR. 5. THE $^{85}$Kr-$^3$He EXPERIMENT.

As it is well known that isotopes of the same element have the same force constants, it is interesting to use an analogous binary mixture having $^{85}$Kr as a tracer, and with approximately the same $\Lambda^*$ and $\frac{\epsilon}{\kappa}$. This mixture is of interest as it might have roughly the same quantum deviations as the preceeding one. Fortunately the mixture $^{85}$Kr-$^3$He having a $\Lambda^* = 0.89$ and an $\frac{\epsilon}{\kappa} \simeq 44$ °K will give us the required properties.

The experimental separation results of such a mixture together with the calculated classical ones for the Lennard-Jones (12.6) potential are given in table III-5.

TABLE III - 4

Separation of $^{85}$Kr- $^{22}$Ne as a function of T.

| $T_{var.}$ | $\ln \dfrac{T_c}{303.3}$ | $\ln \left[ Q_s \right]_{expt.}$ | $\ln \left[ Q_s \right]_{theor.}$ |
|---|---|---|---|
| 101 | 1.110 | - 0.332 $\pm$ .015 | - 0.345 |
| 110 | 1.010 | - 0.326 $\pm$ .015 | - 0.335 |
| 120 | 0.930 | - 0.314 $\pm$ .015 | - 0.320 |
| 130 | 0.840 | - 0.300 $\pm$ .015 | - 0.300 |
| 144.5 | 0.720 | - 0.260 $\pm$ .01 | - 0.275 |
| 155 | 0.670 | - 0.252 $\pm$ .01 | - 0.26 |
| 166 | 0.600 | - 0.228 $\pm$ .01 | - 0.24 |
| 180 | 0.548 | - 0.216 $\pm$ .01 | - 0.22 |
| 183 | 0.500 | - 0.208 $\pm$ .01 | - 0.205 |
| 190 | 0.470 | - 0.192 $\pm$ .008 | - 0.195 |
| 200 | 0.420 | - 0.184 $\pm$ .008 | - 0.18 |
| 210 | 0.370 | - 0.164 $\pm$ .008 | - 0.16 |
| 216 | 0.345 | - 0.148 $\pm$ .008 | - 0.15 |

The calculated classical values will not differ much from those for $^{85}$Kr - $^4$He, since the only difference is the mass difference. By plotting the experimental values as well as the classical ones in a graph showing the relation between $\ln \frac{T_c}{T_h}$ and $\ln Q_s$ as in fig. III-7 we see that there are deviations even at room temperature and that these deviations increase continuously from a few percent at room temperature to about 30% at 50 °K.

If we compare the experimental values of both mixtures $^{85}$Kr- $^4$He and $^{85}$Kr- $^3$He we see that the two results are nearly the same within the experimental error.

In general we can say that the deviation of the two mixtures $^{85}$Kr- $^4$He and $^{85}$Kr- $^3$He from the classical behaviour is the same over the whole range of temperature from room temperature down to about 50 °K.

PAR. 6. THE $^{85}$Kr-H$_2$ EXPERIMENT.

This experiment has been done to see if the deviations from the classical behaviour of a mixture, if one of the components is known to be non-spherical - e.g. H$_2$ in a $^{85}$Kr-H$_2$ mixture -, will show the same order of magnitude as in the mixture $^{85}$Kr- $^4$He and $^{85}$Kr- $^3$He, since it has nearly the same parameters $\Lambda^*$ (for Kr-H$_2$; $\Lambda^* = 0.76$).

The experimental separations as well as the classical ones according to the Lennard-Jones (12, 6) model are given in table III-6.

TABLE III - 5.

Separation of $^{85}$Kr-$^3$He as a function of temperature

| $T_{var.}$ | $\ln \dfrac{T_{var.}}{303.3}$ | $\ln \left[Q_s\right]_{expt.}$ | $\ln \left[Q_s\right]_{theor.}$ |
|---|---|---|---|
| 45 | | - 0.351 | - 1.05 |
| 50 | - 1.7998 | - 0.550 | |
| | | - 0.562 | |
| | | - 0.580 | |
| 60 | - 1.6176 | - 0.635 | - 1.01 |
| | | - 0.650 | |
| | | - 0.665 | |
| 70 | - 1.4637 | - 0.700 | - 0.965 |
| | | - 0.725 | |
| 80 | - 1.3303 | - 0.750 | - 0.935 |
| | | - 0.750 | |
| | | - 0.772 | |
| | | - 0.765 | |
| | | - 0.790 | |
| 90 | - 1.2126 | - 0.712 | - 0.87 |
| | | - 0.740 | |
| | | - 0.747 | |
| 100 | - 1.0778 | - 0.667 | - 0.825 |
| | | - 0.685 | |
| | | - 0.698 | |
| | | - 0.702 | |
| 110 | - 0.9915 | - 0.650 | - 0.755 |
| | | - 0.665 | |
| | | - 0.677 | |
| 120 | - 0.9253 | - 0.635 | - 0.705 |
| | | - 0.642 | |
| | | - 0.647 | |
| 130 | - 0.8453 | - 0.580 | - 0.65 |
| | | - 0.590 | |
| | | - 0.596 | |
| 140 | - 0.7714 | - 0.512 | - 0.60 |
| | | - 0.520 | |
| | | - 0.530 | |
| 150 | - 0.7024 | - 0.465 | - 0.555 |
| | | - 0.470 | |
| | | - 0.474 | |
| 160 | - 0.6380 | - 0.420 | - 0.51 |
| | | - 0.430 | |
| | | - 0.437 | |
| 170 | - 0.5773 | - 0.385 | - 0.465 |
| | | - 0.387 | |
| | | - 0.392 | |
| 180 | - 0.5203 | - 0.326 | - 0.42 |
| | | - 0.330 | |
| | | - 0.337 | |
| 190 | - 0.4665 | - 0.280 | - 0.37 |
| | | - 0.285 | |
| | | - 0.290 | |
| 200 | - 0.417 | - 0.245 | - 0.33 |
| | | - 0.250 | |
| | | - 0.255 | |
| 210 | - 0.368 | - 0.210 | - 0.295 |
| | | - 0.215 | |
| | | - 0.220 | |
| 320 | 0.0537 | 0.0564 | 0.045 |
| | | 0.0497 | |
| | | 0.0497 | |
| 326.8 | 0.0753 | 0.0659 | 0.065 |
| | | 0.0649 | |
| | | 0.0631 | |
| 342.7 | 0.1223 | 0.1142 | 0.10 |
| | | 0.1062 | |
| | | 0.1193 | |
| 354.3 | 0.1554 | 0.1304 | 0.135 |
| | | 0.1320 | |
| | | 0.1345 | |
| 372.1 | 0.2045 | 0.1989 | 0.18 |
| | | 0.1955 | |
| | | 0.1888 | |

If we plot the experimental values of $\ln Q_s$ for each temperature in a graph of $\ln Q_s$ against $\ln T_{var.}$, as in fig... ... we see that there are deviations from the classical behaviour even ... ... from the mixture, and that these deviations increase in ... ... and below a certain value in the temperature region where ... room temperature, there exists an extra deviation from ... ... experimental curve. This is due in the region of energy levels of the ... region which will contribute in a certain way to the ... ... is a low temperature region, where a molecule isolated ... ... probability can be expressed with a rotational energy ... probability with an exchange of total temperature... ...

Quantum needs to explain the phenomenon it ... in its ground state and the necessary grades accessible to ... the excited ... at high temperature accessible. We see ... ... we find that the deviation from the classical ... in these kinds of ... for our three systems we... amplify the extra ... and that this deviation must be due to diffraction effects as explained with the wave nature of the molecules. For a hydrogen atom, the wave length distribution of ... ... °K is 0.8 Å which is less appreciable.

TABLE III - 5.

| $T_{var.}$ | $\ln \dfrac{T_{var.}}{303.3}$ | $\ln [Q_s]_{expt.}$ | $\ln [\overline{Q}_s]_{theor.}$ |
|---|---|---|---|
| 389.2 | 0.2491 | 0.2508 0.2508 0.2546 | 0.24 |
| 412.9 | 0.3081 | 0.2814 0.2784 0.2784 | 0.275 |
| 426.1 | 0.3399 | 0.3134 0.3134 0.3088 | 0.30 |
| 451.5 | 0.3983 | 0.3498 0.3491 0.3498 | 0.355 |
| 464.7 | 0.4267 | 0.3806 0.3785 0.3779 | 0.39 |
| 490.9 | 0.4817 | 0.4244 0.4285 0.4253 | 0.43 |
| 509.9 | 0.5195 | 0.4656 0.4621 0.4637 | 0.46 |
| 533.5 | 0.5646 | 0.5056 0.5001 0.4994 | 0.51 |
| 548.5 | 0.5922 | 0.5296 0.5254 0.5278 | 0.53 |
| 580.8 | 0.6496 | 0.5750 0.5699 0.5692 | 0.58 |
| 594.3 | 0.6724 | 0.6125 0.6109 0.6081 | 0.60 |
| 627.3 | 0.7267 | 0.6523 0.6486 0.6560 | 0.65 |
| 643.3 | 0.7518 | 0.6735 0.6740 0.6781 | 0.675 |
| 666.8 | 0.7875 | 0.7219 0.7228 0.7262 | 0.71 |
| 685.3 | 0.8149 | 0.8289 0.8206 0.8216 | 0.73 |
| 710.3 | 0.8510 | 0.8632 0.8727 0.8752 0.8959 | 0.765 |

If we plot the experimental **values as well** as the classical ones in a graph of $\ln \frac{Tc}{Th}$ against $\ln Q_s$ as in fig. III-8, we see that there are deviations from the classical behaviour even not far below room temperature, and that these deviations increase in magnitude as we go to lower temperature. In the temperature region from about 100 °K to room temperature, there exists an extra deviation from the smooth experimental curve. This is due to the rotational energy levels of the hydrogen molecule which will contribute to a certain extent to the collision process. In this temperature region, when a molecule collides with another, some energy can be exchanged with rotational energy. The probability of such an exchange at room temperature is about $\frac{1}{500}$.

At much lower temperatures the $H_2$ molecule is in the ground state and the measured points appear to match the extrapolated high temperature curve. We can say in general that the deviation from the classical behaviour is of the same order of magnitude for our three mixtures having roughly the same $\Lambda^*$, and that this deviation must be due to diffraction effects accompanied with the wave nature of the molecules. For a hydrogen atom the wave length associated at 300 °K is 0.4 Å which is in fact appreciable.

70

TABLE III - 6

Separation of $^{85}$Kr-H$_2$ as a function of temperature

| T °K | ln T var. | ln [Q$_s$] exp. | ln [Q$_s$] theor. |
|---|---|---|---|
| 50 | - 1.80 | - 0.385 | - 0.485 |
| 55 | - 1.71 | - 0.400 | - 0.487 |
| 60 | - 1.62 | - 0.414 | - 0.490 |
| 65 | - 1.54 | - 0.413 | - 0.490 |
| 70 | - 1.46 | - 0.416 | - 0.490 |
| 80 | - 1.33 | - 0.404 | - 0.485 |
| 100 | - 1.078 | - 0.37 | - 0.452 |
| 105 | - 1.03 | - 0.34 | - 0.442 |
| 110 | - 0.99 | - 0.324 | - 0.435 |
| 115 | - 0.95 | - 0.32 | - 0.425 |
| 120 | - 0.915 | - 0.313 | - 0.418 |
| 125 | - 0.86 | - 0.290 | - 0.402 |
| 130 | - 0.825 | - 0.220 | - 0.392 |
| 135 | - 0.785 | - 0.258 | - 0.38 |
| 140 | - 0.75 | - 0.254 | - 0.37 |
| 145 | - 0.72 | - 0.245 | - 0.36 |
| 150 | - 0.69 | - 0.235 | - 0.35 |
| 155 | - 0.66 | - 0.225 | - 0.336 |
| 160 | - 0.635 | - 0.214 | - 0.32 |
| 165 | - 0.600 | - 0.202 | - 0.315 |
| 170 | - 0.56 | - 0.197 | - 0.302 |
| 175 | - 0.53 | - 0.188 | - 0.285 |
| 180 | - 0.50 | - 0.180 | - 0.272 |
| 185 | - 0.475 | - 0.168 | - 0.260 |
| 190 | - 0.440 | - 0.162 | - 0.245 |
| 195 | - 0.410 | - 0.155 | - 0.23 |
| 200 | - 0.39 | - 0.145 | - 0.22 |
| 205 | - 0.37 | - 0.140 | - 0.21 |
| 210 | - 0.35 | - 0.134 | - 0.20 |



Fig. III-7

The logarithm of the experimental values of the separation Q$_s$ as a function of the logarithm of $^T_c$/303.3 for the $^{85}$Kr-$^3$He mixture, from 50 °K to about 800 °K, together with the theoretical classical curve for the Lennard-Jones (12, 6) potential, with parameters $\sigma_{12}$ = 3.093 Å and $\epsilon_{12}$ = 44.1 °K.
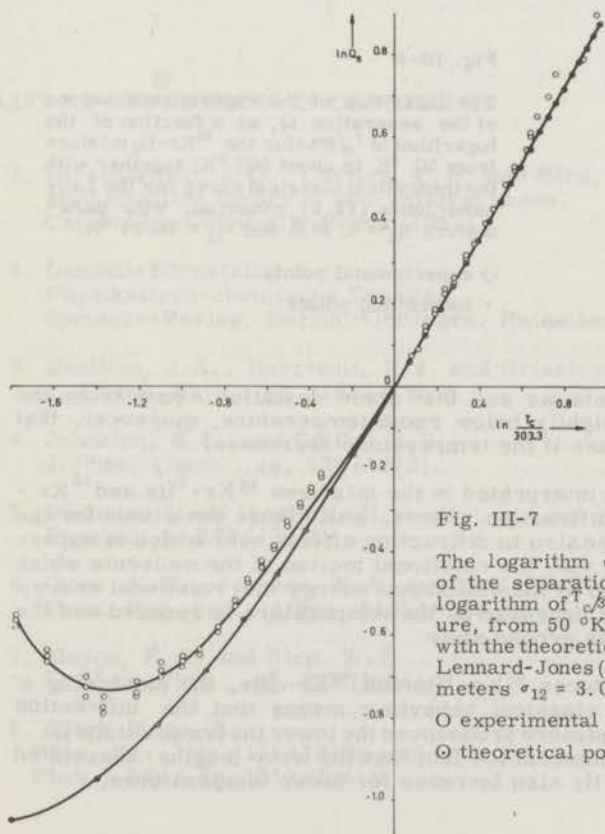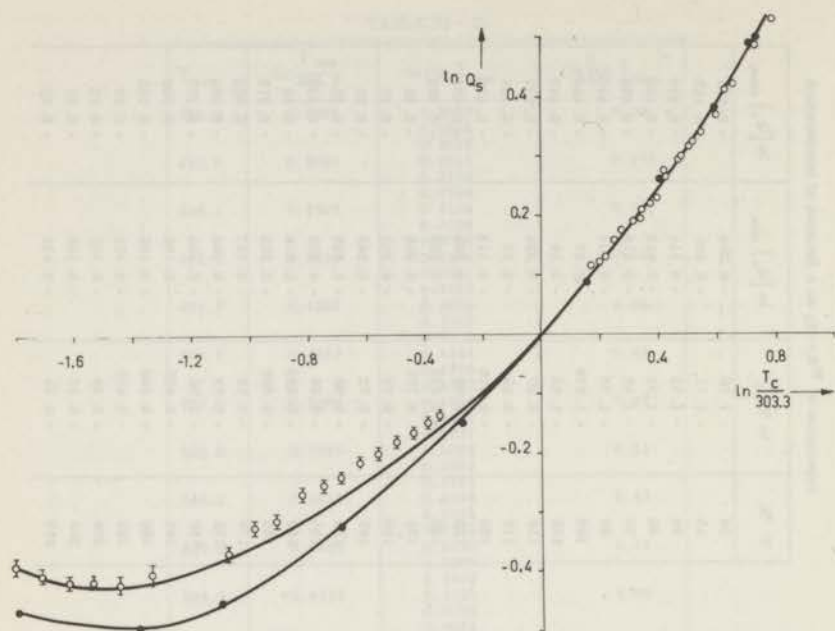
O experimental points

⊙ theoretical points.

Fig. III-8

The logarithm of the experimental values of the separation $Q_s$ as a function of the logarithm of $T_c/303.3$ for the $^{85}Kr-H_2$ mixture from 50 °K to about 800 °K; together with the theoretical classical curve for the Lennard-Jones $(12,6)$ potential, with parameters $\sigma_{12} = 3.29$ Å and $\epsilon_{12} = 78.34$ °K.

O experimental points

• theoretical points

PAR. 7. DISCUSSION.

From these experiments we see that some deviation exists from the classical behaviour slightly below room temperature, moreover, that these deviations increase if the temperature decreases.

These deviations can be interpreted in the mixtures $^{85}Kr-^{4}He$ and $^{85}Kr-^{3}He$ as to be due to diffraction effects, while those deviations for the mixture $^{85}Kr-H_2$ are due also to diffraction effects over which is superimposed another effect viz. the rotational motion of the molecule which will transform a fraction of the collisional energy into rotational energy. These rotational effects decrease as the temperature is reduced and the molecule approaches its ground state.

For the other two mixtures $^{85}Kr-^{4}He$ and $^{85}Kr-^{3}He$, the increasing of the deviation from the classical behaviour means that the diffraction effects become more and more pronounced the lower the temperature is. This is a simple consequence of the fact that the wave lengths associated with the $^{4}He$, $^{3}He$ and $H_2$ also increase for lower temperatures.

We have controlled the correctness of our measurements by studying the $^{85}$Kr- $^{22}$Ne mixture. The wave length associated with a $^{22}$Ne molecule at 300 °K is 0.09 Å, while the wave lengths associated with $H_2$, $^3$He and $^4$He are 0.4 Å, 0.25 Å and 0.2 Å respectively. In the case of $H_2$, $^3$He and $^4$He these wave lengths are appreciable as compared with the molecular dimensions, while for $^{22}$Ne they are small.

By lowering the temperature to 100 °K, the wave lengths of $H_2$, $^3$He and $^4$He, become appreciable ($\lambda_{H_2} = 0.7$ Å, $\lambda_{3He} = 0.4$ Å and $\lambda_{4He} = 0.36$ Å) , so also the deviations. For $^{22}$Ne the wave length is $\sim$ 0.15 Å at 100 °K which may become noticeable. In fact if we compare the experimental points at this temperature with the classical curve, we see that some deviations appear and become more pronounced at 80 °K. Although these deviations are of the order of magnitude of the experimental error, this does not nullify the fact that all the experimental points below 100 °K lie above the classical curve (see fig. III-6), which might confirm that these deviations exist although they are extremely small.

Unfortunately, no quantum calculations have been performed in this intermediate temperature region, due to the extremely difficult nature of the problem. Nevertheless these experiments may encourage some pioneers to perform them and an possible, check will be available at that moment.

LIST OF REFERENCES IN CHAPTER III.

1. Hirschfelder, J.O., Curtiss, C.F. and Bird, R.B.,
   Mathematical theory of non-uniform gases,
   Cambridge University Press (1952).

2. Landolt-Börnstein,
   Physikalisch-chemische Tabellen,
   Springer-Verlag, Berlin, Göttingen, Heidelberg.

3. Beattice, J.A., Barriault, R.J. and Brierley, J.S.,
   J. Chem. Phys., 20, 1613 (1952)

4. Johnston, H.L. and Grilly, E.R.,
   J. Phys. Chem., 46, 938 (1942).

5. Michels, A and Wouters, H.,
   Physica, 8, 923 (1941).

6. Grew, K.E., Johnson, F.A. and Neal, W.E.G.,
   Proc. Roy. Soc., A 224, 513 (1954).

7. Mason, E.A. and Rice, W.E.,
   J. Chem. Phys., 22, 522 (1954).

8. Clark Jones, R.,
   Phys. Rev., 58, 111 (1940) and
   Phys., Rev., 59, 1019 (1941)

9. Waldmann, L.,
   Handbuch der Physik (Ed. Flügge, S.), **XII**, 440,
   Springer-Verlag, Berlin (1958).

10. Mason, E.A.,
    J. Chem. Phys., **32**, 1832 (1960).

11. Mason, E.A. and Rice, W.E.,
    J. Chem. Phys., **22**, 843 (1954)
    Mason, E.A.,
    J. Chem. Phys., **32**, 1832 (1960).

12. Srivastava, K.P.,
    J. Chem. Phys., **26**, 579 (1957).

13. Grew, K.E. and Mundy, J.N.,
    The Phys. of Fluids, **4**, 1325. (1961).

14. Mason, E.A.,
    J. Chem. Phys., **57**, 75 (1957).

15. Mason, E.A.,
    J. Chem. Phys., **57**, 782 (1957).

16. Saxena, S.C. and Mason, E.A.,
    J. Chem. Phys., **28**, 623 (1958).

17. Willers, F.A.,
    Practical analysis,
    Dover Publications, Inc. (1948).

18. Heymann, D.,
    Thesis, Amsterdam (1958).

## LIST OF SYMBOLS USED IN CHAPTER III

| | |
|---|---|
| A | constant |
| a | parameter in the Buckingham 6-exponent |
| $C_1$, C' | constants |
| $\overline{m}_1$, m' | slope of a straight line |
| $T_f$ | fixed temperature, 303.3 °K |
| $T_{ov}$ | temperature of the oven |
| $\beta$ | constant |

CHAPTER IV

. THE THERMAL DIFFUSION COEFFICIENTS IN HYDROGEN-HELIUM
MIXTURES FROM 10-300 °K.

PAR. 1.  INTRODUCTION.

In the experiments described in chapter III, we noticed some influence
of quantum mechanical diffraction effects on thermal diffusion. [1] How-
ever, the disadvantage of these measurements was that the quantum
mechanical calculation of the collision integrals was difficult for the
mixtures used. So no comparison could be made between theory and ex-
periment. The temperature region from room temperature till 50 °K-where
the experiments were performed - is too high to do quantum mechanical
calculations.

In order to do some measurements more accessible to comparison with
quantum theory, we investigated another set of mixtures, viz.:

| | | |
|---|---|---|
| $^4$He  - T$_2$ | H$_2$ - T$_2$ | D$_2$ - T$_2$ |
| $^4$He  - DT | H$_2$ - DT | D$_2$ - DT |
| $^4$He  - HT | H$_2$ - HT | D$_2$ - HT |
| (See fig. IV-1) | (See fig. IV-2) | (See fig. IV-2) |

using tritium as a tracer. These mixtures could be investigated down
to a temperature of about 10 °K, using a liquid hydrogen bath. Because
of the small mass difference and hence the minute separation, these
experiments had to be performed with the utmost accuracy.

For this reason the second apparatus, described in chapter II, has been
built, for which the accuracy in the measurements of the ionisation
current is better than 0.1%.

PAR. 2.  THE MEASUREMENTS ON $^4$He (T$_2$, DT, HT)

The quantum parameters for the above mentioned mixtures are:

| Mixture | $\Lambda^*$ | $\left[\frac{\epsilon}{k}\right]$ | $\left[\sigma_{12}\right]$ |
|---|---|---|---|
| $^4$He  - T$_2$ | 1.65 | 19.45 | 2.74 |
| $^4$He  - DT | 1.75 | 19.45 | 2.74 |
| $^4$He  - HT | 1.88 | 19.45 | 2.74 |

so that quantum effects can be expected.

All mixtures were measured in general at pressures of approximately
5 cm-Hg at any temperature. The exact values of the pressure at the
corresponding temperature will be given in table IV-1.

The tritium used is of high purity - 99,9% T$_2$, as given in the manufacture's
data - and is preserved in small bulbs containing about 2 c.c. of T$_2$ at
N.T.P. The activity of this amount of tritium is about two curies. The
activities used in these mixtures are less than $10^{-9}$ curie/c.c., which
corresponds to a measured current - in our ionisation chamber and at
room temperature - of about $10^{-13}$ A. This current decreases in the
low temperature region - 10 °K to 20 °K - to about $10^{-15}$ A, as most of
the gas goes to the low temperature reservoir.

TABLE IV - 1

Experimental and theoretical values - according to the Lennard - Jones (12, 6) model - of the logarithm of the separation as a function of the temperature.

| Temp. T °K | $\ln \dfrac{T_{var.}}{293.0}$ | $\ln[Q_s]_{expt.}$ | $\ln[Q_s]_{classical}$ | Pressure of the gas - mixture in cm - Hg |
|---|---|---|---|---|
| **DT-⁴He** | | | | |
| 12.5 | - 3.170 | - 0.032 <br> - 0.040 | - 0.229 | 10 |
| 14.0 | - 3.058 | + 0.068 <br> + 0.049 | - 0.229 | |
| 15.7 | - 2.937 | + 0.053 <br> + 0.049 <br> + 0.058 <br> + 0.0 | - 0.228 | |
| 20.3 | - 2.674 | 0.0000 <br> 0.0000 | - 0.222 | 5 |
| 58.0 | - 1.630 | - 0.030 | - 0.161 | |
| 58.5 | - 1.619 | - 0.033 <br> - 0.030 <br> - 0.034 | - 0.160 | |
| 77.5 | - 1.347 | - 0.035 <br> - 0.028 | - 0.137 | |
| 188.3 | - 0.449 | - 0.016 <br> - 0.017 | - 0.046 | |
| **HT-⁴He** | | | | |
| 14.0 | - 3.06 | + 0.012 <br> + 0.013 <br> + 0.011 | - 0.0129 | |
| 15.7 | - 2.937 | + 0.026 <br> + 0.028 <br> + 0.025 | - 0.128 | |
| 20.3 | - 2.674 | + 0.015 <br> + 0.013 <br> + 0.016 | - 0.124 | 6-8 |
| 60.5 | - 1.585 | + 0.000 <br> 0.000 | - 0.081 | |
| 77.5 | - 1.347 | 0.000 <br> 0.000 | 0.070 | 7 |
| 188.3 | - 0.449 | 0.000 <br> 0.000 | - 0.024 | |
| **T₂ - ⁴He** | | | | |
| 12.5 | - 3.17 | + 0.038 <br> + 0.043 <br> + 0.045 <br> + 0.051 | - 1.12 | |
| 14.5 | - 2.98 | 0.000 <br> - 0.002 <br> + 0.003 | - 1.1 | |
| 20.3 | - 2.688 | - 0.138 <br> - 0.163 <br> - 0.166 | 1.06 | 4-6 |
| 53 | ⁻ 1.720 | - 0.117 <br> - 0.114 <br> - 0.110 | - 0.82 | |
| 63 | - 1.542 | - 0.110 <br> - 0.113 <br> - 0.108 | - 0.7 | |
| 77.5 | - 1.336 | - 0.096 <br> - 0.100 | - 0.62 | 5 |
| 188.3 | - 0.449 | - 0.040 <br> - 0.038 <br> - 0.043 | - 0.22 | |

TABLE IV-1

Experimental and theoretical values - according to the Lennard - Jones (12, 6) model - of the logarithm of the separation as a function of the temperature.

| Temp. T °K | $\ln\frac{T \text{ var.}}{293.0}$ | $\ln[Q_s]_{\text{expt.}}$ | $\ln[Q_s]_{\text{classical}}$ | Pressure of the gas - mixture in cm - Hg |
|---|---|---|---|---|
| HT - $H_2$ | | | | |
| 12.5 | - 3.17 | - 0.205 | - 0.271 | |
| | | - 0.254 | | |
| | | - 0.166 | | |
| 14.2 | - 3.037 | 0.000 | - 0.275 | |
| | | 0.000 | | |
| 17.1 | - 2.847 | + 0.049 | - 0.279 | |
| | | + 0.039 | | |
| | | + 0.049 | | |
| 20.3 | - 2.674 | - 0.066 | - 0.280 | 5 |
| | | - 0.056 | | |
| | | - 0.056 | | |
| | | - 0.053 | | |
| | | - 0.053 | | |
| 54 | - 1.698 | - 0.052 | - 0.247 | |
| | | - 0.046 | | |
| 63 | - 1.542 | - 0.045 | - 0.234 | |
| | | - 0.035 | | |
| | | - 0.038 | | |
| 77.5 | - 1.336 | - 0.037 | - 0.215 | 8 |
| | | - 0.045 | | |
| 188.3 | - 0.449 | - 0.016 | - 0.081 | |
| | | - 0.017 | | |
| | | - 0.019 | | |
| DT-$D_2$ | | | | |
| 17.7 | - 2.813 | + 0.022 | - 0.137 | |
| | | + 0.020 | | |
| | | + 0.010 | | |
| 20.3 | - 2.688 | - 0.038 | - 0.135 | 10 |
| | | - 0.036 | | |
| | | - 0.043 | | |
| | | - 0.045 | | |
| 53 | - 1.720 | - 0.034 | - 0.10 | |
| | | - 0.032 | | |
| 77.5 | - 1.34 | - 0.030 | - 0.07 | 10 |
| | | - 0.028 | | |

If we plot the logarithm of the separation as a function of $\ln\frac{T_c}{T_h}$ for the above mentioned mixtures, we obtain the graphs shown in fig. IV-1. From these graphs we see that all the three mixtures have shown a minimum and a maximum for the separation, which means that the thermal
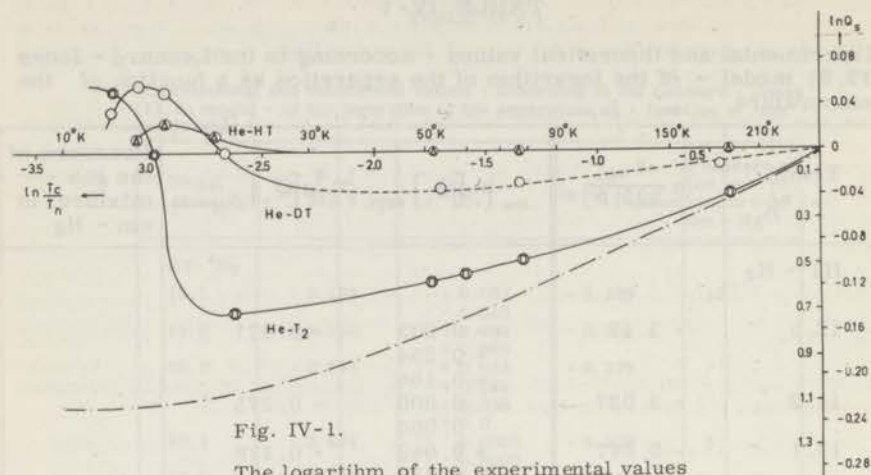
Fig. IV-1.

The logartihm of the experimental values of the separation $Q_s$ as a function of the logarithm of $\frac{T_c}{T_h}$, from room temperature to about 10 °K.

O    Experimental values for DT-$^4$He mixture.

    Experimental values for $T_2$-$^4$He mixture.

    Experimental values for HT-$^4$He mixture

-.-. Theoretical classical curve for $T_2$-$^4$He mixture only, with the inner scale for ln $Q_s$. The Lennard-Jones potential (12, 6) was used with $\frac{\varepsilon_{12}}{k}$=19.45 °K and $\sigma_{12}$=2.742 Å.

diffusion factor $\alpha$ shows a reversal of sign two times. This change of sign of $\alpha$ in the mixture $^4$He-$T_2$ appears to occur at about 20 °K and 13 °K, while for $^4$He-DT this happens at about 21 °K and 14 °K, which corresponds to a reduced temperature of 1 and 0.8 respectively. For the $^4$He-HT mixture, the reversal of sign of $\alpha$ occurs at about 15 °K in the positive part of the separation, while in the negative part no such change was detected.

For $^4$He-$T_2$ mixture, the calculated classical curve has been also shown in the same figure for which the force constants have been taken from Hirschfelder.[1] By comparing the experimental results with this classical curve we notice the large discrepancy which amounts from some percents at room temperature to about 100% at the low temperature region from 20 °K to 10 °K. These measurements show reasonable agreement in the neighbourhood of 300°K with the measurements done by Slieker and De Vries above 300 °K[2]. The inclination of the curve is about the same.

The $^4$He-DT mixture shows the same general behaviour as $^4$He-$T_2$. The only difference is in the magnitude of the separation, which is due to the mass difference, and in our belief to a large extent to the unsymmetry of the DT molecule, as the centre of mass of the DT molecule is not in

the middle of the two atoms. Our measurements do not agree with recent measurements done in this Laboratory by Slieker. He finds a separation with his Trennschaukel experiment between 100 °K and 300 °K which come very close to the measured $^4$He-T$_2$ curve of us.

For the mixture $^4$He-HT, no separation was detected from room temperature till about 30 °K. This is due to the fact that both $^4$He and HT molecules have the same mass and if there are some differences between them, this will be due to the mass distribution, which has contributed to the separation in the temperature region from 20 °K to 10 °K.

PAR. 3. THE MEASUREMENTS ON H$_2$-(T$_2$, DT, HT).

Unfortunately the results of the experiments H$_2$-T$_2$ and H$_2$-DT cannot be trusted due to the fact that some exchange takes place - even instantaneously - in the metal part of the ionisation chamber at room temperature according to the relations:

$T_2 + H_2 \rightleftarrows 2\,HT$  and

$H_2 + DT \rightleftarrows HD + HT$  or

$H_2 + 2\,DT \rightleftarrows 2\,HD + T_2$
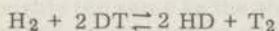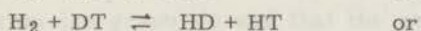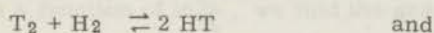
which leads to a large uncertainty.

By checking the experimental results of the H$_2$-T$_2$ mixture with those of H$_2$-HT, we have found that the two sets of values are approximately the same within the experimental error confirming the above supposition.

The activities and the pressures used for these mixtures are roughly the same as mentioned in Par. 2 of this chapter.

If the logarithm of the separation - for the H$_2$-HT mixture - is plotted as a function of $\ln\frac{T_c}{T_h}$, we obtain the curve shown in fig. IV-2.

Our H$_2$-HT measurements between 50 °K and 100 °K do not agree with recent measurements done by Slieker in this Laboratory and by Waldmann c. s.[3] done above 300 °K. The derivative of our curve is smaller than of these mentioned research workers.

From this figure we see that the experimental curve for this mixture follows the same behaviour as for the $^4$He mixtures discussed in Par. 2. For this mixture, the thermal diffusion factor changes sign at about 25 °K and 16 °K, which corresponds to reduced temperatures of about 0. 67 and 0. 43 respectively. In the temperature region between 11 °K and 13 °K the separation changes very abruptly. This may be due to adsorption of the HT molecule in the cold reservoir or to condensation. Another important reason is that the hydrogen pressure at this region of temperature is too small so that we may get pressure dependence as will be discussed now.

To deal with the condensation problem we notice that at 12 °K the vapour pressure of HT is 0. 73 mm, while that for H$_2$ is 12. 7 mm. As our activity has a partial pressure of about $10^{-6}$ atmosphere, then the radioactive pressure inside our apparatus will be $10^{-3}$ mm-Hg, which is far below the saterated vapour pressure of HT at 12 °K. No condensation is likely to occur.

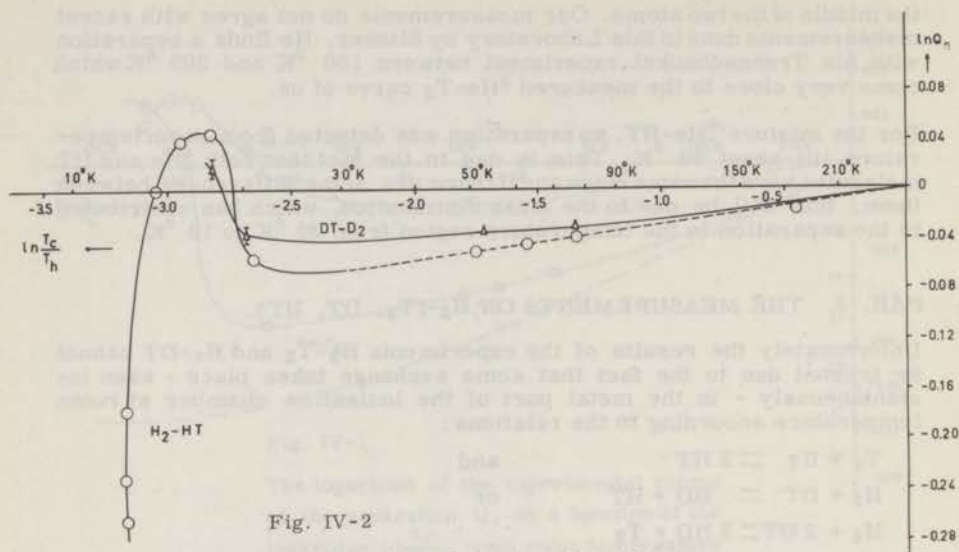There remains the problem of adsorption. As the geometrical area of our

Fig. IV-2

The logarithm of the experimental values
of the separation $Q_s$ as a function of the
logarithm of $\frac{T_c}{T_h}$, where $T_c$ is the variable
temperature, from room temperature to
$10\ ^\circ K$, and $T_h$ is the hot temperature fixed
always at $293\ ^\circ K$.

Δ  Experimental values for the DT-$D_2$
mixture.

O  Experimental values for the HT-$H_2$
mixture.

lower reservoir is about 100 cm$^2$ and if we suppose that this area is completely covered with one tenth of a monolayer of adsorbed HT molecules, which seems reasonable at a partial HT pressure so very far away from the saturation pressure, then the number of necessary HT molecules that will cover this area, will be $10^{17}$. The number of HT molecules per c. c. in the $H_2$-HT mixture is about $5 . 10^{16}$. This means that the number of HT molecules contained in the bottom reservoir is $5 . 10^{18}$, which is much more than the supposed one tenth monolayer contains. The adsorption therefore seems to be of minor influence.

Moreover, the measuring technique described in chapter II indicates that each time small quantities of gas are taken via the bypass from the cold reservoir to the ionisation chamber.

The only fear which remains is that the insufficient pressure of $H_2$ at 12 $^\circ K$ will cause a pressure dependance of the thermal diffusion factor. For temperatures above 12 $^\circ K$ this is not possible since then our working pressure has always been about 5 cm-Hg. Below 14 $^\circ K$ we are limited by the vapour pressure of hydrogen and our working pressure is of the order of 1 cm-Hg. According to Kotousov's [4] publication at room temperature a rapid decrease in the thermal diffusion factor occurs below pressures of 1 or 2 cm-Hg.

Here in our case the last three experimental points at about 12 °K lie very low, but correspond with a very large $\alpha$, which can never be understood from the Kotousov effect.


PAR. 4. THE MEASUREMENTS ON $D_2$-($T_2$, DT, HT).

From the mixtures $D_2$-$T_2$ and $D_2$-HT, although measured, the results will not be given for the same reason as mentioned in Par. 3 of this chapter, viz. because of disturbing exchange effects.

The only remaining mixture is $D_2$-DT which has a quantum parameter of 1.16.

The thermal diffusion factor $\alpha$ for this mixture shows a change of sign at about 21 °K. The measurements for this mixture have not been extended to 12 °K because of the low vapour pressure of $D_2$ at this temperature (0.73 mm-Hg). If we plot the logarithm of the experimental separation as a function of $\ln\frac{T_c}{T_h}$, we find the graph shown in fig, IV-2.

From the graph we see that the general behaviour of this mixture is roughly the same as the above mentioned ones. The problem of condensation and adsorption in case of this mixture does not play any role except for the last measured point only.


LIST OF REFERENCES IN CHAPTER IV

1. Hirschfelder, J.O., Curtiss, C.F. and Bird, R.B.,
   Molecular theory of gases and liquids,
   John Wiley & Sons, Inc., New York (1954).

2. Slieker, C.J.G. and De Vries, A.E.
   Societe de Chemie Physique, Paris 4-8 June 1962.
   Communication no. 33.

3. Slieker, C.J.G. (to be published)
   Schirdewahn, J., Klemm, A., Waldmann, L.
   Z. Naturforsch 16a, 133-144 (1961).

4. Kotousov, L.S.,
   Soviet Physics-Technical Physics, 7, 159 (1962).

LIST OF SYMBOLS IN CHAPTER IV

$\Lambda^*$      quantity used for comparing quantum deviations due to the associated wave length with a molecule.

$\epsilon$      depth of the potential field for the Lennard-Jones potential field

$\sigma$      distance of closest approach between colliding particles.

CHAPTER V

THEORETICAL CONSIDERATIONS

COMPARISON OF THEORY AND EXPERIMENT

Par. 1. GENERAL INTRODUCTION

As we have mentioned in chapter I, in order to calculate the thermal diffusion factor $\alpha$, we are in need of collision integrals as $\Omega^{1,1}$, $\Omega^{1,2}$ .... etc. For the calculation of these collision integrals the knowledge of the phase shifts $\eta_\ell(k)$ for every type of a binary mixture is necessary. These phase shifts can be calculated by solving the radial Schrödinger equation numerically. This exhibits an enormous amount of work beyond our existing ability.

To get a somewhat rough estimation - though not bad - avoiding the tremendous numerical work, we have found that it may be fruitful to interpolate the calculations from the existing theoretical work done by other people. These existing calculations are not complete. They have been done for different mixtures at very low temperatures from nearly zero till $T^* = 0.6$. This means from nearly zero to about 5 °K for $^4$He. Nevertheless by reasonable interpolation we hope that we are not too far from reality for those mixtures which will mainly be of interest to us in this chapter, viz. for Kr-$^4$He, Kr-$^3$He and Kr-$H_2$.

Par. 2. CLASSIFICATION OF THE COLLISION INTEGRALS

In order to perform such approximations, we have classified firstly the collision integrals available in the form of a table (see table V-1) as well as in graphs to give the required impression for the approximation.

Before discussing the interpolation procedure, we must mention that there are two ways of reducing the different quantities in classical and in quantum mechanics. In classical mechanics the normal way of reducing the cross section as well as the collision integrals, is to divide these by the corresponding regid sphere values. In quantum mechanics the reduction appears in a logical way by reducing the Schrödinger equation in the form: [4]

$$\frac{d^2}{dr^{*2}}(r^*\psi) + \left[ k^{*2} - \frac{\ell(\ell+1)}{r^{*2}} + \frac{16\pi^2}{\Lambda^{*2}}\left( \frac{1}{r^{*12}} - \frac{1}{r^{*6}} \right) \right] (r^*\psi) = 0$$

in which $r^* = \dfrac{r}{\sigma}$, $k^* = k\sigma$ and $\Lambda^* = \dfrac{h}{\sigma\sqrt{m\epsilon}}$

From this equation the cross section was derived and is given by:

$$Q^\ell(k) = \frac{2\pi}{g} \int_0^\pi (1 - \cos^\ell x)\,\alpha(k,x)\,\sin x\,dx$$

TABLE V-1.

Tabulation of the collision integrals

| | | Averaged cross-section : $\Omega^{\star}{}^{z}_{1j}$ | | | | values of $A_{ij}$ $B_{ij}$ $C_{ij}$ | | |
|---|---|---|---|---|---|---|---|---|
| | T | $\Omega^{\star(1,1)}_{ij}$ | $\Omega^{\star(1,2)}_{ij}$ | $\Omega^{\star(1,3)}_{ij}$ | $\Omega^{\star(2,2)}_{ij}$ | $A_{ij}$ | $B_{ij}$ | $C_{ij}$ |
| | $H_2$ - isotopes.[*] | | | | | | | |
| OO | 0.05 | 8.286 | | | 7.890 | 0.1905 | 0.7856 | 1.0234 |
| | 0.1 | 8.317 | | | 7.825 | 0.1641 | 0.7710 | 0.9879 |
| | 0.2 | 7.974 | | | 5.642 | 0.1415 | 0.7821 | 0.9632 |
| | 0.3 | 7.644 | | | 5.106 | 0.1336 | 0.7723 | 0.9558 |
| | 0.4 | 7.399 | | | 4.840 | 0.1308 | 0.7633 | 0.9566 |
| | 0.5 | 7.230 | | | 4.706 | 0.1302 | 0.7551 | 0.9612 |
| | 0.6 | 7.124 | | | 4.640 | 0.1303 | 0.7475 | 0.9662 |
| PP | 0.05 | 9.908 | | | 9.592 | 0.1936 | 0.8471 | 0.9441 |
| | 0.1 | 8.726 | | | 7.306 | 0.1675 | 0.7420 | 0.9346 |
| | 0.2 | 8.007 | | | 5.567 | 0.1391 | 0.7804 | 0.9559 |
| | 0.3 | 7.614 | | | 5.065 | 0.1331 | 0.7696 | 0.9505 |
| | 0.4 | 7.365 | | | 4.819 | 0.1309 | 0.7540 | 0.9553 |
| | 0.5 | 7.206 | | | 4.699 | 0.1304 | 0.7471 | 0.9635 |
| | 0.6 | 7.099 | | | 4.634 | 0.1306 | 0.7434 | 0.9709 |
| OD | 0.05 | 4.222 | | | 7.677 | 0.3637 | 0.8306 | 0.9319 |
| | 0.1 | 3.562 | | | 6.764 | 0.3799 | 0.8200 | 0.8784 |
| | 0.2 | 2.830 | | | 5.652 | 0.3995 | 0.7809 | 0.8661 |
| | 0.3 | 2.491 | | | 5.111 | 0.4103 | 0.7491 | 0.8902 |
| | 0.4 | 2.326 | | | 4.842 | 0.4164 | 0.7239 | 0.9190 |
| | 0.5 | 2.243 | | | 4.706 | 0.4198 | 0.7079 | 0.9457 |
| | 0.6 | 2.200 | | | 4.641 | 0.4219 | 0.6975 | 0.9702 |

[*] The $H_2$-isotope collision integrals are given as $\Omega^*$ not as $\Omega^{\star}$.

| | | | | | | | | |
|---|---|---|---|---|---|---|---|---|
| | $^3$He-$^4$He [2,3] | | | | | | | |
| | 0.00 | | | | 2.21 | 0.400 | 0.600 | 1.200 |
| | 0.025 | 1.24 | | | 1.54 | 0.357 | 0.656 | 0.690 |
| | 0.05 | 0.862 | | | 1.68 | 0.361 | 0.569 | 0.865 |
| | 0.10 | 0.869 | | | 2.32 | 0.386 | 0.630 | 1.04 |
| | 0.20 | 0.989 | | | 2.67 | 0.465 | 0.655 | 1.14 |
| | 0.30 | 1.14 | | | 2.91 | 0.474 | 0.655 | 1.14 |
| | 0.40 | 1.26 | | | 2.91 | 0.460 | 0.655 | 1.14 |
| | $^3$He-$^3$He [2,3] | | | | | | | |
| | 0.00 | | | | | 0.400 | 0.600 | 1.20 |
| | 0.025 | 0.648 | | | 0.858 | 0.265 | 0.543 | 1.13 |
| | 0.05 | 0.878 | | | 1.02 | 0.232 | 0.657 | 1.17 |
| | 0.10 | 1.07 | | | 1.11 | 0.208 | 0.811 | 1.06 |
| | 0.20 | 1.13 | | | 1.42 | 0.250 | 0.574 | 1.06 |
| | 0.30 | 1.29 | | | 1.93 | 0.301 | 0.429 | 1.21 |
| | 0.40 | 1.54 | | | 2.46 | 0.318 | 0.408 | 1.28 |
| | $^4$He-$^4$He [2,3] | | | | | | | |
| | 0.00 | | | | | 0.267 | 0.800 | 0.800 |
| | 0.025 | 4.73 | | | 4.34 | 0.184 | 0.845 | 0.602 |
| | 0.05 | 2.36 | | | 1.87 | 0.158 | 0.539 | 0.680 |
| | 0.10 | 1.77 | | | 2.71 | 0.305 | 0.247 | 1.14 |
| | 0.20 | 2.50 | | | 3.72 | 0.297 | 0.750 | 1.21 |
| | 0.30 | 2.81 | | | 3.75 | 0.267 | 0.831 | 1.08 |
| | 0.40 | 2.95 | | | 3.42 | 0.232 | 0.773 | 1.02 |

for which the first and second approximations are :

$$Q^{(1)} = 2\left(\frac{2\pi}{k^2}\right) \sum_{\ell=0,1,2,\ldots}^{\infty} (\ell + 1) \sin^2 (\eta_{\ell+1} - \eta_\ell) \qquad \text{and}$$

$$Q^{(2)} = \left(\frac{2\pi}{k^2}\right) \sum_{\ell=0,1,2,\ldots}^{\infty} \frac{(\ell+1)(\ell+2)}{(\ell+\frac{3}{2})} \sin^2 (\eta_{\ell+2} - \eta_\ell).$$

These are the cross sections when the two colliding particles are not identical. However, when the two colliding particles are identical, they obey either Fermi-Dirac statistics or Bose-Einstein statistics. [2,4] In the first case only summation over odd values of $\ell$ should be taken, in the second case only summation over even values of $\ell$. So for two identical particles, taking the spin s into consideration, the cross sections become :

$$Q^{(n)}_{B.E.} = \frac{S+1}{2S+1} Q^{(n)}_{B.E.} + \frac{S}{2S+1} Q^{(n)}_{F.D.} \qquad \text{and}$$

$$Q^{(n)}_{F.D.} = \frac{S+1}{2S+1} Q^{(n)}_{F.D.} + \frac{S}{2S+1} Q^{(n)}_{B.E.}$$

The reduced cross section is written as $Q^* = \dfrac{Q}{\sigma^2}$

and the collision integrals are given by :

$$\Omega^{n,r}(T) = \sqrt{\frac{kT}{\pi m}} \int_0^\infty e^{-\gamma^2} \gamma^{2r+3} Q^{(n)}(k) \, d\gamma$$

which when reduced, become :

$$\Omega^{*n,r} = \frac{\Omega^{n,r}}{\sigma^2 \sqrt{\epsilon/m}}$$

So the relation between the reduced quantum collision integrals and the reduced classical collision integrals, given by Hirschfelder, is :

$$\Omega^{+\ell,s}_{ij} = \sqrt{\frac{2\mu_{ij}}{\epsilon_{ij}}} \frac{1}{\sigma^2_{ij}} \Omega^{\ell,s}_{ij} =$$

$$= \sqrt{\frac{2\mu_{ij}}{\epsilon_{ij}}} \frac{1}{\sigma^2_{ij}} \sqrt{\frac{kT}{2\pi\mu_{..}}} \tfrac{1}{2}(S+1)! \left[ 1 - \tfrac{1}{2} \frac{1+(-1)^\ell}{1+\ell} \right] \pi \sigma^2_{ij} \Omega^{*\ell,s}_{ij} =$$

$$= \sqrt{T^*} \frac{\sqrt{\pi}}{2} (s+1)! \left[ 1 - \tfrac{1}{2} \frac{1+(-1)^\ell}{1+\ell} \right] \Omega^{*\ell,s}_{ij}$$

After these reductions have been made, the graphs of $\Omega^{*\ell,s}_{ij}$ as a function of $T^*$ were plotted as shown in fig. V-1.

In the case that we plot $C_{ij}$ (see I-32d) as a function of $T^*$ the following reductions were performed :

$$C^*_{ij} = \frac{\Omega^{*1,2}_{ij}}{\Omega^{*1,1}_{ij}} = \frac{\dfrac{\sqrt{\dfrac{2\pi\mu_{ij}}{kT}}\,\left[\Omega^{\ell,s}_{ij}\right]^{1,2}}{\left[\frac{1}{2}(s+1)!\left\{1-\frac{1}{2}\frac{1+(-1)^{\ell}}{1+\ell}\right\}\pi\sigma^2_{ij}\right]^{1,}}}{\dfrac{\sqrt{\dfrac{2\pi\mu_{ij}}{kT}}\,\left[\Omega^{\ell,s}_{ij}\right]}{\left[\frac{1}{2}(s+1)!\left\{1-\frac{1}{2}\frac{1+(-1)^{\ell}}{1+\ell}\right\}\pi\sigma^2_{ij}\right]^{1,1}}} = \frac{\Omega^{1,2}_{ij}/6}{\Omega^{1,1}_{ij}/2} =$$

$$= \frac{\Omega^{1,2}_{ij}}{3\,\Omega^{1,1}_{ij}} = \frac{1}{3}\left(\frac{2\,\Omega^{1,2}_{ij}}{5\,\Omega^{1,1}_{ij}}\right)\frac{5}{2} = \frac{5}{6}\,C_{12}$$

To perform the interpolation of the quantum curve, we have to discuss the curves in fig. V-1. For the curves in fig. V-1a, the collision integrals between like molecules $\Omega^{*1,1}_{i,i}$ have been drawn as a function of the temperature $T^*$. In evaluating these collision integrals, the statistics of the molecules - i.e. not only the wave function, but also the spin function have been taken into consideration.

Whereas these statistical effects differ from one atom to another, we see the strange behaviour of the collision integral cruves differing considerably from the classical behaviour which should give a limit. According to these curves we see that the more the quantum parameter $\Lambda^*$ decreases, the more these curves deviate from the classical curve, Moreover, the $^3$He-$^3$He curve goes in the opposite direction from the classical curve.

As is well known the more the quantum parameter $\Lambda^*$ approaches zero, the more the quantum curves approach the classical ones. For a true comparison of mixtures obeying different statistics, the different parameters occurring in the calculations must be the same. In our mixtures we lack such a correspondence. For this reason we think it much safer that the interactions between identic particles are not taken into consideration. For the interaction of unlike particles we have only one sort of statistics which encouraged us in that case to try further calculations. So we have found it safer not to interpolate the curves for $\Omega^{*1,1}_{i,i}$.

Another reason that makes these interpolations very difficult is that these collision integral cruves have been calculated for only small values of $T^*$ - viz. $T^* < 0.6$. To find values for these integrals at $T^* \approx 2$, holding for our mixtures Kr-$^4$He, Kr-$^3$He and Kr-$H_2$, is subject to a large uncertainty which will introduce a large error in the interpolated curve.

The curves of fig. V-1b of the collision integrals $\Omega^{*2,2}_{i,i}$ between like particles as a function of temperature, are more reasonable. The deviations of these curves from the classical one increase as the corresponding values of $\Lambda^*$ increase. As our quantum parameter $\Lambda^*$ for most of our $^{85}$Kr mixtures has a mean value of about 0.8, the collision integrals for this value of $\Lambda^*$ must lie between the curve corresponding to $\Lambda^* = 1.22$ for either $pD_2$-$pD_2$ or $oD_2$-$oD_2$ and the classical curve corresponding to $\Lambda^* = 0$. If we examine these graphs carefully, we can see how difficult and unreliable such an interpolation will be.
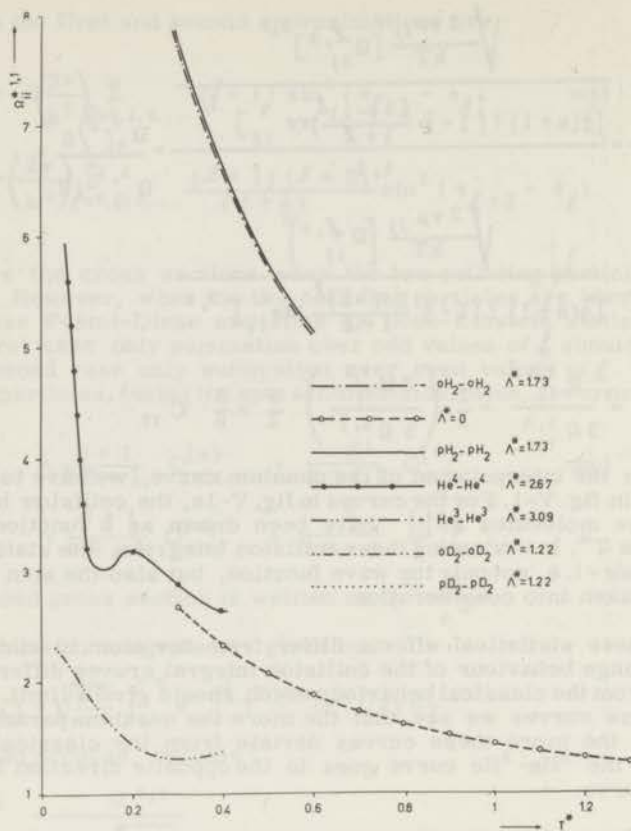
Fig. V-1a.

The reduced values of the collision integral $\Omega^{*}{}^{1,1}_{1,1}$ between identical particles, both quantum mechanical and classical as a function of the reduced temperature. The $pD_2$ and $oD_2$ data have been taken from E. A. de Kerf's and M. H. J. J. Ernst, work before publication, for which we thank him very much. [1]
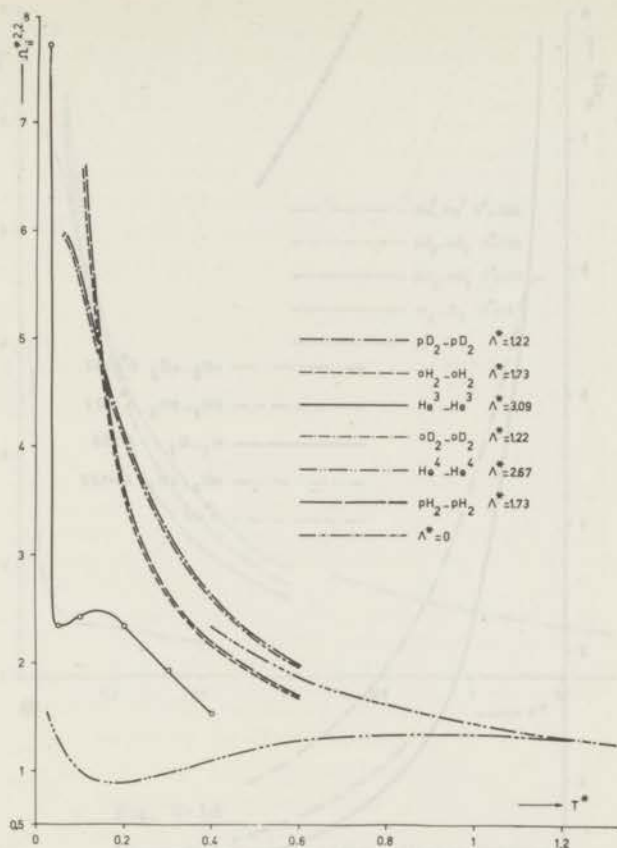
Legend:
- $oH_2$-$oH_2$ $\Lambda^{*} = 1.73$
- $\Lambda^{*} = 0$
- $pH_2$-$pH_2$ $\Lambda^{*} = 1.73$
- $He^4$-$He^4$ $\Lambda^{*} = 2.67$
- $He^3$-$He^3$ $\Lambda^{*} = 3.09$
- $oD_2$-$oD_2$ $\Lambda^{*} = 1.22$
- $pD_2$-$pD_2$ $\Lambda^{*} = 1.22$

Fig. V-1b.

The reduced values of the collision integral $\Omega^{*2,2}_{i\ i}$ between identical particles, both quantum mechanical and classical as a function of the reduced temperature.

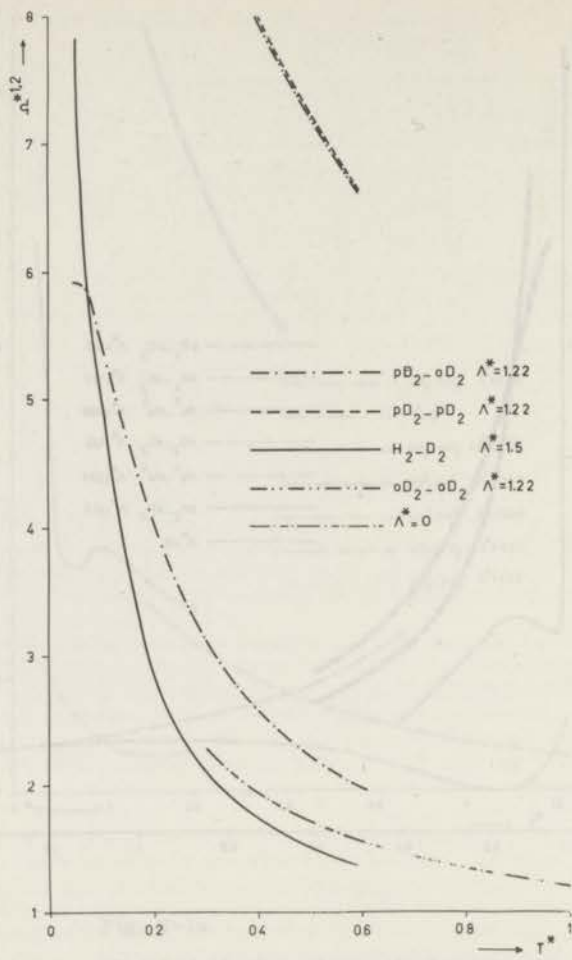$pD_2$ and $oD_2$ from E.A. de Kerf and M. H. J. J. Ernst.

Fig. V-1c.

The reduced values of the collision integral $\Omega^{*1,2}$ between identical as well as different particles, both quantum mechanical and classical as a function of the reduced temperature.

$pD_2$ and $oD_2$ as well as $H_2$-$D_2$ from E. A. de Kerf and M. H. J. J. Ernst.
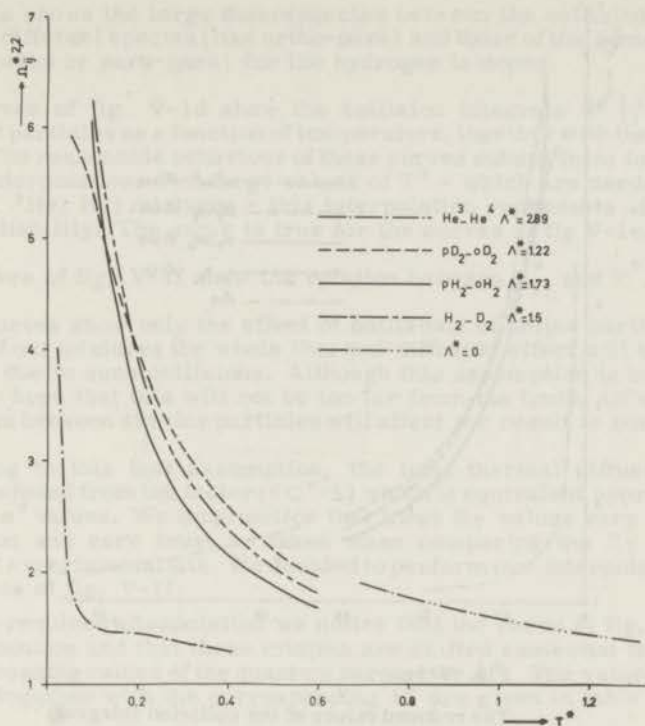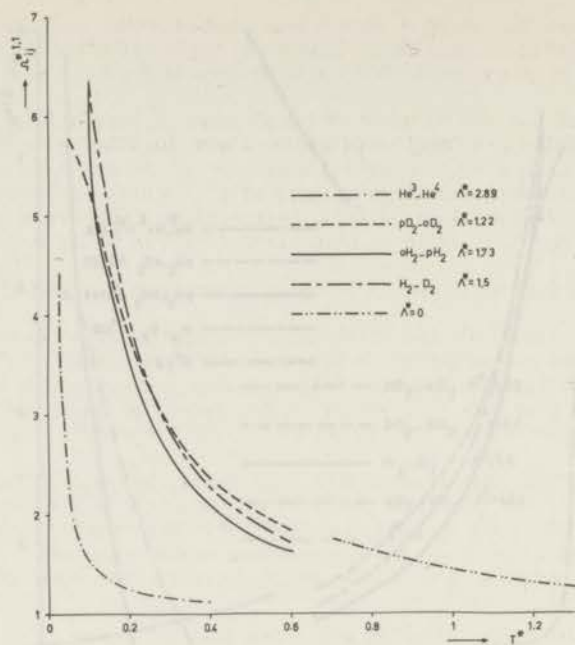
Fig. V-1d

The reduced values of the collision integrals
$\Omega_{ij}^{*2,2}$ between different particles, both
quantum mechanical and classical as a
function of the reduced temperature.
$pD_2$ and $oD_2$ as well as $H_2 - D_2$ from E. A.
de Kerf and M. H. J. J. Ernst.

Legend in figure:
$He^3 - He^4 \quad \Lambda^* = 2.89$
$pD_2 - oD_2 \quad \Lambda^* = 1.22$
$pH_2 - oH_2 \quad \Lambda^* = 1.73$
$H_2 - D_2 \quad \Lambda^* = 1.5$
$\Lambda^* = 0$

89

Fig. V-1e.

The reduced values of the collision integral $\Omega^{*\,1,1}_{i\,j}$ between different particles, both quantum mechanical and classical as a function of the reduced temperature.
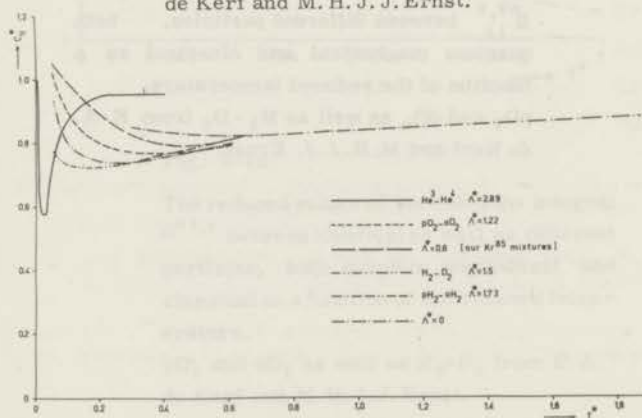$pD_2$ and $oD_2$ as well as $H_2 - D_2$ from E. A. de Kerf and M. H. J. J. Ernst.



Fig. V-1f.

The reduced values of $C^{*}_{i\,j}$, both quantum mechanical and classical as a function of the reduced temperature.
$pD_2$ and $oD_2$ as well as $H_2 - D_2$ from E. A. de Kerf and M. H. J. J. Ernst.

Fig. V-1c shows the large discrepancies between the collision integrals $\Omega^{*\,1,2}$ of different species (like ortho-para) and those of the same species (Ortho-ortho or para-para) for the hydrogen isotopes.

The curves of fig. V-1d show the collision integrals $\Omega^{*\,1,1}_{ij}$ between different particles as a function of temperature, together with the classical curve. The reasonable behaviour of these curves submit them to a certain kind of interpolation. For large values of $T^*$ - which are needed for our $Kr$-($^4He$, $^3He$, $H_2$) mixtures - this interpolation represents difficulties and unreliability. The same is true for the curves of fig V-1e. ($\Omega^{*\,2,2}_{ij}$)

The curves of fig. V-1f show the relation between $C^*_{ij}$ and $T^*$.

These curves show only the effect of collisions of unlike particles. And in case of our mixtures the whole thermal diffusion effect will be assumed to be due to such collisions. Although this assumption is not strictly true, we hope that this will not be too far from the truth. Of course the collisions between similar particles will affect the result to some extent.

According to this last assumption, the total thermal diffusion effect should be found from the factor $(6C^*-5)$ which is equivalent approximately to $R_T$ or $\alpha^*$ values. We must notice that these $R_T$ values vary with concentration and care must be taken when comparing the $R_T$ values of different experimentalists. We decided to perform our interpolation from the curves of fig. V-1f.

To do the required interpolation we notice that the curve of fig. V-1f has certain minima and that these minima are shifted somewhat to the right with decreasing values of the quantum parameter $\Lambda^*$. The values of these minima together with the corresponding $\Lambda^*$ are given in table V-2a.

TABLE V-2a

| $\Lambda^*$ | $T^*$ | $[C^*_{ij}]_{min.}$ |
|---|---|---|
| 2.89 | 0.025 | 0.575 |
| 1.73 | 0.165 | 0.720 |
| 1.50 | 0.250 | 0.739 |
| 1.22 | 0.390 | 0.765 |
| 0.00 | 0.600 | 0.820 |

Here $T^*$ represents the temperature of the minimum value and $[C^*_{ij}]$ min. represents the value of $C^*_{ij}$ at this minimum.

By plotting a graph between $\Lambda^*$ and $C^*_{ij}$, we see that at a $\Lambda^* = 0.78$ we have a minimum value for $C^*_{ij}$ of 0.792.

Moreover, by plotting a graph between $\Lambda^*$ and $T^*$, we see that this minimum value of $C^*_{ij}$ - for $\Lambda^* \simeq 0.78$ - occurs at a reduced temperature 0.5.

Some extra points have been interpolated according to the fact that the ratio of the distances between any pair of points on the curves of fig. V-1f must be proportional to the ratio between their corresponding $\Lambda^*$. In this way another set of points was derived, giving the required interpolated curve for our mixtures ($\Lambda^* \simeq 0.8$).

In this way the corresponding curves of $\alpha^*$ were obtained, as was shown in chapter I, fig. I-3.and fig. V - 2 in this chapter.
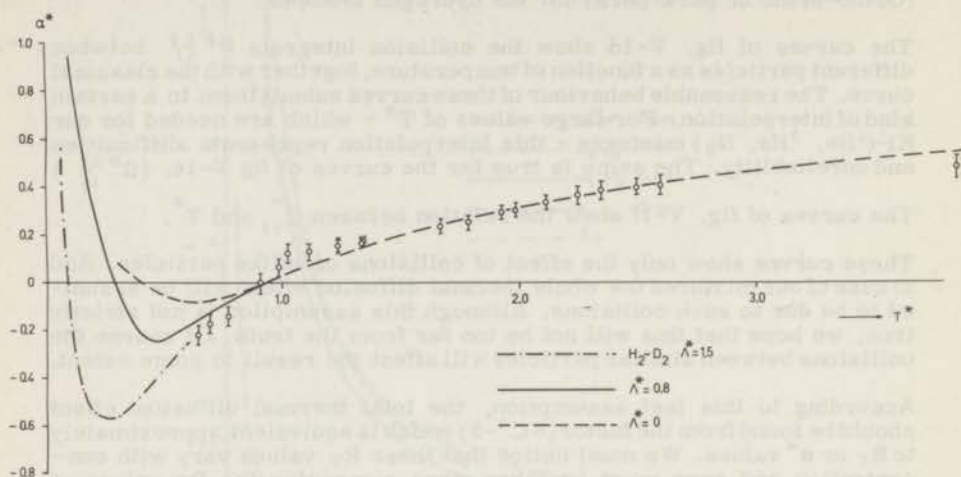


Fig. V-2

The reduced values of the thermal diffusion
factor $\alpha^*$ for $^{85}$Kr-$H_2$ mixture as a function
of the reduced temperature.

-.-. theoretical quantum curve for $\Lambda^* = 15$

——— interpolated curve for $\Lambda^* \simeq 0.8$

- - - classical curve for $\Lambda^* = 0$

⊥
○   experimental points with standard
⊤
    deviation

## Par. 4. INTERPRETATION OF THE $^{85}$Kr-$H_2$ RESULTS.

By drawing the tangent to the experimental curve showing the relation
between $\ln\frac{T\,\text{var.}}{303.3}$ against $\ln Q_s$, the thermal diffusion factor was deter-
mined as mentioned in chapter III. These thermal diffusion factors have
been given in table V-2 as a function of temperature.

The thermal diffusion factor for the $^{85}$Kr-$H_2$ mixture is given by:

$$\alpha = \frac{- M_2 + \frac{3S}{A_{12}}\left[ M_1^2\,(M_1 - M_2) \right] + 4S\,M_1 M_2}{6\,M_1^2 + 5\,M_2^2 - 4\,M_2^2 B_{12} + 8\,M_1 M_2 A_{12}}\; 5\,(C_{12} - 1)$$

92

## TABLE V-2

The experimental values of the thermal diffusion factor and the reduced thermal diffusion factor as a function of temperature for the $^{85}Kr - H_2$ mixture.

| T °K | T* | $\ln \dfrac{T_{var.}}{303.3}$ | $\alpha$ expt. | $\alpha^* = \dfrac{\alpha \text{ expt.}}{\alpha_{R.E.S.}}$ |
|---|---|---|---|---|
| 50.0 | 0.64 | - 1.80 | - 0.23 | - 0.22 |
| 54.2 | 0.69 | - 1.70 | - 0.18 | - 0.17 |
| 60.0 | 0.77 | - 1.62 | - 0.15 | - 0.14 |
| 70.8 | 0.90 | - 1.45 | 0.00 | - 0.00 |
| 76.8 | 0.98 | - 1.35 | + 0.07 | + 0.06 |
| 80.0 | 1.02 | - 1.33 | + 0.13 | + 0.12 |
| 87.0 | 1.11 | - 1.25 | + 0.15 | + 0.14 |
| 96.0 | 1.23 | - 1.15 | + 0.16 | + 0.15 |
| 104.0 | 1.33 | - 1.07 | + 0.17 | + 0.16 |
| 105.0 | 1.34 | - 1.06 | + 0.18 | + 0.17 |
| 130.0 | 1.66 | - 0.85 | + 0.24 | + 0.23 |
| 140.0 | 1.78 | - 0.77 | + 0.27 | + 0.25 |
| 150.0 | 1.92 | - 0.70 | + 0.30 | + 0.29 |
| 155.0 | 1.98 | - 0.67 | + 0.32 | + 0.30 |
| 165.0 | 2.11 | - 0.61 | + 0.35 | + 0.33 |
| 175.0 | 2.24 | - 0.55 | + 0.38 | + 0.36 |
| 183.0 | 2.34 | - 0.50 | + 0.40 | + 0.38 |
| 195.0 | 2.49 | - 0.44 | + 0.42 | + 0.39 |
| 203.0 | 2.59 | - 0.40 | + 0.43 | + 0.41 |
| 303.3 | 3.86 | - 0.00 | + 0.50 | + 0.47 |

$$\alpha_{R.E.S.} = 1.06 \quad \left[\frac{\epsilon_{12}}{k}\right]_{^{85}Kr-H_2} = 78.4 \ ^{\circ}K \quad [\sigma_{12}]_{^{85}Kr-H_2} = 3.29 \ \text{Å}$$

where $s = \left(\dfrac{\sigma_{12}}{\sigma_2}\right)^2 \dfrac{1}{\sqrt{2M}} \dfrac{\Omega^{*2,2}(T_{12}^*)}{\Omega^{*2,2}(T_2^*)}$ and $A_{12}=0.4, B_{12} = 0.6, C_{12}=1.2,$

For rigid elastic spheres all $\Omega^{*l}$ s are put equal to 1. The values taken for the parameters $\sigma$ are the Lennard-Jones values $\sigma_{12} = 3.29$ and $\sigma_2 = 2.93$ from Hirschfelder.

From these values it was found that $\alpha_{R.E.S.} = 1.06$

By dividing the experimental value $\alpha_{expt.}$ by the above value $\alpha_{R.E.S.}$ we get what we will call $\alpha_{expt.}^*$ or $\left[R_T\right]_{expt.}$ . These experimental values of $R_T$ - as shown in table V-2 - have been plotted as a function of $T^*$

together with their standatd deviations.

By comparing these results with the interpolated quantum curve, we see that there is some agreement between the experimental and the interpolated values. ($\Lambda^* = 0.8$).

## Par. 5. INTERPRETATION OF THE $^{85}$Kr-$^4$He AND $^{85}$Kr-$^3$He RESULTS

The same process as used in par. 4 has been used for the $^{85}$Kr-$^4$He and the $^{85}$Kr-$^3$He measurements. The plot of the experimental values of $R_T$ against $T^*$, as tabulated in table V-3, has been shown in fig. V-3.
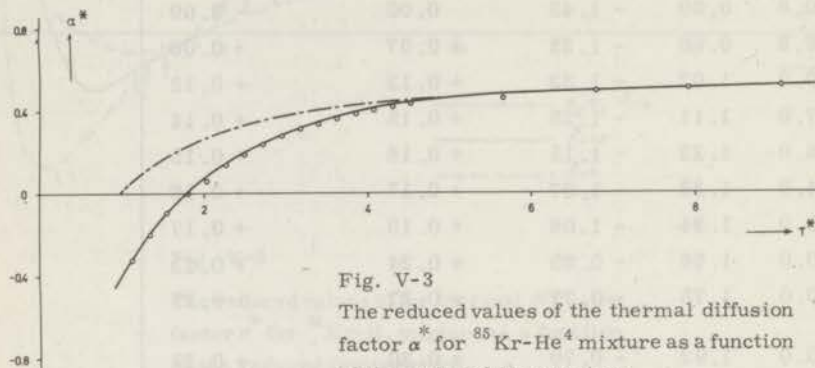


Fig. V-3

The reduced values of the thermal diffusion factor $\alpha^*$ for $^{85}$Kr-He$^4$ mixture as a function of the reduced temperature.

- - - - classical curve for $\Lambda^* = 0$

o     experimental points

By comparing the experimental curve for this mixture with the classical calculated $R_T = 5(C_{12} - 1)$ curve, we see that the zero value of the experimental thermal diffusion factor occurs at a $T^*$ value of about 2. This is in contradiction with the classical thermal diffusion factor which equals zero at about $T^* = 1$. Moreover, the position of this zero value of $\alpha^*_{expt.}$ nearly occurs at the same absolute temperature as for the mixture $^{85}$Kr-H$_2$. Above this temperature the experimental $R_T$ values deviate appreciably from the classical curve and approach it asymtotically at about room temperature.

The behaviour is very strange. Some trials have been done - as mentioned in chapter III - to explain the $^{85}$Kr-$^4$He results on a completely classical basis. We showed in fig. III-5a that at high temperatures the Lennard-Jones (12, 6) potential fits nicely, whereas in the low temperature region the softer Lennard-Jones (4, 8) potential model gives better agreement.

The same difficulties rise if one wants to explain the $^{85}$Kr-$^3$He results.

## Par. 6. THE TRITIUM MIXTURES.

By using the same interpolation technique, we have not succeeded to interpret the positive separation in the low temperature region for the tritium mixtures. Moreover, the large discrepancies between the theoretical classical curve - according to the Lennard-Jones potential - and the experimental one cannot also be explained by such an interpolation.

## TABLE V-3

The experimental values of the thermal diffusion factor and the reduced thermal diffusion factor as a function of temperature for the $^{85}Kr - {}^4He$ mixture.

| T °K | T* | $\alpha$ tang. expt. | $\alpha$* |
|------|------|---------|---------|
| 50   | 1.13  | - 0.55  | - 0.47  |
| 60   | 1.36  | - 0.34  | - 0.29  |
| 70   | 1.59  | - 0.16  | - 0.137 |
| 80   | 1.81  | - 0.00  | 0.000   |
| 90   | 2.04  | + 0.10  | 0.086   |
| 100  | 2.27  | 0.24    | 0.206   |
| 110  | 2.50  | 0.33    | 0.283   |
| 120  | 2.72  | 0.41    | 0.352   |
| 130  | 2.95  | 0.45    | 0.386   |
| 140  | 3.18  | 0.54    | 0.463   |
| 150  | 3.40  | 0.58    | 0.498   |
| 160  | 3.63  | 0.62    | 0.532   |
| 170  | 3.86  | 0.66    | 0.566   |
| 180  | 4.08  | 0.69    | 0.593   |
| 190  | 4.31  | 0.72    | 0.618   |
| 200  | 4.53  | 0.74    | 0.635   |
| 250  | 5.67  | 0.81    | 0.695   |
| 300  | 6.80  | 0.85    | 0.73    |
| 350  | 7.93  | 0.87    | 0.747   |
| 400  | 9.07  | 0.88    | 0.755   |
| 450  | 10.02 | 0.89    | 0.764   |
| 500  | 11.33 | 0.89    | 0.764   |

$$\alpha_{R.E.S.} = 1.165 \qquad \left[\frac{\epsilon_{12}}{k}\right]_{{}^{85}Kr-H_2} = 44 \; °K \qquad \left[\sigma_{12}\right]_{{}^{85}Kr-{}^4He} = 3.093 \; \text{Å}$$

If we keep in mind that the quantum calculations - all the collision integrals - have been calculated according to the Lennard-Jones spherical potential field, then some doubt might exist as to the validity of these calculations for non-spherical molecules. This leads us to try some other field which may explain these experimental results in the future.

For the interaction of two $H_2$ molecules which is calculated from first principles by de Boer[5], there is clearly a temperature dependent part in the averaged potential. De Boer showed that for the interaction of two $H_2$ molecules this temperature dependent part can be neglected. However, when working with asymmetric molecules, it might be that the linear azimuthal terms in the potential would not cancel out as is the case with the symmetric $H_2$-molecule. We therefore applied a method, developed by Kihara, Midzuno and Kaneko[6] for estimating the influence of nonsphericallity of symmetric molecules to asymmetric molecules. The scheme followed is outlined here.

We will assume with Kihara[6] that within each diatomic molecule there is a distribution of charges $\varrho(\overline{s}) \geqslant 0$ and that this distribution satisfies the normalised volume integral :

$$\int \varrho\,(\overline{s})\ d\overline{s} = 1 \qquad (V-1)$$

where $\overline{s}$ is the radius vector from the centre of the molecule to the source element. The centre of the molecule will be defined as the mean value of the distribution, so that :

$$\int \overline{s}^2 \varrho(\overline{s})\ d\overline{s} = \frac{\text{o symmetric}}{\text{const. x } \delta^2 \text{antisymmetrical}} \qquad (V-2)$$

where $\delta$ is half the distance between the two molecules.

We will also suppose that the interaction between the molecules 1 and 2 will be given by :

$$V(\overline{r}) = \int \varrho\,(s_1)\ d\overline{s}_1 \int \varrho\,(\overline{s}_2) u(/\overline{r} + \overline{s}_2 - s_1/)\ d\overline{s}_2 \qquad (V-3)$$

Now, by assuming that the charge distributions inside the molecule, can be approximated by a net point charge situated at the "mean centre" then the deviation of the real distribution from the assumed one is given by:

$$\int \overline{s}^2\,(\overline{s})\ d\overline{s} = \frac{\delta^2 \text{ symmetrical}}{\text{const. x } \delta^2 \text{ antisymmetrical}} \qquad (V-4)$$

We will assume also that the effective potential field $V_{eff.}$ will be given by Kirkwood's equation :

$$V_{eff.}\ (\overline{r}) = \frac{\iint V(r)\ e^{-\frac{V(r)}{KT}}\ d\omega_a\,d\omega_b}{\iint e^{-\frac{V(r)}{KT}}\ d\omega_a\ d\omega_b} \qquad (V-5)$$

where the factor $e^{-\frac{V(r)}{KT}}$ is a Boltzmann weighing factor to account for the fact that statistically the molecules spend more time in those orientations for which the energy is small.

When evaluating equation (V-5), we get :

$$V_{eff.} = <V(r)>_{average} + \frac{1}{2\,kT}\,[<V>^2_{average} - <V^2>_{average}\,] \qquad (V-6)$$

Taking these equations and assumptions into consideration we have found for the effective field of $T_2$-$^4$He the following expression:

$$V_{eff.}(r) = u(r) + \frac{\delta^2}{12}\left[\frac{5u'}{r} + u''\right] \tag{V-7}$$

and for HT-$^4$He mixture :

$$V_{eff.}(r) = u(r) + \frac{9\delta^2}{48}\left[\frac{5u'}{r} + u''\right] + \frac{\delta^2}{12kT}(u')^2$$

from which we see that with antisymmetrical molecules a temperature term appears in the potential field. This may contribute to some extent to the discrepancies between the different mixtures.

As we see also in the case of asymmetric molecules only a second order correction appears as well in the temperature dependent part as in the temperature independent part. The influence of these corrections is very small however.

LIST OF REFERENCES IN CHAPTER V.

1. Kerf, E. A. de, Ernst, M. H. J. J.
   Physica, (Incourse of publishing)

2. Cohen, E. G. D., Offerhaus, M. J., Roos, B. W. and Boer, J. de
   Physica, 22, 791 (1956).

3. Cohen, E. G. D., Offerhaus, M. J. and Boer, J. de,
   Physica, 20, 501 (1954) and
   Physica, 20, 515 (1954).

4. Hirschfelder, J. O., Curtiss, C. F. and Bird, R. B.,
   Molecular theory of gases and liquids,
   John Wiley & Sons, Inc., New York (1954).

5. Boer, J. de,
   Physica, 9, 363 (1942).

6. Kihara, T., Midzuno, Y. and Kaneko, S.,
   J. Phys. Soc. (Japan), 11, 362 (1956).

## LIST OF SYMBOLS USED IN CHAPTER V.

$A, B, C$ — numbers involved in the equation of the thermal diffusion factor

$A^*, B^*, C^*$ — reduced values of the above values

$g$ — relative velocity between two colliding particles

$i, j$ — atomic species

$\kappa$ — Boltzmann constant $1.38 \times 10^{-16}$ erg/degree

 — wave number corresponding to the relative velocity of two colliding molecules

$k^*$ — equals to $\frac{k}{\sigma}$

$\ell$ — angular momentum quantum number between two colliding particles

$M_1, M_2$ — equal $\frac{m_1}{m_1 + m_2}$, $\frac{m_2}{m_1 + m_2}$ respectively

 — where $m_1$ and $m_2$ are the masses of the two particles

$Q^\ell(k)$ — $\ell^{\text{th}}$ approximation in the cross section

$r^*$ — reduced distance between two colliding molecules equals $\frac{r}{\sigma}$

$\bar{s}$ — radius vector from the centre of the molecule to the source element

$T$ — absolute temperature

$u', u''$ — equal to $\frac{du}{dr}$, $\frac{d^2u}{dr^2}$

$V(r)$ — potential field between two colliding particles

$\alpha(k, \varkappa)$ — probability of finding a particle within a solid angle $d\omega$

$\gamma$ — equals to $\sqrt{\dfrac{k^2}{mKT}}$

$\delta$ — equals half the distance between the two atoms of a molecule

$\epsilon$ — depth of the potential field in the Lennard-Jones (12, 6) model

$\eta_\ell(k)$ — phase shift between two colliding particles

$\Lambda^*$ — a quantity used for comparing quantum deviations

$\mu$ — reduced mass of two colliding particles equals $\dfrac{m_1 m_2}{m_1 + m_2}$

$\varrho(\bar{s})$ — charge density

$\sigma$ — distance of closest approach between two colliding particles

$\lambda$ — angle of deflection

$\Psi$ — wave function of two colliding particles

$d\omega_a, d\omega_b$ — solid angles

SUMMARY

The aim of this work was to study the thermal diffusion factor as a function of temperature in binary mixtures of the quasi-Lorentzian type. For this purpose we used $^{85}$Kr as a heavy radioactive tracer molecule in the successive gases $^{22}$Ne, $^4$He, $^3$He and $H_2$. The research was done with the purpose:

a. to check the Lennard-Jones collision parameters given by Hirschfelder for a classical Chapman - Enskog description of the thermal diffusion factor.
b. to see if below 100 °K quantum effects would become noticeable which can be expected according to the quantum parameters $\Lambda^*$ and the ($\epsilon/k$) values of the above mixtures.


The temperature range was taken from 800 °K till 50 °K. The lower limit was determined by the vapour pressure of the krypton gas, although very minor quantities of this gas could be used because of its radioactivity. We used counting technics, and the so called two-bulb method The experiments with $^{22}$Ne were only done to check the measuring method as this gas mixture certainly should behave classically ($\Lambda^*$ = 0.28, $\epsilon/k$ = 77 °K and $\sigma_{12}$ = 3.22 Å). Indeed, perfect agreement was found between experiments and theory (Chapter III), down till 80 °K.

The measurements done with $^{85}$Kr in respectively $^4$He and $^3$He show a completely similar behaviour. Above room temperature the description is classical, with a Lennard-Jones (12, 6) potentail with $\epsilon_{12}/k$ = 44 °K and $\sigma_{12}$ = 3.095 Å. Below 100 °K the description would fit much better with a L.J. (4, 8) potential. One might say that the decrease in the reduced experimental thermal diffusion factor $\alpha^*_{exp}$ is due to the increased softness of the repulsive force below $T^*$ = 3.

The $^{85}$Kr- $H_2$ measurements (Chapter III) showed good agreement in the high temperature region (100 °K < T < 800 °K) with classical calculations on basis of a L.J. (12, 6) potential model with $\sigma_{12}$ = 3.29 Å and $\epsilon_{12}/k$= 78 °K. The quantum deviations below 100 °K down till 50 °K are of the same order of magnitude as in the Kr - He case, which, perhaps, can be expected from $\Lambda^*$ being 0.76 for Kr-$H_2$. Moreover, we observe an extra deviation between 100 °K and 300 °K, which probably has to do with the excitation of the first rotational energy level in the $H_2$ molecule.


In Chapter V we have tried to classify all known quantum collision integrals. We think that the ($C^*_{ij}$, $T^*$) curves are the most important as they give the $\alpha^*$ due to collisions between unlike particles. It was possible to interpolate a curve between the various theoretical ($C^*_{ij}$, $T^*$) curves for the (Kr-$H_2$) case with $\Lambda^*$ = 0.8. A comparison with the experimentally found $\alpha^*_{exp}$ gives qualitative agreement within the experimental uncertainties (15% at 50 °K). For Kr-He such a comparison was not possible.

To get experimental data in a temperature region where more complete quantum calculations are available we studied also hydrogen - helium mixtures between 10 °K and 300 °K, using tritium $H^3$ as a radioactive tracer-gas. We had to use ionisation chamber technics now. We investigated the following mixtures.

$^4$He - T$_2$  with $\Lambda^* = 1.65$ 　　　　　 H$_2$ - HT  with $\Lambda^* = 1.52$

$^4$He - DT  with $\Lambda^* = 1.75$ 　　　　　 D$_2$ - DT  with $\Lambda^* = 1.16$

$^4$He - Ht  with $\Lambda^* = 1.88$

with  $\sigma_{12} = 2.742$ Å 　　　　　　　　　　 with  $\sigma_{12} = 2.928$ Å

and  $\epsilon_{12}/k = 19.5$ °K 　　　　　　　　　 and  $\epsilon_{12}/k = 37.0$ °K

All of these mixtures show two zero values for the thermal diffusion factor $\alpha$, one at about 20 °K and the other one at about 15 °K. There are big quantum effects.

# SAMENVATTING

Het in dit proefschrift beschreven werk heeft betrekking op de thermo-diffusie-factor van quasi Lorentz-mengsels. Als zware component werd het radioactieve $^{85}$Kr-isotoop gebruikt, terwijl de lichte dragergassen respectievelijk $^{22}$Ne, $^4$He, $^3$He en $H_2$ waren. De thermodiffusie-factor voor deze mengsels werd gemeten in een groot temperatuurinterval van 50 $^o$K tot 800 $^o$K.

Het doel van deze metingen was, om enerzijds in het hoge temperatuur-gebied de overeenstemming van de experimentele waarden en de uit de Chapman-Enskog theorie berekende theoretische waarden na te gaan, anderzijds om in het lage temperatuurgebied de grootte van de quantum-effecten te kunnen bepalen.

De metingen werden gedaan in een twee-bollenopstelling, waarbij voor het meten van de scheiding de $^{85}$Kr-concentratie bepaald werd met behulp van een proportionele teller.

Bij de botsing van twee moleculen zullen de quantummechanische dif-fractie-effecten invloed gaan uitoefenen, indien de De Broglie golflengte van dezelfde orde van grootte wordt als de diameter van de moleculen. Een maat voor deze quantumeffecten is de quantumparameter $\Lambda^*$ gede-finieerd door $\Lambda^* = \dfrac{h}{\sigma \sqrt{m \epsilon}}$

Indien $\Lambda^*$ gedeeld door $\sqrt{T^*}$ van de orde van grootte van 1 is, kunnen quantumeffecten optreden. Hierbij is $T^*$ de gereduceerde temperatuur, $T^* = k\,T/\epsilon$. De grootte van de afwijkingen wordt bepaald door $\Lambda^*$.

Voor het mengsel $^{22}$Ne-$^{85}$Kr zijn de bepalende parameters $\Lambda^* = 0,28$, $\epsilon/k = 77$ $^o$K en $\sigma_{12} = 3,22$ Å. De metingen met Ne zijn uitgevoerd tot 80 $^o$K en, zoals te verwachten valt, zijn hierbij geen quantumeffecten gemeten. De overeenstemming met de klassieke theoretische thermodif-fusie factor is uitstekend.

Voor de mengsels $^3$He-$^{85}$Kr en $^4$He-$^{85}$Kr zijn de quantumparameters respectievelijk 0,89 en 0,78. Voor beide mengsels is $\sigma_{12} = 2.095$ Å en $\epsilon/k = 44$ $^o$K. De overeenstemming tussen de experimentele en theoretische waarden is boven kamertemperatuur uitstekend. Hieronder treden afwij-kingen op, welke evenwel niet verklaard kunnen worden met de quantumme-chanische theorie van de transportverschijnselen. Een vergelijking van de experimentele thermodiffusie factor met de theoretische waarde, wel-ke volgt uit het door Clark-Jones gebruikte 8,4 Lennard-Jones-model, geeft in de buurt van 100 $^o$K een redelijke overeenstemming. Mogelijk is dit afwijkend gedrag te verklaren met een potentiaal, die als functie van de temperatuur varieert.

De parameters voor $H_2$-$^{85}$Kr-mengsels zijn $\Lambda^* = 0,76$, $\sigma_{12} = 3,29$ Å en $\epsilon_{12}/k = 78$ $^o$K. Tot ca 100 $^o$K is de overeenstemming tussen theorie en ex-periment uitstekend te noemen. Tussen 100 $^o$K en 300 $^o$K is er een geringe discrepantie tussen de theorie en het experiment, welke waar-schijnlijk het gevolg is van de excitatie van het eerste rotatieniveau van waterstof. Beneden 100 $^o$K is er een discrepantie tussen de klassiek be-rekende waarden van de diffusiefactor en de experimenteel gemeten waarden.

In hoofdstuk V hebben wij de voor diverse quantumparameters berekende waarden van $C_{ij}^*$ getabelleerd als functie van $T^*$. Het is nu mogelijk gebleken om grafisch te interpoleren tussen krommen met verschillende quantumparameters, hoewel bij deze methode grote voorzichtigheid geboden is. Op deze wijze hebben wij de kromme voor het $H_2 - {}^{85}Kr$ mengsel met $\Lambda^* = 0.8$ geinterpoleerd. Het bleek dat de overeenstemming tussen het experiment en de theorie nu zeer bevredigend was.

Teneinde meer experimentele gegevens omtrent de quantumafwijkingen te krijgen, hebben we vervolgens de thermodiffusie factoren gemeten van verschillende mengsels van waterstof en helium. Hierbij werd gebruik gemaakt van een tritiumverbinding in sporenhoeveelheden, teneinde scheidingsfactoren te kunnen meten met behulp van ionisatiekamers. Gemeten werd in een temperatuurinterval van $10\,^{\circ}K - 300\,^{\circ}K$. We onderzochten de volgende mengsels :

$^4He - T_2$,   $\Lambda^* = 1,65$         $H_2 - HT$,   $\Lambda^* = 1,52$

$^4He - DT$,   $\Lambda^* = 1,75$         $D_2 - DT$,   $\Lambda^* = 1,16$

$^4He - HT$,   $\Lambda^* = 1,88$

met $\sigma_{12} = 2,742\,\text{Å}$         met $\sigma_{12} = 2,928\,\text{Å}$

$\epsilon_{12}/k = 19,5\,^{\circ}K$         $\epsilon_{12}/k = 37\,^{\circ}K$

Bij al deze mengsels bleek de thermodiffusie factor op 2 punten nul te worden. Het ene nulpunt ligt bij ca $20\,^{\circ}K$, het andere bij ca $15\,^{\circ}K$. De quantumafwijkingen blijken bijzonder groot te zijn. Een vergelijking met de theorie bleek voor deze mengsels weinig zinvol te zijn.

# STELLINGEN

by A. I. Ghozlan

## 1

The idea of Mason that there is something peculiar about krypton is not correct.

Fender, B. E. F., J. Chem. Phys. **35**, 2243 (1961)
Mason, E. A., J. Chem. Phys. **35**, 2245 (1961)

## 2

The discrepancies between the quantum calculations for the transport coefficients found respectively by Ross and de Boer, are due to the correspondence principle.

Choi, S. I. and Ross, J., J. Chem. Phys. **33**, 1324 (1960)
Boer, J. de and Bird, R. B., Physica **20**, 185 (1954)

## 3

The term "phocuson" which is used to describe momentum transfer in a solid lattice is misleading.

Anderson, G. S., J. Appl. Phys. **34**, 659 (1963)

## 4

The anomaly of the thermal diffusion factor of HT and component X as component to the thermal diffusion factor of $D_2$ and the same component X, has been determined, assuming that the diffusion coefficients behave normally. This assumption is not justified.

Schirdewahn, J., Klemm, A. and Waldmann, L.,
Z. Naturforsch. **16a.** 133 (1961)
Slieker, C. J. G. and Vries, A. E. de, J. Chim. Phys. **60**, 172 (1963)

## 5

The mean energy of sputtered particles as measured by Kopitzki contains a major error especially in the case of the angular dependent measurements.

Kopitzki, K. and Stier, H. E., Z. Naturforsch. **17a**, 346 (1962)
Kistemaker, J. and Snoek, C., Colloques Internationaux du Centre
National de la Recherche Scientifique, 4-8 décembre 1962

It has sometimes more physical meaning to determine the quotient of the parallel and perpendicular electrical component of the light than the polarisation degree $\pi$

Heddle, D. W. O. and Lucas, C. B., Proc. Roy. Soc. A **271**,
129 (1963)

The discrepancy between the heat of sublimation of strontium at room temperature found by Hartmann and Schneider and that found by Priselkov and Nesmeianov, is due to the uncorrect way of performing the experiment by the former research workers.

Hartmann, H. and Schneider, R., Z. anorg. Chem. 180, 275 (1929)
Priselkov, I. A. and Nesmeianov, A. N.,
Doklady Acad. Nauk. S.S.S.R. **95**, 1207 (1954)

The idea of using superconducting coils in plasma physics will be only useful for simple field configurations.

Post, R. F., Conference on Plasma Physics and Controlled Nuclear
Fusion Research, Salzburg, Sept. 1961

The study of the influence of fast neutrons en superconductivity is necessary for the eventual application in thermonuclear plasma physics.

International Conference on High Magnetic Fields,
Cambridge, Massachusetts, November 1-4, 1961

A base pressure of $10^{-7}$. Torr or less in thermonuclear experiments is often not necessary as long as the influence from impurities from the wall is not removed. Impurity radiation may prove to be a bigger problem in reaching fusion than plasma instabilities.

It is generally believed by non-Moslems that a Moslem-man could marry more than one wife. This is not correct.

The new idea of the uniqueness of God stated by Agnaton, the Egyptian pharao, was a necessity.

Elhakim, T., Agnaton, the pharao, admitting God's uniqueness,